Spring 2020

Application of geophysics and remote sensing techniques for economic mineral exploitation in Libya

Awad Abdussalam Henish Lemnifi

Department: Mining Engineering

APPLICATION OF GEOPHYSICS AND REMOTE SENSING TECHNIQUES FOR ECONOMIC MINERAL EXPLOITATION IN LIBYA

by

AWAD ABDUSSALAM HENISH LEMNIFI

A DISSERTATION

Presented to the Faculty of the Graduate School of the

MISSOURI UNIVERSITY OF SCIENCE AND TECHNOLOGY

In Partial Fulfillment of the Requirements for the Degree

DOCTOR OF PHILOSOPHY

in

MINING ENGINEERING

2020

Approved by:

Taghi Sherizadeh (Advisor)
Nassib Aouad (Co-advisor)
Lana Alagha
Ryan Smith
Abdulmohsin Imqam

ABSTRACT

This study investigates crustal thickness and properties within the north central Africa region. Results obtained from 15 seismic stations belonging to the Libyan Center for Remote Sensing and Space Science are reported, in addition to 3 seismic stations publically available, using receiver functions, the first P-to-S receiver function investigation of the 410 km and 660 km depth discontinuities bounding the mantle transition zone (MTZ), and P wave tomography methods. The results from the first method show crustal thicknesses ranging from 24 km to 36 km (with uncertainties ranging between ±0.10 km and ±0.90 km). More specifically, crustal thickness ranges from 32 km to 36 km in the southern portion of the Libyan territory then becomes thinner, between 24 km and 30 km, in the coastal areas of Libya and thinnest, between 24 km and 28 km, in the Sirt Basin.

The observed high *Vp/Vs* value of 1.91 at one station located at the AS Sawda Volcanic Province in central Libya indicates the presence of either partial melt or an abnormally warm area. The results from the second method show thinning of the MTZ was observed beneath the Miocene – Holocene volcanic provinces in central Libya, and the thickness of the MTZ increases from 249 km to 270 km. The third methods results show that Low-velocity anomalies probably representing deep and hot materials are visible extending to depths of ~350–350 km under the volcanic provinces in North Central Africa.

These results indicate that the source materials beneath the volcanic provinces are deeper than previously believed and are mostly attributable to a mantle plume.

ACKNOWLEDGMENTS

I am highly indebted to my advisor, Dr. Taghi Sherizadeh and my co-advisor, Dr. Nassib Aouad, for his technical knowledge, inspiration, and support leading to the successful completion of this project. I would like to thank the examining committee members: Dr. Taghi Sherizadeh (Advisor), Nassib Aouad (Co-advisor), Dr. Lana Alagha, Dr. Ryan Smith, and Dr. Abdulmohsin Imqam for their support. Special thanks to Dr. Kelly Liu and Stephen Gao for helpful discussions and comments.

TABLE OF CONTENTS

Page

LIST OF FIGURES

Page

LIST OF TABLES

Page

1. INTRODUCTION

1.1. BACKGROUND

In the last decades, many studies have suggested that the current continental crust reflects multiple accretionary processes resulting from continent-continent collision, volcanic arcs, continental rifting, and basaltic volcanism at hot spots (Christensen & Mooney, 1995; Clarke & Silver, 1993; Griffin & O'Reilly, 1987; Lemnifi et al., 2017; Rudnick & Fountain, 1995; Rudnick & Gao, 2003). Most of the African subcontinental lithospheric mantle (SCLM) is believed to be of Archean origin but strongly affected by metasomatization during later geological events (Begg et al., 2009). The subcontinental lithosphere is composed of cratons and smaller cratonic fragments that are linked together by younger fold belts. The boundaries of these fragments are fed by magmas that over time generate a fertilization of the SCLM. These weak margins undergo many cycles of rifting, extension, subduction, and renewed accretion (Begg et al., 2009).

The North African portion of the subcontinental lithospheric mantle has undergone a series of complex tectonic processes, where the most notable being the Pan-African events. The Pan-African events (Late Proterozoic to Early Paleozoic) developed continental-scale convergence structures, such as crustal thickening, and may be related to volcanic arcs and possibly deeper alterations indicated by drop a Bouguer gravity anomaly (Doucouré & de Wit, 2003; Liégeois et al., 2013, 2005; Liu & Gao, 2010; Van Der Meijde et al., 2003).

Libya includes a portion of the largest Archean craton of Africa, which is the Sahara Metacraton (SMC). The SMC extends from the Tuareg Shield to the Arabian-Nubian

Shield (Abdelsalam et al., 2002; Lemnifi et al., 2015). According to geochronological and isotopic data, the whole craton appears to have behaved as a single block during the Phanerozoic (Abdelsalam et al., 2002; Liégeois et al., 2013). In addition, the Late Paleozoic oceanic crust is found north of the continental crust of Libya and Egypt (Granot, 2016; Speranza et al., 2012).

A series of uplifts have been recognized on the surface of the SMC, such as the western Tihemboka uplift, the Tibesti-Sirt uplift, the Tripoli-Tibesti uplift, the Al Garaqaf arch, the Haruj Uplift, and the eastern Calanscio-Awayant uplift (Craig et al., 2008; Hassan & Kendall, 2014). The Phanerozoic period in the north of Africa involved episodic compressional and extensional tectonism (Nyblade et al., 1996). During the Mesozoic and early Cenozoic, the North African part was affected mainly by subduction of the Mesozoic lithosphere along the Hellenic arc and Calabrian arc (Capitanio et al., 2009; Marone et al., 2003). In the same period, deep-seated rifting and marine transgression across the region was initiated. As a result, many basins were formed, such as the Sirt, the Murzuk, the Al Kufrah, and the Ghadamis Basins. In the northern part of central Africa, there is significant continental extension (represented by normal faults) affecting an area of 500 kmin width and 500 km in length along the Sirt Basin. This extension developed during the Late Cretaceous to the Eocene, and perhaps into the Holocene, and may have been controlled by the slab pull force developed during the Hellenic convergent event in the north of the region (Capitanio et al., 2009; Nyblade et al., 1996).

Volcanism in Libya began in the Eocene and continued developing into the late Pleistocene. Some evidence suggests volcanism continued along the western and southwestern margins of the Sirt Basin into the Holocene (Elshaafi & Gudmundsson, 2016,

2017a; Nixon et al., 2011). Volcanic units of the Al-Haruj province of Libya are dominated by primarily olivine- and clinopyroxene-rich magma types, which were likely sourced from the juvenile asthenosphere (Cvetkovi´c et al., 2010). It has been proposed that the extrusion of these volcanic units occurred during the reactivation of older lithospheric faults from the uplift events (Cvetkovi´c et al., 2010). Basaltic rocks of Libya's volcanism were produced by melting of predominately anhydrous mixed peridotitic mantle source in an upper mantle plume with an asthenosphic potential temperature around 1400∘C (Ball et al., 2016; Nixon et al., 2011).

The origin of magma beneath Libya and North Africa at large scale is still poorly understood and widely debated. For example, Hegazy (1999) argues that the Libyan intraplate volcanism is related to hot mantle plumes in the underlying asthenosphere. Keppie et al. (2011) propose a conceptual model, using available geophysical and geological constraints, outlining the geometry of a channel plume underlying North Africa, which laterally feeds geographically discrete volcanic fields, similar to a model of the Afar plume (cf. Ebinger & Sleep, 1998). Tomographic models by Begg et al. (2009) argue that topography of the bottom of cratonic blocks in Africa has caused an important role in guiding the upwelling hot mantle, whereby magma might ascend to the surface through metasomatized lithospheric channels. Based on geochemistry and isotope data, Nixon et al. (2011) infer that the North African Tertiary-Quaternary volcanism can be partly explained in terms of diapiric upwellings originating from the upper mantle.

The main volcanic provinces in Libya mostly coincide with the current elevated basement regions. There are at least two alternative mechanisms that may explain this relationship between basement and volcanic provinces in Libya: (i) the regions have been

subject to magmatic underplating that led to further increase in the elevation (cf. Craig et al., 2011) and (ii) the basement highs have been subject to subcrustal arching (Al-Hafdh & El-Shaafi, 2015; Vail, 1971).

All these studies and related models to a large degree depend on having a reasonably accurate knowledge of the crustal thickness, mantle transion zone (MTZ), and P-wave tomography beneath Libya. However, the crustal thickness, thickness of MTZ and P-wave tomography of Libya and of the central North Africa, in general, has been rather poorly constrained, partly because of the paucity of seismic broadband stations.

1.2. STATEMENT OF THE PROBLEM

Economic minerals related to source materials beneath Libya are sparsely studied and poorly constrained. In particular, the origin of volcanic materials and hydrothermal processes, lucks of understanding the plumbing system of Libya's enigmatic volcanism and substantial characterization of ore deposits within and around the study area (e.g., Lemnifi et al., 2015) are still debated and many interpretations are based on mainly geochemical and isotopic data and rarely from regional geophysical studies (Elshaafi and Gudmundsson, 2018). Tomographic models by Begg et al. (2009) argue that topography of the bottom of cratonic blocks in Africa has caused an important role in guiding the upwelling hot mantle, whereby magma might ascend to the surface through metasomatized lithospheric channels. The main volcanic provinces in Libya mostly coincide with the current elevated basement regions. Previous models have mostly centered on two hypotheses. Some studies (e.g., Burke, 1996; Gourgaud and Vincent, 2004; Nixon et al., 2011) consider the origin of the volcanic materials are coming from deep source beneath

the region. By contrast, other studies (e.g., Liegeois et al., 2003; Less et al., 2006) completely rule out that the origin of the volcanic materials coming from deep source. Beccaluva et al. (2007) also suggest that the volcanism in Libya and adjacent regions is mostly related to passive asthenospheric mantle upwelling triggered by extensional stress in the lithosphere during Cenozoic reactivation. Cvetkovi´c et al. (2010) proposed that volcanic activity was most likely initiated during the early stage evolution of the Sirt Basin. Numerous global and regional tomographic studies (e.g., Marone et al., 2003; Li´egeois et al., 2005; Pasyanos and Nyblade, 2007; Montagner et al., 2007; Fishwick, 2010; Bardintzeff et al., 2012) have shown weak velocity anomalies, but the depths of their investigations were limited. The volcanic provinces throughout northern Central Africa are mainly associated with negative Bouguer anomalies, and the lithospheric thicknesses indicated from surface wave tomography are relatively, perhaps anomalously thin, at approximately 90 to 100 km [Fishwick, 2010].

There are at least two alternative mechanisms that may explain this relationship between basement and volcanic provinces in Libya: (i) the regions have been subject to magmatic underplating that led to further increase in the elevation (cf. Craig et al., 2011) and (ii) the basement highs have been subject to subcrustal arching (Al-Hafdh & El-Shaafi, 2015; Vail, 1971). Part of a more complete understanding relies on further knowledge of the mechanical interactions between subsurface layers in the Earth and their role in the widespread magmatism throughout the region since the Early Miocene.

Mapping and understanding the depth and physical properties of the sediment-crust, crust-mantle, and lithosphere-asthenosphere boundaries is essential for not only interpreting the processes occurring within the layers and between the boundary plates but

also to develop a more complete understanding of the tectonic evolution of the Earth, source of the volcanic materials (McKenzie and Priestley, 2008; Liu and Gao, 2018).

Thus, this research will open and advance frontiers on the use of the geophysical models to study relationship between the earth's layers and estimate the depth of the source of surface volcanic materials. Thus, this information can lead to discovery of ore deposits.

1.3. RESEARCH OBJECTIVES AND SCOPE

Despite a proliferation of literature concerning the tectonic evolution of north central Africa as well as the characteristics of the crustal thickness and the source of the ore deposit beneath the region, numerous significant questions remain. The main objective of this research is to develop a comprehensive local geological model, which considers the relationship between the different layers such as crust-mantle and sediment-crust boundaries. The study area lucks deal geophysical study shows that how the mechanical interaction between Moho, crust and sediment. Also, a further question concern how these boundaries affect different hydrothermal and partial melting. The answering to such questions cannot be answered by using only one method. Thus, this proposed research study will address these weaknesses. This study will apply three distinct analytical techniques receiver function constraints, p wave tomography, and remote sensing techniques. This research encourages further research in the development of local 2D/3D geodynamic models using new seismic data and encourage geological field work.

This research initiative is limited to lack of geophysical information by using new seismic data. The study will provide an independent set of measurements with a higher resolution than most previous studies. Additionally, the results from this study are less

affected by the thick sedimentary layers which led to an approximately 1.5–2 s delay of the first P arrival on the radial receiver function.

1.4. INDUSTRIAL AND ACADEMIC CONTRIBUTIONS

Exploration for minerals requires a range of different techniques and technology. As such, this project will use data from both seismic stations and satellites in the areas around volcanic provinces in Libya in order to better estimate their mineral resource potential. In a simple sense, ores and mineral deposits require hot fluids to flow through faults and fractures (i.e. permeable networks). It is well recognized that the geometrical arrangement of crustal structures influences the deposition of hydrothermal minerals (Hildenbrand et al., 2000). As the relationship between ore formation and lithospheric thickness is still poorly constrained and unknown, some inferences are needed in order to assess any potential mineralization in the Libyan region.

The complex tectonic history in the region is exhibited by periods of uplift, subsidence, tilting, faulting, and intrusion. The effects of these tectonic events throughout the region are broad (Al-Heety, 2013). For example, external impacts on mining operations can produce a serious threat as they occur rapidly and unexpectedly. Such a rapid onset external impact is seismic activity. Although the region is not considered as highly seismically active (Al-Heety, 2013), many earthquakes of Mw >6 have occurred historically. Fortunately, both telesesimic and microseismic measurements are collected and commonly used in the fields of geo-science, geo-engineering and geo-resources. The data from such measurements can be used to monitor the seismic structure in and around tunnels, which benefits schedule planning, budget and safety for any planned mining

activities. The beauty of teleseismic and microseismic investigations is that they can be applied over different scales to observe fluctuations in stress field across a regional fault caused by changes of stability level. They can also be incorporated into risk planning associated with mining activity. The new information and expertise from this research would be a great help to build a new base for mining activities and estimation of the amount of future investment and profit from mining activities in the region.

This research effort is expected to expand frontiers and advance knowledge with the use of seismicity data to create a geodynamic model link with mantle-crust-sediment layering. This study will build a bridge between engineering, geological and geophysical research fields. The knowledge and discoveries from this study will create new research frontiers for further research initiatives.

1.5. ORIGINALITY OF PHD RESEARCH

This fundamental research work is a novel effort towards providing a local geodynamics model by using different techniques. The research pioneers the efforts in studying the crustal thickness, sediment thickness, and source of any ore's deposits beneath Libya. A major problem for the seismicity studies of Libya in the past decades was the absence of any extensive seismological network until 2005, at which time, the first Libyan seismological network was established (Al-Heety, 2013). Specifically, this study uses seismologic data acquired from 2005 to 2009 and allows us to infer in much greater detail than has been possible before the depth of the Moho, and the source of the ore deposits in various parts in Libya and, in particular, the origin of the partial melting within the volcanic provinces.

1.6. STRUCTURE OF THE PHD DISSERTATION

Section 1 presents background information about the study area and associated problems. The research problem, as well as the research objectives and methodology, are outlined. Section 2 provides an extensive review of literature that has been done so far in the region. The extensive review of literature will be in the following areas including seismology, global geophysical model, geochemical isotopes, and remote sensing. We will focus in weaknesses in the existing techniques that used in the literatures, and lack of available studies conducted into seismology and remote sensing. The data and methods are presented in Section 3. The methods that we will use are receiver functions, p wave tomography. The results and observation from the methods are captured in Section 4. Section 5 provides discussion and comparisons of our findings with previous studies. Summary of the conclusions and recommendations from the research are covered in Section 6.

2. LITERATURE REVIEW

The contributions and limitations of relevant books and technical publications have been reviewed. This section will outline the summary contributions from published literature with significant impact on receiver function (RFs), P-wave tomography.

2.1. PREVIOUS GEOPHYSICAL STUDIES ON CRUSTAL THICKNESSES USING RECEIVER FUNCTION METHOD

Many geophysical studies have focused on crustal thicknesses beneath northern and central Africa (Begg et al., 2009; Marone et al., 2003; Pasyanos & Nyblade, 2007; Pasyanos & Walter, 2002) using different global velocity models. Marone et al. (2003) estimated the crustal thickness at the Eurasia-Africa plate boundary on basis of receiver function analysis, reflection and refraction surveys, and gravity and anomaly measurements. They inferred a typical Moho depth of about 30 km. They interpreted the sharp change in crustal thickness along the coast of Africa (from 25 km to 35 km) as being due to extension of the North African margin. In this area Moho depth and structure are poorly constrained, making it difficult to provide reliable models of associated local geological processes.

Sandvol et al. (1998) used H-κ stacking to estimate the crustal structure in the Middle East and in a segment of North Africa but did not include data from Libya. Van Der Meijde et al. (2003) studied the crustal structure beneath the Mediterranean region using H-κ stacking and found that the crustal thickness varies from 22 km beneath the intraoceanic islands to 47 km beneath the continental margins. They found a deeper Moho of 30 ± 2.1 km at station GHAR and 31 ± 1.5 km at station MARJ. In their study, they

chose the peaks by using a very broad grid search method, so the Moho depth could range from 30 km to 36 km for both stations in their study. Pasyanos and Nyblade (2007) estimated crustal thickness beneath Africa and Arabia using forward modeling of surface waves and found that the crustal thickness in the study area varies between 25 km and 35 km. They found that the crustal thickness at the coastline is about 25 km in the west and 30 km to 35 km in the east. They also have examined the sedimentary cover thickness in the African and Arabian platforms, including that in the study area, providing estimates indicating that the sediment layers are thicker in the coastal areas (about 3.5 km to 5.5 km) and thinner in the central portions (about 1.0 km to 3.0 km).

The gravity field of the eastern Mediterranean Sea, including the coastline of the study area, was studied by Cowie and Kusznir (2012) whose results indicate that close to the coastline the offshore crust is about 35 km thick but 20–25 km thick farther seaward, while in the interior of Libya the crust reaches its maximum thickness of 40–45 km. They concluded that the thickness of sedimentary deposits along the southern coastline of the Mediterranean Sea is ranging from 4 km to 6 km.

High heat flow of 80–120 mW/m2 in northwestern Africa is associated with a regional thermal anomaly in the lithosphere (Lesquer et al., 1990). Specifically, the Tertiary-late Quaternary volcanic activity in Algeria, in the Hoggar massif, indicates that the upper mantle beneath northwestern Africa is still partially molten (Lesquer et al., 1990; Nyblade et al., 1996). Very low shear wave velocities (Vs) have been observed beneath eastern Africa and branches throughout northern Africa, which may reflect the presence of partial melt at the crust-mantle boundary (Begg et al., 2009; Deen et al., 2006).

2.2. PREVIOUS GEOPHYSICAL STUDIES ON MANTLE TRANSION ZONE USING RECEIVER FUNCTION METHOD

The study of mantle discontinuities beneath Libya and adjacent regions are relatively sparse. This is partly due to the limited number of broadband seismic stations deployed in the area. Van der Meijde et al. (2005) studied seismic discontinuities in the Mediterranean region using P-to-S converted phases which were identified through receiver function analysis. They found that the MTZ was 10–30 km thicker than the global average in the areas surrounding the Mediterranean Sea (including the north-eastern parts of Libya). These findings were interpreted as resulting from past subduction. Bonatto et al. (2015) investigated the MTZ thickness beneath the Ibero-Magherbian region (to the west of the study area) using data from 258 seismic stations. Their method was also based on receiver function analysis and two different cross-correlation functions. They observed lateral variations in terms of the depths of the 410 km depth discontinuity (d410) and the 660 km depth discontinuity (d660) and the thickness of the MTZ which they attributed as the Betic Aboran slab subducted beneath the Alboran Sea, as well as the presence of a garnet enriched layer beneath the western Moroccan region, and plume material beneath the Gulf of Cadiz.

The origin of Libya's volcanism (Tibesti, Al Haruj, As Saawada and Gharyan) and adjacent areas is widely debated and many interpretations are based on mainly geochemical and isotopic data and rarely from regional geophysical studies (Elshaafi and Gudmundsson, 2018). Previous models have mostly centered on two hypotheses. Some studies (e.g., Burke, 1996; Gourgaud and Vincent, 2004; Nixon et al., 2011) consider there to be a hotspot mantle plume beneath the region. By contrast, other studies (e.g., Liegeois et al., 2003; Less et al., 2006) completely rule out the mantle plume theory.

Ebinger et al. (1989) propose that nearly all of the volcanic activity in North and Central Africa, such as the volcanoes found in Darfur, Tibesti and Cameroon, are associated with the Afar plume. The hypothesis relies on the lateral flow of plume materials beneath the lithosphere feeding the volcanoes in this region (Azzouni-Sekkal et al., 2007). Keppie et al. (2011) offer a conceptual model based on geological constraints and geophysical data to depict the geometry of the super-plume underlying North Africa. This super-plume laterally feeds geographically discrete volcanic fields analogous to the Afar plume (cf. Ebinger et al., 1989, Ebinger and Sleep, 1998; Begg et al., 2009). Burke (1996) proposes that the North African intraplate volcanism is related to mantle plumes in the underlying asthenosphere. Gourgaud and Vincent (2004) also allude to the existence of a mantle plume beneath the Tibesti volcanic province, southernmost Libya, using geochemical data.

By contrast, the tomographic model of Liegeois et al. (2005) does not support the existence of mantle plumes beneath the Libyan volcanic provinces. This model instead assumes that the shallow mantle is warmer with melt fractions at depths between 100 km to 150 km. These estimated depths are in good agreement with the depths of 80–150 km reported from geochemistry and isotopic studies on the lavas and mantle xenoliths from the Al Haruj and Waw an Namous provinces (Bardintzeff et al., 2012). In addition, the relatively low magmatic temperatures that have been obtained through the studied peridotite xenoliths (spinel lherzolites) (Peregi et al., 2003; Less et al., 2006; Elshaafi and Gudmundsson, 2017) from the Al Haruj Volcanic Province, do not support the presence of a mantle plume beneath this volcanic region but instead they suggest the existence of a relatively cold lithosphere. Beccaluva et al. (2007) suggest that the volcanism in Libya and

adjacent regions is mostly related to passive asthenospheric mantle upwelling triggered by extensional stress in the lithosphere during Cenozoic reactivation. Cvetkovi´c et al. (2010) proposed that volcanic activity was most likely initiated during the early stage evolution of the Sirt Basin.

Nixon et al. (2011) inferred that Libya's volcanism formed by diapirs and upwelling originating in the upper mantle. They concluded that the primary magmas originated at depths of 70 km for tholeiitic magmas with partial melt of 13.5% and 74 km for alkali magmas with partial melt of 18.9%. The primitive mantle normalized multi-element patterns of Libya's basaltic rocks are highly enriched in incompatible trace elements, similar to within plate basalts, particularly oceanic island basalts (OIB) spectrum (St Helena-type) which represent basaltic melts from an enriched asthenospheric mantle source, most likely associated with an uprising mantle plume (Asran and Aboazom, 2004). St. Helena is also formed by a mantle plume similar to that of many volcanic islands, such as Hawaii and Iceland.

Previous seismological investigations of the crust and mantle beneath Libya and adjacent areas have been global scale low-resolution studies (e.g., Pasyanos and Nyblade, 2007; Fishwick, 2010). Tomography studies indicate that the volcanic areas in Libya are associated with a low-velocity mantle structure limited to the top 150 km (Liegeois et al., 2003) as previously mentioned. Large positive velocity anomalies in the upper 100 km of North Africa were interpreted as the cratonic roots of cratonic terranes called the Sahara Metacraton (Grand, 2002; Lemnifi et al., 2015). The delamination of cratonic roots have been proposed to explain the observed negative velocity anomalies at the depths of 100–175 km (Abdelsalam et al., 2011). The interior of North Africa has also been imaged, with

limited resolution, to show high velocity anomalies at depths above the 660 km discontinuity which suggests that the area is dominated by an accumulation of subducted slabs (Piromallo and Morelli, 2003). The central portion of Libya was characterized as having a thinner lithosphere, which is about 90–100 km thick, based on studies of surface wave tomography (Fishwick, 2010). It is likely that partially molten magma reservoirs are active beneath the AS Sawda Volcanic Province, as detected recently by slow Vs waves in comparison to the Vp waves (Lemnifi et al., 2017a).

Most of the existing global or continental scale tomography models of the study area (Marone et al., 2003; Li´egeois et al., 2005; Pasyanos and Nyblade, 2007; Montagner et al., 2007; Fishwick, 2010; Bardintzeff et al., 2012) show weak anomalies but with limited depth investigation. P-and S-wave velocity perturbations have been observed in previous studies (e.g., Grand, 2002; Simmons et al., 2012). Shear wave splitting measurements obtained adjacent to North Africa (Miller et al., 2013; Lemnifi et al., 2014; 2015) are attributed to mantle flow and represent the horizontal movement of the African continent to the north with local deflection of the mantle flow (Lemnifi et al., 2015).

2.3. PREVIOUS GEOPHYSICAL STUDIES ON MANTLE STRUCTURE BENEATH NORTH CENTRAL AFRICA USING TELESEISMIC P-WAVE TOMOGRAPHY

Over the last two decades, seismic tomography has become one of the most powerful tools for mapping the three-dimensional (3-D) heterogeneous velocity structure of the Earth’s interior. Through tomography on both regional and global scales, seismology can provide useful information to answer questions related to geodynamics and tectonics. Certainly, tomography can be used to estimate the volume of subducted lithosphere and

locate upwellings of hot (low-velocity) material from different depths in the mantle more realistically than other studies (e.g., Piromallo and Morelli, 2003).

Categorizing the structure of the lithosphere is of fundamental importance for studying the evolution of the crustal thickness and the development of volcanic provinces (Cochran and Karner, 2007; Lemnifi et al., 2019). The Pan-African orogeny, an orogenic cycle reflecting the opening and closing of a large ocean and the collision of buoyant crustal blocks (Kröner and Stern, 2005), exerted compressional stresses on the African plate during the Neoproterozoic and caused varying lithospheric thicknesses (Stoeser and Camp, 1985; Stern, 1994; Lemnifi et al., 2015). Related to these complicated geological phenomena, North Central Africa also contains many volcanic provinces that were shaped from the Miocene to the Holocene (e.g., Hoernle et al., 1995; Bardintzeff et al., 2012; Lemnifi et al., 2019]. These volcanic provinces are thought to originate from within the lower mantle (Lemnifi et al., 2019). Previous geophysical investigations have indicated that the crustal thickness beneath North Central Africa varies from 20 to 37 km using the gravity field and receiver functions (e.g., Cowie and Kusznir, 2012; Lemnifi et al., 2017). Lesquer et al. (1990) found that this area is characterized by a high heat flow of 80–120 mW/m2, especially in the Hoggar massif, indicating that the upper mantle beneath northwestern Africa is still partially molten (Lesquer et al., 1990; Nyblade et al., 1996).

Numerous models have been developed to explain the tectonics of North Central Africa, including those involving teleseismic receiver functions (e.g., Sandvol et al., 1998; Cowie and Kusznir, 2012; Lemnifi et al., 2017; 2019), shear-wave splitting analyses (e.g., Lemnifi et al., 2015), and global tomography (e.g., Liegeois et al. 2005). However, the dynamic evolutionary processes of this region are still debated because the lack of seismic

data and deep seismic soundings prohibit its detailed imaging. Recent receiver function investigations beneath Libya in the As Sawda volcanic province revealed an obvious low-velocity (low-V) anomaly in the mantle transition zone (MTZ) (Lemnifi et al., 2019), suggesting higher-than-normal temperatures therein.

2.4. SUMMARY

Literature on geological and geophysical studies on the region have been reviewed. We summarize from the previous studies that have done in the region, the origin of the surface volcanic materials observed receiver functions and p wave tomography is still poorly understood. The vast majority of the previous receiver functions and p wave tomography investigations in the study area was based on the data from three seismic stations. Major problem for the seismicity studies of Libya in past decades was the absence of any extensive seismological network until 2005 at which time the first Libyan seismological network was established (Al-Heety, 2013). Specifically, this study uses seismologic data acquired from 2005 to 2009 and allows us to infer in much greater detail than has been possible before the depth of Moho in various parts in North Central Africa. Section 3 presents the data and methods and equations that used in this study.

3. DATA AND METHODS

We used receiver functions (RFs) and P wave tomography obtained from 15 seismic stations managed by the Libyan Center for Remote Sensing and Space Science (LCRSSS) and 3 seismic stations from the Incorporated Research Institutions for Seismology (IRIS) and Data Management Center (DMC). Figure 3.1 shows the distribution of earthquakes used in this study from both seismic networks.

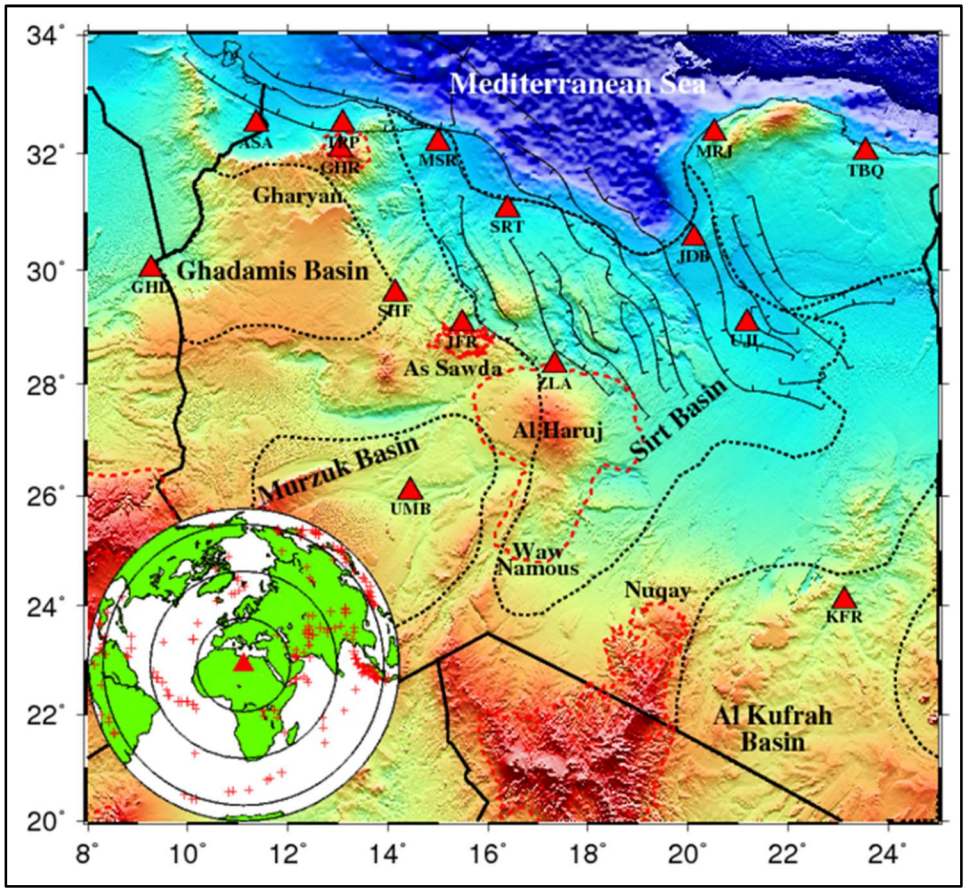

Figure 3.1. Elevation map of the study area (North Central Africa) and distribution of seismic stations (red triangles) used in this study. The circular inset shows the epicentral distribution of the teleseismic events (red crosses) used in this study. The red triangle indicates the center of the study area, and the numbers show the epicentral distances in degrees from the center of the study area.

The operation period of the Libyan Network stations ranged from early 2005 to late 2009, while the data were acquired from early 2000 to 2013 for the public seismic stations. All 18 stations were used to estimate H and κ values, mantle transition zone thickness, and mantle structure beneath north central Africa.

3.1. RECEIVER FUNCTIONS METHODS TO ESTIMATE H AND κ VALUES

The three component seismograms are adjusted to 20 s earlier and 260 s after the first P wave arrival based on the IASP91 Earth model, and seismograms were filtered in the 0.04–0.8 Hz frequency band to enhance the signal-to-noise ratio. All seismic events in this study have magnitudes between 5.2 and 6.2 and occurred at epicentral distances from 30° to 180° (cf. Liu et al., 2017; Nair et al., 2006; Reed et al., 2014) (Figure 3.2).

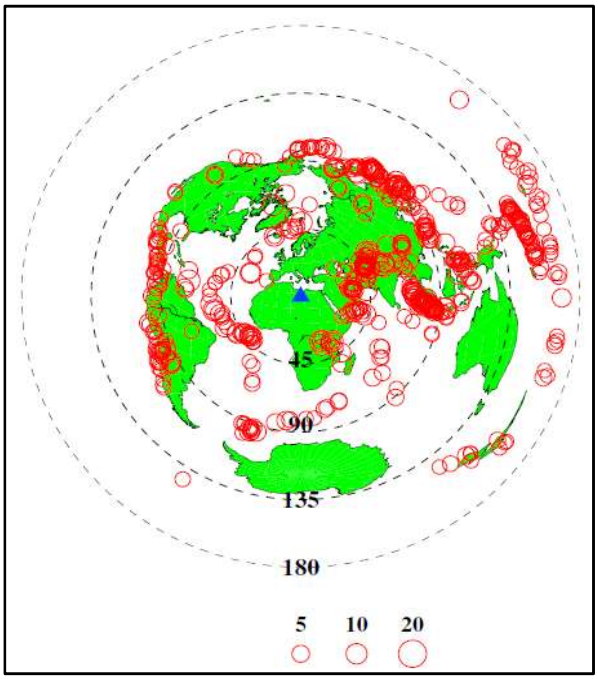

Figure 3.2. Location of the events used in this study. The size of the red circles is proportional to the number of high-quality receiver functions from that event. The blue triangle indicates the area of study.

In this study, the cutoff magnitude (Mc) was defined as Mc = 5.2 + (De − 30.0)⁄(180.0−30.0) −Hf⁄700, where De is epicentral distance in degree and Hf is focal depth in kilometer (Liu & Gao, 2010). We applied the procedure of Ammon (1991) to deconvolving the vertical component from the radial component to filter seismograms with a P wave signal. A signal-to-noise ratio of 4.0 or greater was used in order to generate radial RFs on the radial component utilizing the frequency domain water level deconvolution. This method uses the relative arrival times of the P wave and associated P to S converted phases PxS by grid searching each station's stacked trace across a range of candidate values for H and κ. A constant P wave crustal velocity of 6.5 km/s was assumed in this study. The optimal pair of H and κ values was investigated in the range of 15–55 km and 1.65–1.95, with the intervals of 0.1 km and 0.01 km, respectively.

Moreover, the high-quality seismograms were manually selected with a robust first arrival of the direct P phase on the vertical component in order to identify the optimal pair of H and κ corresponding to the maximum stacking amplitude (Zhu & Kanamori, 2000). Thus, iterating the moveout corrections and stacking were used to determine the parameters (H and κ) and their standard deviations (uncertainties) through 10 bootstrap computation using the Efron and Tibshirani (1986) method for random resampling in order to obtain a reliable estimate. We used a producer that is described by Zhu and Kanamori (2000) to stack the RFs. The following equation describes the stacking of the receiver functions at each of the station.

$$A(H_i, \kappa_j) = \sum_{k=1}^{N} w_1 \times S_k\left(t_1^{(i,j)}\right) + w_2 \times S_k\left(t_2^{(i,j)}\right) - w_3 \times S_k\left(t_3^{(i,j)}\right), \qquad (1)$$

Where N is the number of high-quality radial RFs from the station, Sk(t) is the amplitude of the point on receiver function at time t after the direct P arrival, t1, t2, t3 are the moveout times for the PxS, and the w1,w2, and w3 are the weighting that satisfy w1 + w2 + w3 = 1 (Zhu & Kanamori, 2000). More detailed descriptions of this method can be found in Nair et al. (2006) and in Reed et al. (2014). The stations results were ranked as: A (excellent), B (good), and C (poor), according to the peak clarity of the PxS on the H-κ. The stations assigned a rank of C were not included in the results.

The study area has four major sedimentary basins as already mentioned, and stations SRT, MSR, UJL, ZLA, SHF, UMB, GHD, and KFR are located within the sedimentary basins (Figure 3.1). The Mesozoic Sirt Basin situated in north central Libya is bounded by the Paleozoic Ghadamis, Murzuk, and Al Kufrah Basins. These basins have thick sedimentary deposits, ranging from 1 km to 7 km (Abadi et al., 2008; Hassan & Kendall, 2014; Pasyanos & Nyblade, 2007). The increasing thickness and decreasing velocity of the sedimentary layers can generate a reverberatory characteristic in the RFs (Yu et al., 2015). Therefore, larger sedimentary thicknesses can produce errors in the H results when applying the method described above. Thus, the conventional H-κ stacking procedure causes overestimates of H because the strong reverberations by multiple reflections (between the bottom of a loose sedimentary layer and the Earth's surface) associated with a low-velocity sedimentary layer can mask the Moho converted phases. In order to remove these effects of the sedimentary layers, we have applied the technique by Yu et al. (2015), which uses the arrival time of the PxS phases and the two-way travel time of the sedimentary layers to correct the RFs. The removal of the reverberations clarifies the arrival of Ps from the Moho discontinuity (Figure 3.3). This procedure corrects the time

delay and calculates the thicknesses of the unconsolidated sediment layer as well as the subsediment H and κ. Further details of the technique procedure are given by Yu et al. (2015).

On the other hand, an average P wave velocity of 3.5 km/s was used for the sedimentary layers during this study based on several studies related to oil surveys in Libya (e.g., Ben, 2000; Makris & Yegorova, 2006). The sediment velocity (3.5 km/s) for stacking would lead to an error of 0.024 km to 0.78 km in the resulting H value and 0.0052 to 0.13 in the resulting κ value. After the removal of the effects caused by the sedimentary layers, the amplitude of the first Ps phase from the base of the sedimentary layer (PbS) and the Moho phases appears more clearly (Figures 3.3-3.5).

For each pair of (Hi , ϕj) we will calculate PmS was calculated by using [Dueker and Sheehan, 1998]

$$t_1^{(i,j)} = \int_{-Hi}^{0} \left[\sqrt{(V_p(z)/\phi_j)^{-2} - p^2} - \sqrt{V_p(z)^{-2} - p^2} \right] dz \quad (2)$$

Where p is the P wave ray parameter, H_i is the depth of the candidate discontinuity, ϕ_j is the candidate Vp/Vs and Vp(z) is the P wave velocity at depth z.

The moveout, $t_2^{(i,j)}$ of PPmS can be calculated by using

$$t_2^{(i,j)} = \int_{-Hi}^{0} \left[\sqrt{(V_p(z)/\phi_j)^{-2} - p^2} + \sqrt{V_p(z)^{-2} - p^2} \right] dz \quad (3)$$

and for PSmS, $t_3^{(i,j)}$ can be calculated by

$$t_3^{(i,j)} = \int_{-H_i}^{0} 2\sqrt{(Vp(z)/\phi_j)^{-2} - p^2}\ \mathrm{dz} \quad (4)$$

At each station the receiver functions have been stacked by using

$$A(H_i, \phi_j) = \sum_{k=1}^{n} w_1 S_k(t_1^{(i,j)}) + w_2 S_k(t_2^{(i,j)}) - w_3 S_k(t_3^{(i,j)}) \quad (5)$$

where n is the number of high –quality radial RFs from the station, Sk(t) is the amplitude of the point on the receiver function at time t after the direct P arrival, t1, tt2, t3, are moveout for PxS, w1, w2 and w3 are weighting factors that satisfy w1+w2+w3= 1 (Zhu and Kanamori, 2000).

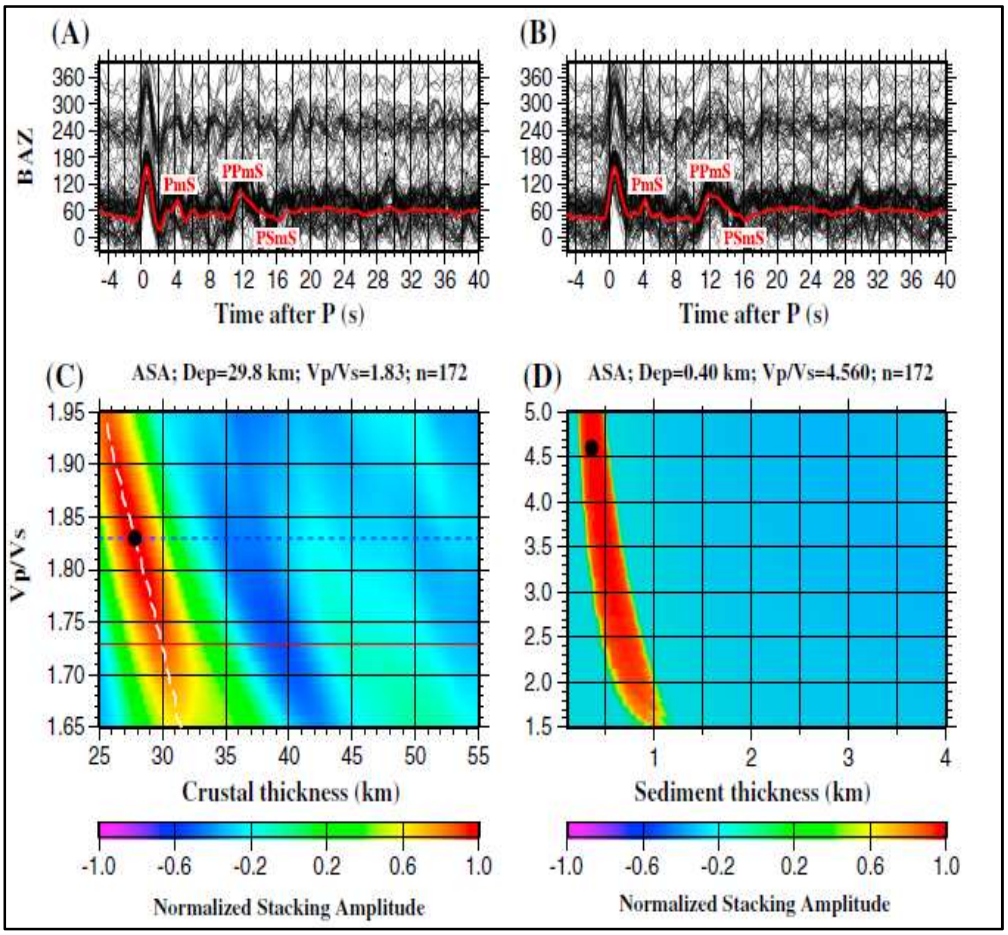

Figure 3.3. Application of H-κ plot for station ASA before and after the sediment correction, using the procedure of Yu et al. (2015). (a) Radial RFs plotted against the back azimuth, with a simple time series stack (red) before sediment moveout, (b) same as Figure 3.3a but after resource-removal filtering, and (c) H-κ grid plot for normalized stacking amplitude after the sediment moveout correction. The optimal H and κ pair are indicated by a black dot. (d) Same as Figure 3.3c but for the H-κ grid plot for the stacking amplitude to determine sediment thickness.

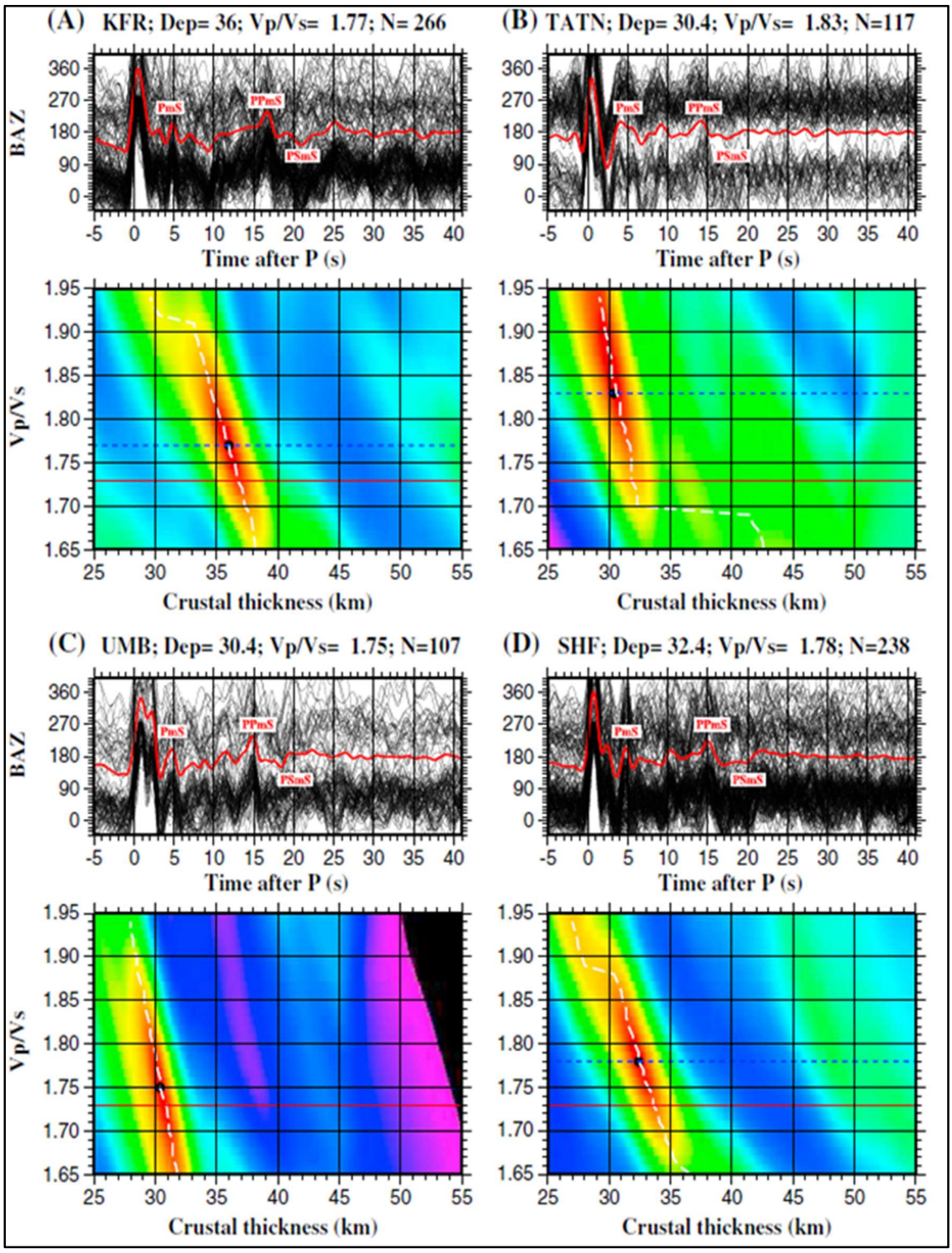

Figure 3.4. (a–d) Application of H-κ stacking for stations KFR, TATN, UMB, and SHF. The top panels show radial RFs (black) plotted against the back azimuth. The bottom panels are normalized amplitude grid with optimal H and κ pair indicated by a black dot. The red line represents stacking amplitudes for κ = 1.73, the dashed blue line represents stacking amplitudes for the optimal κ and stacking amplitude along the dashed white.

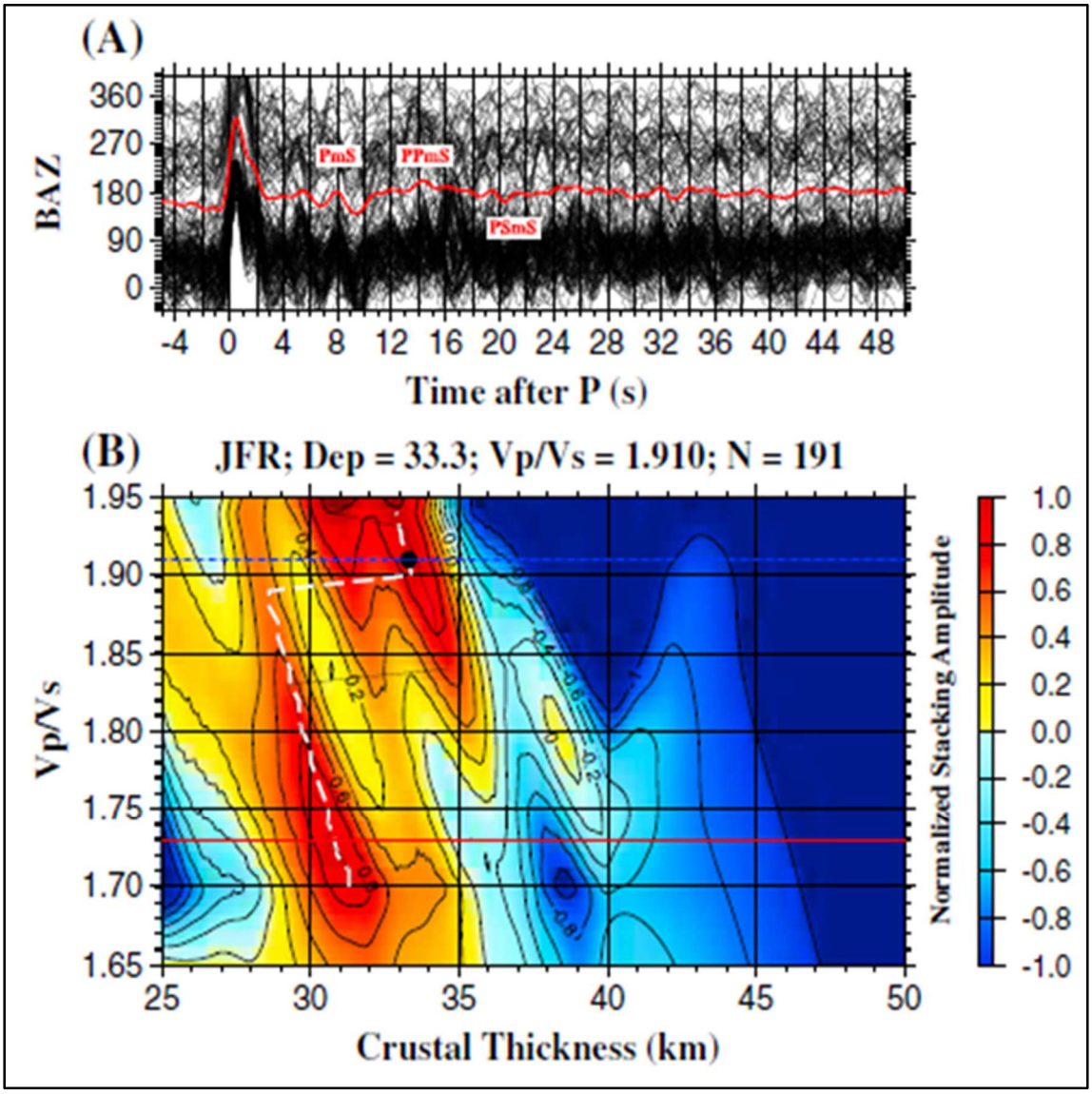

Figure 3.5. Same as Figure 3.4 but for station JFR at the AS Sawda Volcanic Province. Note that the κ value (1.91) most likely indicates partial melting beneath this region.

3.2. RECEIVER FUNCTIONS METHODS TO ESTIMATE THE MANTLE TRANSION ZONE THICKNESS

The mantle layer between the 410 km and 660 km discontinuities (here after referred to as d410 and d660, respectively) is denominated as the Mantle Transition Zone (MTZ). Mineral physics and seismic studies (Ringwood, 1975) suggest that d410 is characterized as the phase transition from olivine to wadsleyite, while d660 is formed by

the transformation of spinel to perovskite and magnesiowüstite. Previous determinations revealed Clapeyron slopes of +1.5 to+3.0 MPa K−1 for the olivine wadsleyite (d410) and -4.0 to -0.4 MPa K−1 for the postspinel transition (d660) (Gao and Liu, 2014b; Tauzin and Ricard, 2014). Therefore, the depths of the d410 and d660 phase changes are anticorrelated in depth of thermal anomalies. The d410 phase becomes shallower when it hosts colder material, and deeper with hotter material.

The d660 phase exhibits the opposite behavior. Therefore, the MTZ is thinner in higher temperature regions, and thicker in colder regions (such as near subducted slabs) (Helffrich, 2000; Lawrence and Shearer, 2006; Bonatto et al., 2015). Previous studies have established that the depth variability of the d410 and d660 can indicate the existence of cold subducted slabs and high temperature anomalies (e.g., Anderson, 1967; Collier et al., 2001; Contenti et al., 2012; Li and Yuan, 2003; Shearer and Masters, 1992; Wicks & Richards, 1993; Yu et al., 2017). Kennett and Engdahl (1991) and Kennett et al. [1995] established that in most global models, the average thickness of the MTZ is 250 km, known because mineral phase variations between α olivine and β olivine occur at 410 km (Ringwood, 1975) and the spinel to bridgmanite variation occurs at 660 km (Ito & Katsura, 1989; Yamazaki and Karato, 2001).

Nevertheless, MTZ thickness variations depend not only on the temperature of the material, but also on water concentration and chemical composition (Gu et al., 1998; Flanagan and Shearer, 1998; Meier et al., 2009). Litasov et al. (2005) demonstrated that the presence of water within olivine, wadsleyite and ringwoodite has the effect of increasing the magnitude of the clapeyron slope and thus amplifies variations in depth. The effect is to deflect the d410 upward and the d660 downward, making it harder to observe

the temperature changes because thickening of the MTZ will always occur when a enough water is present (Yu et al., 2017).

The present work focuses on MTZ studies by using new data from eighteen broadband seismic stations, which are managed by the Libyan Center for Remote Sensing, and Space Science (LCRSSS), in addition, data from three seismic stations are publicly available and archived from the Incorporated Research Institutions for Seismology (IRIS) Data Management Center (DMC) (Figures 3.2 and 3.6). The main aim of this project is using receiver function analysis to map the depth of the discontinuities and the thickness of the MTZ beneath Libya and so infer related geodynamical processes and understand better the origin of Libya's volcanism.

The seismic events were selected based on epicentral distance, from 30° to 100° and cut-off magnitude, which is determined by the epicentral distance and focal depth, as defined by Liu and Gao (2010). We calculated the receiver functions (RFs) based on the frequency-domain water-level deconvolution procedure (Ammon, 1991). The seismograms were filtered in the frequency range of 0.02-0.50 Hz. An SNR based procedure was applied to select high-quality RFs, further details about the quality of RFs are given by Gao and Liu (2014a). We stacked the moveout-corrected RFs within each 2° radius bin based on the locations of the ray-piercing points at the depth of 535 km (Gao and Liu, 2014a). We stack the RFs based on the piercing point locations calculated at each of the candidate discontinuity depths (e.g., Liu et al., 2003). The IASP91 reference Earth model (Kennett and Engdahl, 1991) was employed to stack the receiver functions using the non-plane wavefront assumption [Gao and Liu, 2014a]. RFs placed within each of the bins are resampled over 50 iterations (Efron and Tibshirani, 1986; Liu et al., 2003; Dahm et al.,

2017) to calculate the mean and standard deviation of the discontinuity depths and the thickness of the MTZ. The moveout-corrected RFs were converted into a depth range of 300–800 km with a vertical interval of 1 km.

Bins with less than 5 RFs were not used in this study in order to minimize the possibility of misidentifying the arrivals from the targeted discontinuities. In order to increase the reliability of the results, we manually picked the maximum amplitude near the theoretical arrival of the converted S waves from the MTZ discontinuities.

To provide restrictions on the explanation on the observation of the results MTZ, we pick P-wave travel-time manually relative to the IASP91 Earth model on the vertical and transverse components. The P wave arrival was measured relative to the IASP91 Earth model. The picking residuals accuracy is dependent on the signal strength relative to the background noise, as well as the sharpness of the arrivals (further details are given by Yu et al., 2015). In this study, we use 5.3 km s−1 for the P-waves. We apply Eq. (6) to correct for travel-times due to variations in station elevation (Nolet, 2008; Yu et al., 2015).

$$\delta t_{ij} = \delta_{ij} - \frac{hi}{v\ x\ \cos\{a\ \sin(Rij\ x\ v)\}} \tag{6}$$

where, δtij is the original residual (in seconds) found at the ith station from the jth event, Rij is the ray parameter (in s km−1), hi is the elevation (in km) for the ith station, and v is the average velocity (in km s−1) in the layer above sea-level.

3.3. TELESEISMIC P-WAVE TOMOGRAPHY

In this study, we use data collected from the LCRSS. The LCRSS consists of 15 relatively new seismic stations. The epicentral distances of the events used in the project vary from 25° to 95°. Most of the events used here are in the Pacific and Atlantic Oceans

(Figure 3.1); hence, these events represent a sufficient azimuthal coverage around the study region.

Here, based on theoretical arrival times computed using the IASP91 Earth model (Kennett and Engdahl, 1991), we hand-picked the first P-wave arrival times from high-quality seismograms (Figure 3.7) with an accuracy of approximately 0.1–0.2 s. We then applied various important steps, including a careful visual check of all the vertical-component seismograms to reject all those lacking a clear P-wave onset (see Yu et al. (2017) for more details regarding the procedure). Each of the events used in the study was recorded by at least four seismic stations. A total of 2093 direct P-wave arrivals (Figure 3.7) were used for the tomographic inversion. The ray paths show good coverage in all directions (vertical and horizontal planes) down to a depth of 700 km (Figure 3.8).

We computed the relative travel-time residual for each event to decrease the effects of uncertainties in the hypocenter locations and origin times by using the tomography method of Zhao et al. (1994) to subtract the mean residual from the raw residuals prior to the tomographic inversion. For the tomographic inversion, we used the IASP91 Earth model as the starting one-dimensional velocity model. For more details for the calculation of the relative travel-time residuals, see Zhao et al. (1994); Lei and Zhao (2016); Zhao et al. (1992); Yu at el. (2015); (2017). An average P-wave velocity of 6.5 km/s was assumed in this study. The ray path length in the crust was calculated by considering the angle of incidence, which was calculated using the ray parameter.

Damping and smoothing regularization were used to solve the large and sparse system of observation equations (Zhao et al., 1994; Zhao, 2015; Yu et al., 2017) by employing the conjugate-gradient algorithm (Paige and Saunders, 1982).

Figure 3.9 shows the optimal values of the damping and smoothing parameters established based on the trade-off curve between the data variance reduction and model norm (Hansen, 1992; Yu et al., 2017).

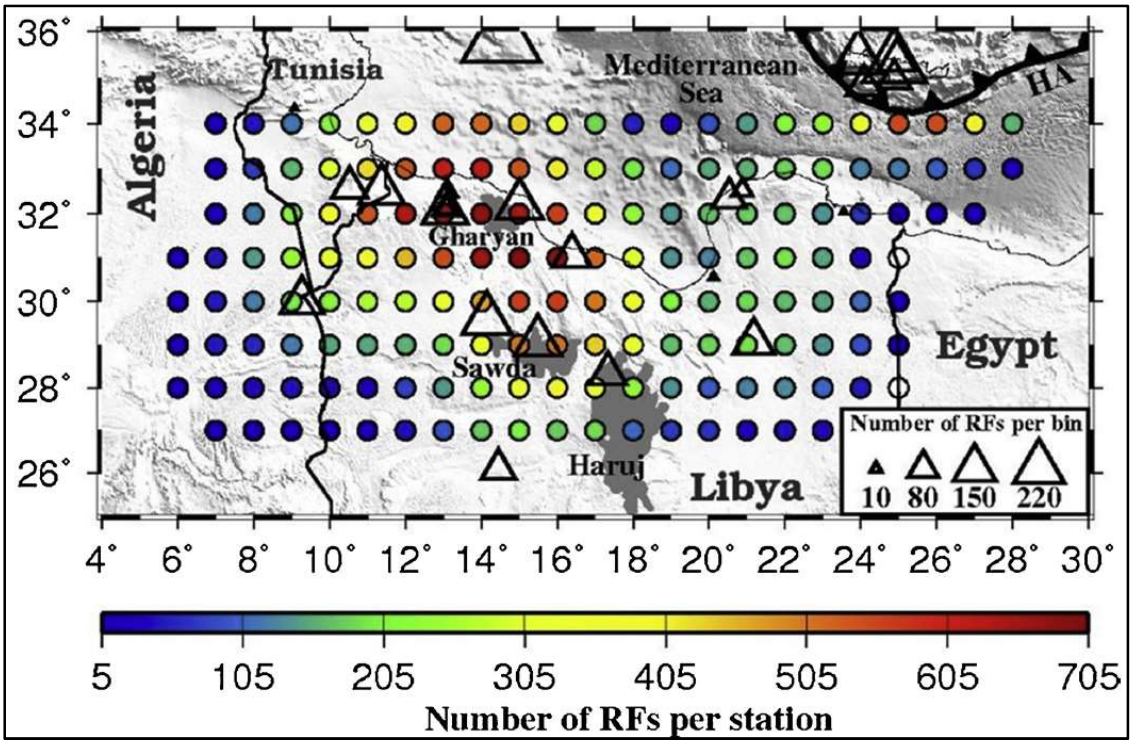

Figure 3.6. Topographic map overlaid with circles representing the central point of each 2° radius bins. The triangles represent the seismic stations used in this study. HA: Hellenic Arc. The different sizes of the triangles represent the number of RFs obtained from each station. The color of the circles represents the number of RFs per bin.

3.4. SUMMARY

Over the last two decades, receiver functions, seismic tomography techniques have become one of the most powerful tools for mapping of earth's layer of the Earth's interior. These techniques can provide useful information to answer questions related to geodynamics, origin of the surface materials especially in the volcanic provinces and tectonics. The results all methods we used are presented in Section 4.

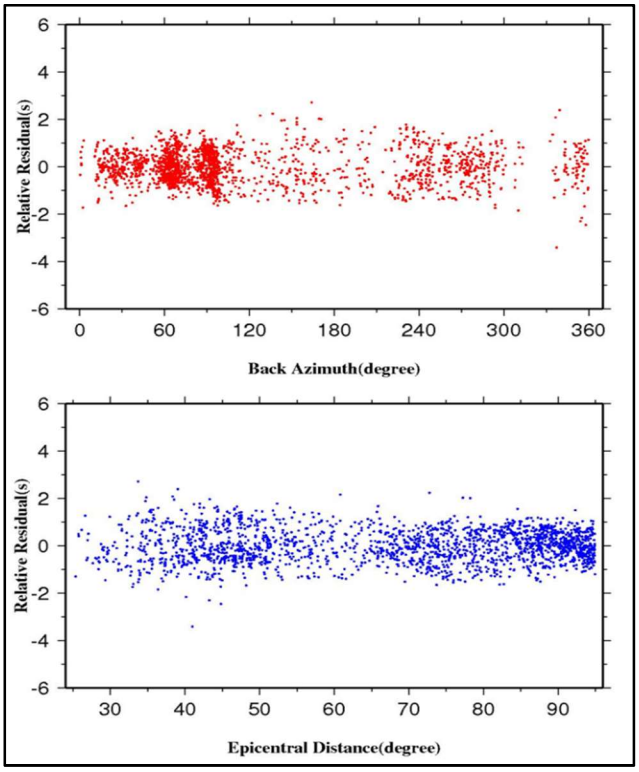

Figure 3.7. (A) All 2093 raw travel-time residuals (in seconds) versus the backazimuth (in degrees). (B) Raw travel-time residuals (in seconds) versus the epicentral distance (in degrees).

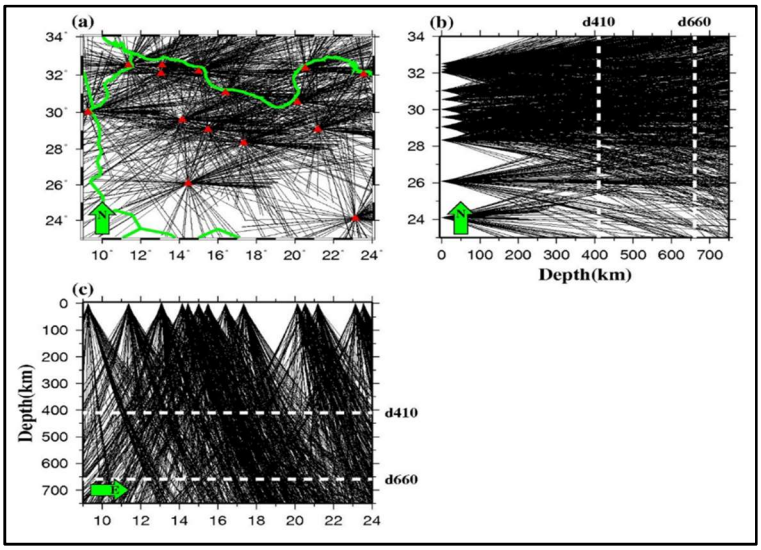

Figure 3.8. Distribution of P-wave ray paths (A) in map view and (B) on north-south and (C) east-west vertical cross-sections through the region. The ray paths from each station are projected onto the cross-section. The red triangles represent the seismic stations. The white dashed lines in B and C illustrate the 410 km (d410) and 660 km (d660) discontinuities.

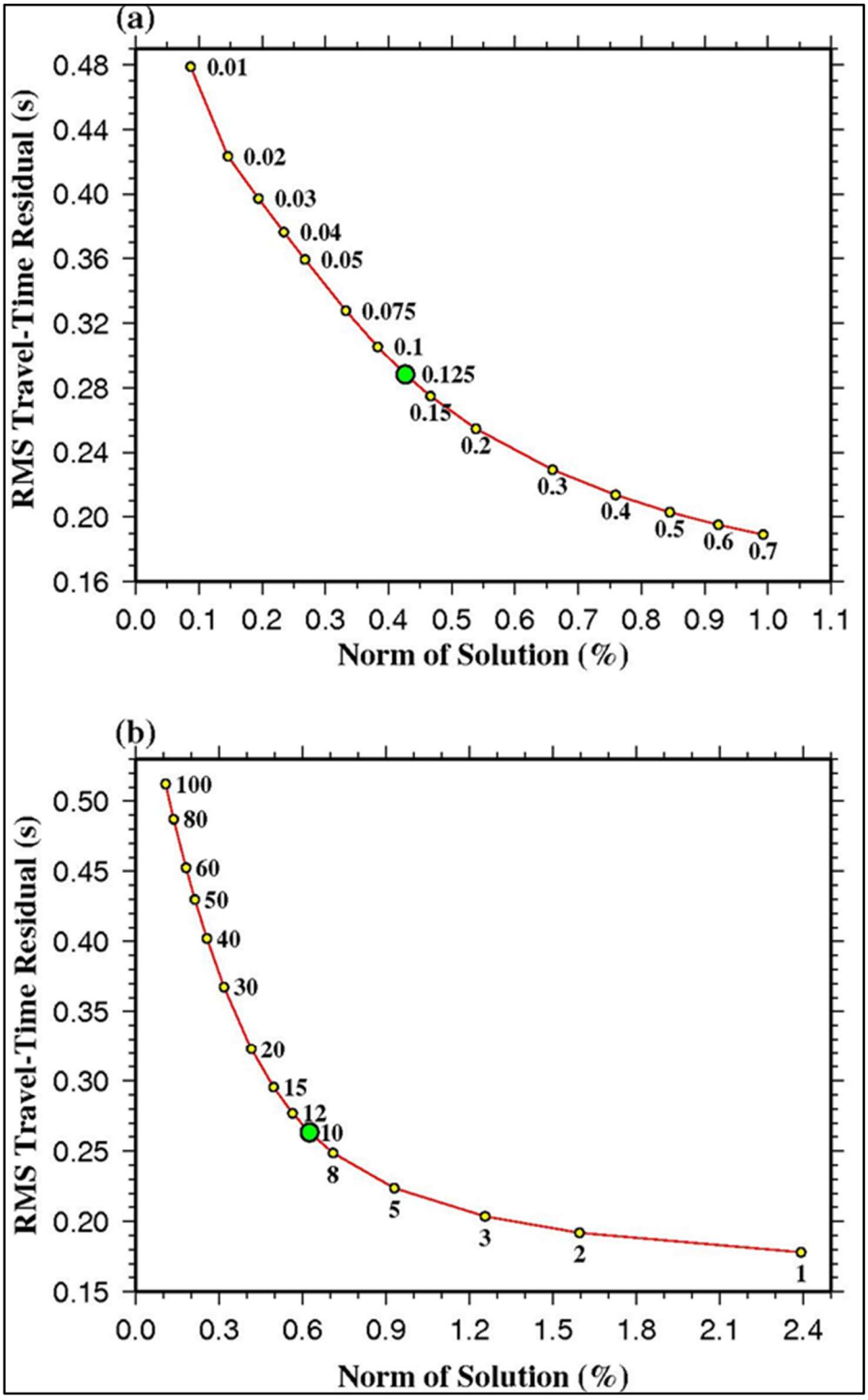

Figure 3.9. Trade-off curves between the norm of the 3-D velocity model and the root-mean-square (RMS) travel-time residuals for the tomographic inversions with different values of the damping parameter. The green circles in (A) and (B) indicate the optimal values of the smoothing and damping parameters used in this study, respectively.

4. RESULTS

In this section will present the results from three methods (receiver function, first P-to-S receiver function investigation of the 410 km and 660 km depth discontinuities bounding the mantle transition zone (MTZ), and P wave tomography).

4.1. RECEIVER FUNCTION TO ESTIMATE H AND κ VALUES

The values for H and κ for the crustal thickness and unconsolidated sediment layer thickness obtained from the 18 seismic stations are shown in Tables 4.1, Figures 4.1 and 4.2 and Table 4.2. Each station was manually checked based on the displayed PmS, as well as both the PPmP and PSmS arrivals. Figures 3.4 and 3.5 show an example from stations ASA, KFR, TATN, UMB, SHF, and JFR that display a clear arrival phase in a singular stacking point on the corresponding H-κ plot after the removal of effects from the sedimentary layers.

For the entire area of investigation, the resulting H values range from 24 km to 36 km, with a mean value of 32 km (with uncertainties ranging between ±0.10 km and ±0.90 km). The κ values range from 1.71 to 1.91, with a mean value of 1.83 (with uncertainties ranging between ±0.01 and ±0.04). The results suggest that the thinnest crust occurs mainly beneath the stations SRT, TRP, and JDB, whereas the thickest crust occurs beneath station KFR (the east central portion of the study area). In the coastal area, the H ranges from 24 km to 31 km, and the κ value ranges from 1.71 to 1.85. The northwestern part of the region is characterized by some of the lowest κ values, especially at stations GHAR and SRT (Figure 4.2). Stations GHD and ZLA were not used in the study because of the very strong

influence of a thick sedimentary layer that led to an approximately 1.5–2 s delay of the first P arrival on the radial RFs. The waveform does not have a dominant period; thus, the sedimentary removal procedure cannot be reliably applied in this case.

Additionally, station TBQ was not used because it recorded an unreliable number of RFs (<10). Our result for the stations GHAR and GHR shows that H is approximately 33 km, which is similar to the finding recorded by Van Der Meijde et al. (2003) who reported an average thickness of about 31 km.

To characterize the observed systematic spatial variations in the crust, we tested the correlations between crustal thickness, elevation, Vp/Vs, and Bouguer gravity anomalies for the region (Figure 4.2). We used a grid resolution for Bouguer gravity anomaly and elevation of 2 min and 1 min, respectively. Such resolutions are useful for large-scale geological studies and give critical information about the compensation mechanism of the Libyan territory (cf. Tontini et al., 2006). The H is directly proportional to the surface elevation with cross-correlation coefficient (r) of 0.55 (Figure 4.3a), and the H is inversely proportional to the Bouguer gravity anomaly with r = −0.70 (Figure 4.3c). We also compare the κ values with H, surface elevation, and Bouguer gravity anomaly and find no significant correlation with r = −0.02, −0.34, and 0.03, respectively (Figures 4.3e and 4.3f).

We additionally observed a good correlation between elevation and Bouguer gravity anomalies (r = 0.57) for 56 points where we picked up four measurements for both parameters at 2.5 km around each seismic station (Figure 4.1b). Hence, the greater surface elevations commonly correspond to the lower Bouguer anomalies and thicker crust, which may indicate an isostatically compensated crust.

4.2. RESULTS FROM RECEIVER FUNCTIONS METHODS TO ESTIMATE THE MANTLE TRANSION ZONE THICKNESS

The RFs in the study area produced 162 bins with observable arrivals from the d410 and d660. As shown in Figure 4.4, the P-to-S conversion from the d410 and d660 can be easily identified when the traces are sorted according to depth. All of the stacked traces plot along eight latitudes from 27 °N to 34 °N as shown in Figure 4.5. The average depth of the d410 in the study area is 413 ± 6 km, and the average depth of the d660 is 663 ± 8 km. The average MTZ thickness calculated is 249 ± 14 km, which fully agrees with the IASP91 Earth model depth value of 250 km.

The observed depth of the d410 increases towards the central part of the study area, from approximately 400 km to 420 km (Figure 4.5a, b, c, e, and f). The apparent depth of the d660 increases from 650 to 670 km from longitudes 6° to 13° but returns to 650 km from longitudes 14° to 28°. The depths of the d410 and the d660 increase by 10 km to 420 km and 670 km beneath the areas hosting volcanoes. We find that the depths of the d410 and d660 are generally uncorrelated, and the cross-correlation coefficient (R) is 0.21 (Figure 4.6). To provide spatial series images for the results at the bins selected we used a continuous curvature surface gridding algorithm, with a tension factor of 0.5 (Smith and Wessel, 1990; Yu et al., 2015). The Standard deviation (STD) of MTZ thickness in the region is less than 10 km (Figure 4.7d).

The weak correlation between the two depths studied indicates that the MTZ beneath the study area is influenced by materials with anomalously high or low temperatures (e.g., Bonatto et al., 2015). MTZ thicknesses in the west and southeast are similar to the global average but the MTZ thickness in the northeast of Libya is about 20

km thicker than average (Figure 4.7c), while the south-central area, approximately centered at 14 °E, 28 °N, is about 10 km thinner. The thinnest portion of the MTZ, to the south of the As Sawda Volcanic Province (SVP), is affected by a depressed d410 and an uplifted d660. Therefore, the weak correlation might indicate slower upper mantle velocities. To the northeastern part of Libya, a thicker MTZ is caused by shallowing of the d410 and deepening of the d660, which demonstrates a negative correlation between the d410 and d660 and as such indicates the presence of cold material. This finding is entirely supported by mineral physics studies (Ito and Takahashi, 1989; Fei et al., 2004).

We have hand-picked P-wave residuals from the teleseismic events (Figure 4.8). The observations represent the residuals from individual station event pairs which are plotted at the ray-piercing point at the depth of 100 km from west to east along the study area. The P-wave travel time residuals decrease in the central part of the region, and this again occurs spatially with the location of volcanic provinces.

Table 4.1. Observations of Crustal Thickness (H) and Vp/Vs(k).

Station	Latitude (deg)	Longitude (deg)	*N*	*H* (km)	V_p/V_s (κ)	Rank
ASA	32.51	11.37	172	29.8 ± 0.37	1.83 ± 0.01	A
GHAR	32.12	13.10	41	33.4 ± 0.80	1.73 ± 0.03	A
GHR	32.07	13.05	203	33.0 ± 0.12	1.76 ± 0.01	A
JDB	30.55	20.12	11	24.10 ± 0.00	1.86 ± 0.00	B
JFR	29.06	15.49	191	33.30 ± 0.12	1.91 ± 0.01	A
KFR	24.10	23.13	266	36.0 ± 0.19	1.77 ± 0.00	A
MRJ[a]	32.35	20.53	60	27.0 ± 0.28	1.71 ± 0.03	A
MSR	32.19	15.01	184	30.90 ± 0.26	1.81 ± 0.01	A
SHF	29.59	14.15	238	32.37 ± 0.21	1.78 ± 0.01	A
SRT	31.05	16.39	80	26.10 ± 0.44	1.72 ± 0.04	B
TANT	32.58	10.53	117	30.40 ± 0.58	1.83 ± 0.02	A
TRP	32.51	13.10	32	24.20 ± 0.79	1.85 ± 0.02	B
UJL	29.07	21.18	149	28.80 ± 0.16	1.82 ± 0.01	A
UMB	26.08	14.45	107	30.44 ± 0.13	1.75 ± 0.01	A

[a]Merged two stations.

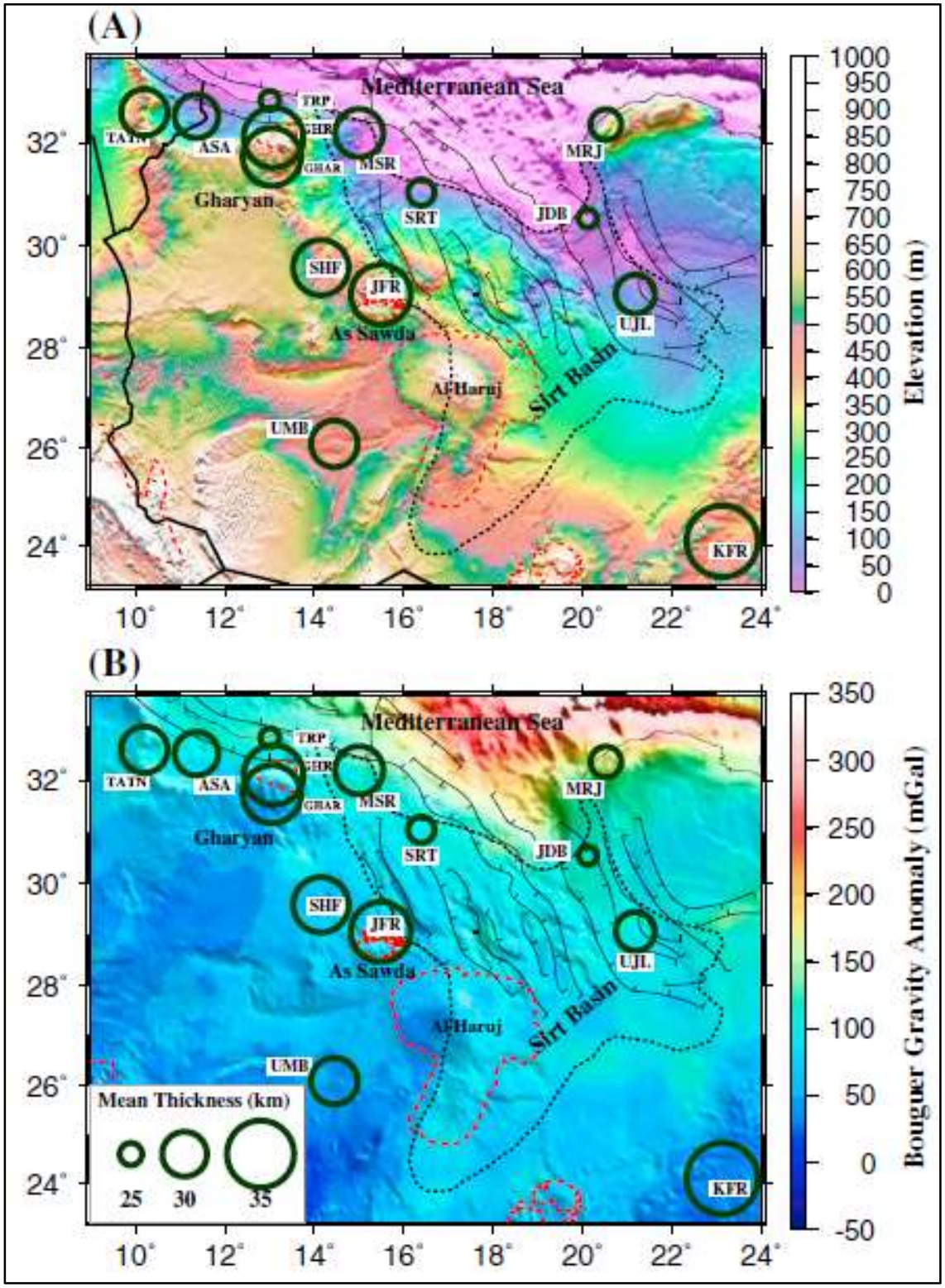

Figure 4.1. (a) Topographic relief map of the study area, with 1 min resolution, showing crustal thickness, and (b) resulting crustal thicknesses plotted on top of the Bouguer gravity map, which produced from the WGM2012 Bouguer gravity model with a resolution of 2 min. Note that circle diameter correlates with crustal thickness

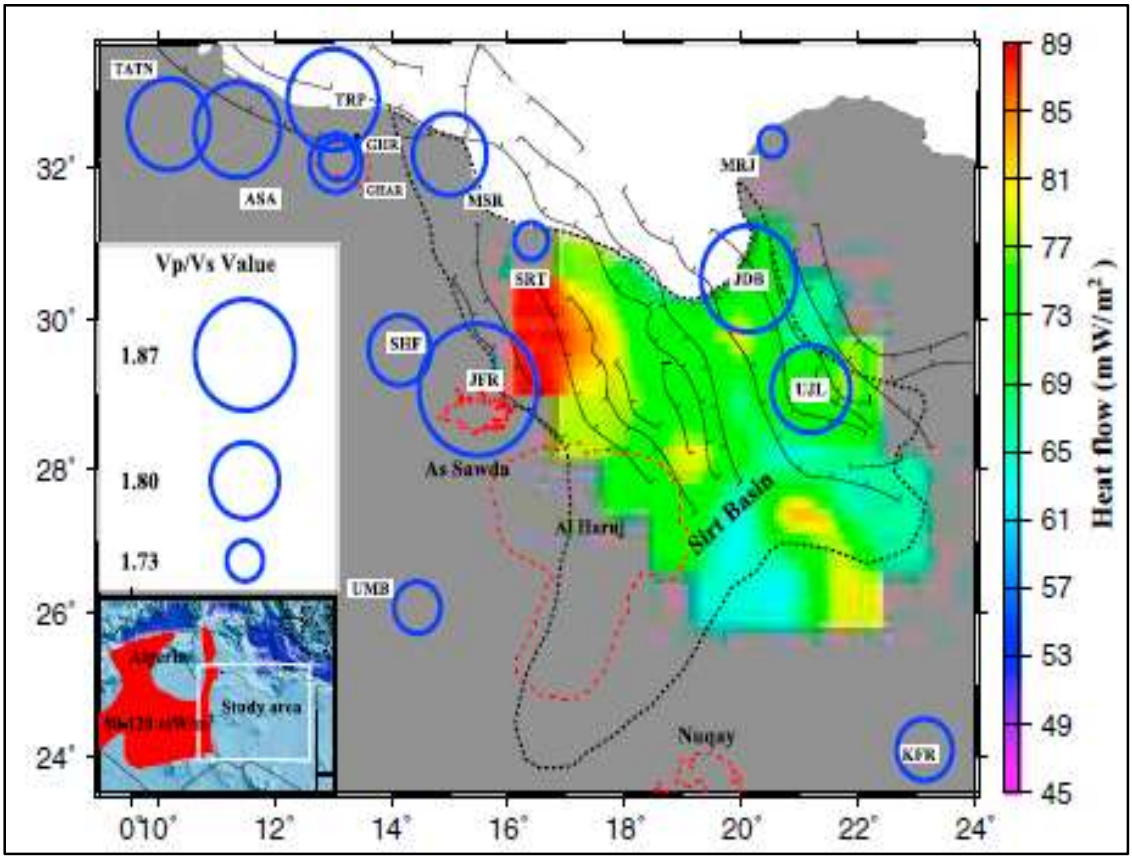

Figure 4.2. Vp⁄Vs values in the study area and patterns of heat flow across the Sirt Basin. The inset map shows the heat flow (80–120 mW/m2) in the NW part of Africa at Algeria, which is indicated by a deep red color. The heat flow in the volcanic areas seems likely much higher than central and eastern parts of the Sirt Basin. The heat flow data are taken from Nyblade et al. (1996). Expanding circle diameters indicate increasingly κ values. The highest κ value (1.91) was recorded beneath the AS Swada Volcanic Province at station JFR. The main volcanic provinces represent by red dashed lines, and Mesozoic rifts represent by teeth on downthrown blocks (black lines).

Table 4.2. Observations of Crustal Thickness (H) and Vp/Vs(k).

Station	Latitude (deg)	Longitude (deg)	N	H (km)	V_p/V_s (κ)	Rank
ASA	32.51	11.37	172	0.40 ± 0.02	4.56 ± 0.13	A
JDB	30.55	20.12	6	2.17 ± 0.06	4.21 ± .08	B
MSR	32.19	15.01	184	0.80 ± 0.26	4.79 ± 0.01	A
SHF	29.59	14.15	238	1.90 ± 0.21	2.29 ± 0.01	A
SRT	31.05	16.39	80	2.00 ± 0.44	3.48 ± 0.04	B
TRP	32.51	13.10	32	3.70 ± 0.79	2.21 ± 0.02	A
UJL	29.07	21.18	149	1.50 ± 0.16	4.75 ± 0.01	A

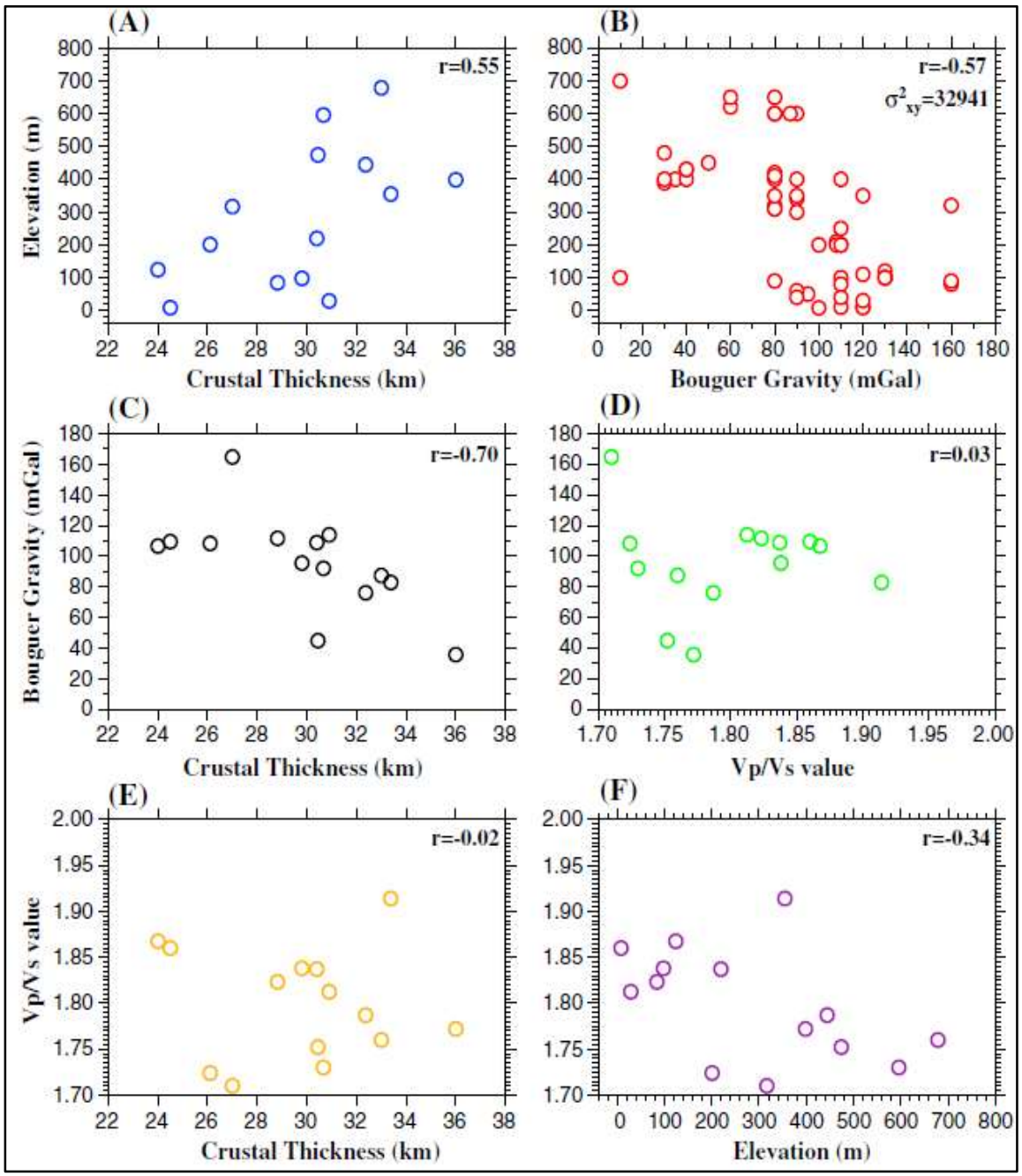

Figure 4.3. Graphs showing the correlations between crustal thickness, elevation, Bouguer Gravity, and Vp⁄Vs. (a) Correlation between crustal thickness and elevation with r = 0.55 where r is the cross-correlation coefficient. (b) Correlation between Bouguer gravity anomaly and elevation with r = −0.57, σ2(x, y) = 32, 941, where σ(x, y) is the sum of variance elevation (x) plus Bouguer gravity anomaly (y) due to both x and y are correlated. (c) Correlation between crustal thickness and Bouguer gravity anomaly with r = −0.70. (d) Correlation between Bouguer gravity anomaly and Vp⁄Vs values with r = 0.03. (e) Correlation between crustal thickness and Vp⁄Vs values with r = −0.02. (f) Correlation between elevation and Vp⁄Vs values with r = −0.34.

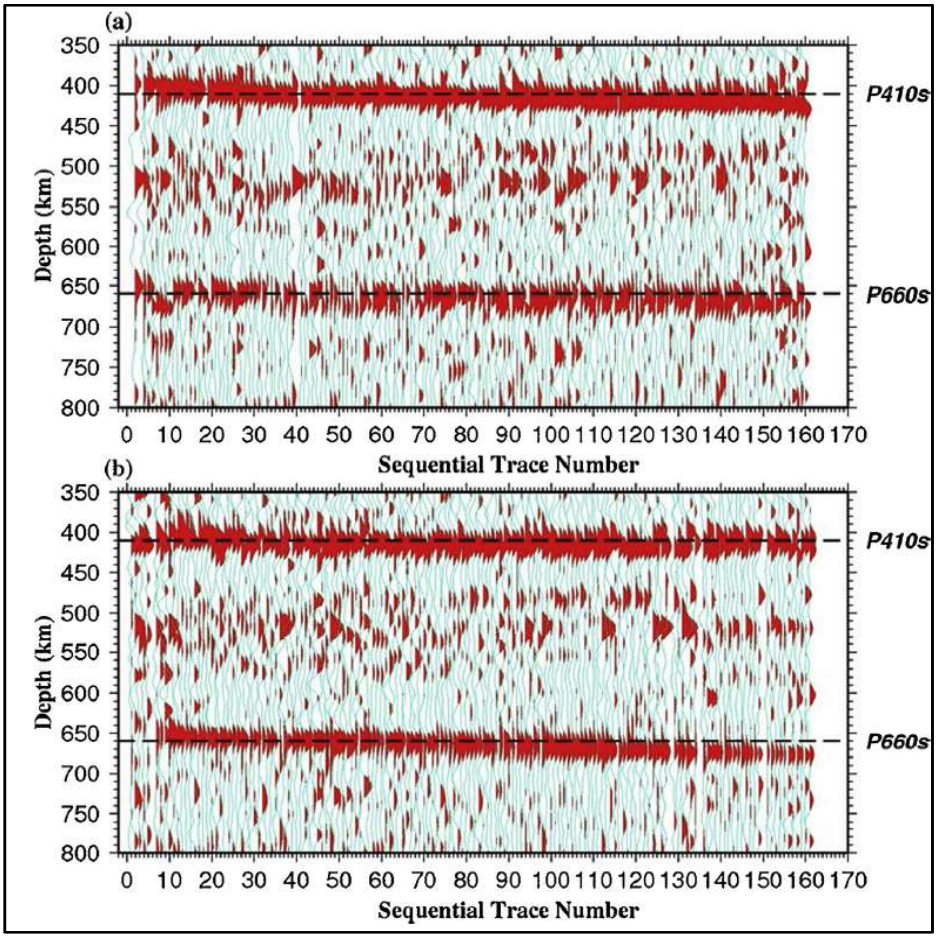

Figure 4.4. (a) The results of stacking normal moveout-corrected RFs, plotted with the sequentially increasing depth of the d410, and (b) same as (a) but for the d660.

4.3. P-WAVE TOMOGRAPHU RESULTS

In this study, the tomography resolution was examined by performing a checkerboard resolution test at many different depths using different grid intervals (Figure 4.9).

4.3.1. Resolution Analyses. Here, we allocated alternating negative and positive velocity anomalies of up to 3% to the 3-D grid nodes in the modeling space. A grid interval of 1° was adopted to represent the optimal tomographic inversion of real-world data. The checkerboard resolution test outcomes are good for the depth range of 150–700 km beneath

the study area. As the depth increases, the resolution increases due to the presence of vertically incident rays (Figure 3.8).

The spatial resolution beneath the volcanic provinces becomes significantly higher with increasing depth due to the improving ray path coverage. In some areas, the biased velocity anomalies are spatially limited, especially in the west and east, which may be due to the azimuthal coverage of incoming rays and the limited number of seismic stations. Therefore, our interpretation will focus on the areas with a high number of seismic stations, good resolution test outcomes, and a high back azimuthal coverage.

4.3.2. Tomography Results. Here, we adopted velocity anomalies ranging from –3% to 3%, as shown in Figures 4.9 and 4.10. At 80 km depth, both low- and high-velocity bodies are clearly shown, especially around the Al Haruj volcanic province (Figure 4.10). The results at a depth of 150 km are mostly the same as those at a depth of 80 km with low-velocity anomalies between the Al Haruj and As Sawada volcanic provinces.

The resolution gradually increases with depth and is greatly improved at a depth of 300 km, which reflects the improved ray coverage (Figure 3.8). A high-velocity anomaly is revealed beneath the As Sawada volcanic province that extends to a depth of 750 km. However, low velocities are observed between Al Haruj and As Sawada volcanic provinces. In the northwestern part of the study area, especially beneath the Gharyan volcanic province, a high-velocity anomaly is observed in the shallow (depths <80 km) and deep (depths >80 km) lithosphere, while in the southeastern part of the province, the underlying depth range of 100–300 km is dominated by a low-velocity body (Figure 4.11). A high-velocity anomaly covers the entire As Sawada and Gharyan volcanic provinces in the depth slices at 350 and 750 km.

The most prominent features seen on the cross-sections in Figure 4.11 are low- and high-velocity anomaly zones in the depth range of 100–400 km beneath the volcanic provinces. A low-velocity anomaly exists from the surface to a depth of ~200 km beneath the Al Haruj and As Sawada volcanic provinces, while a high-velocity body extends to a depth of approximately 700 km beneath the volcanic provinces.

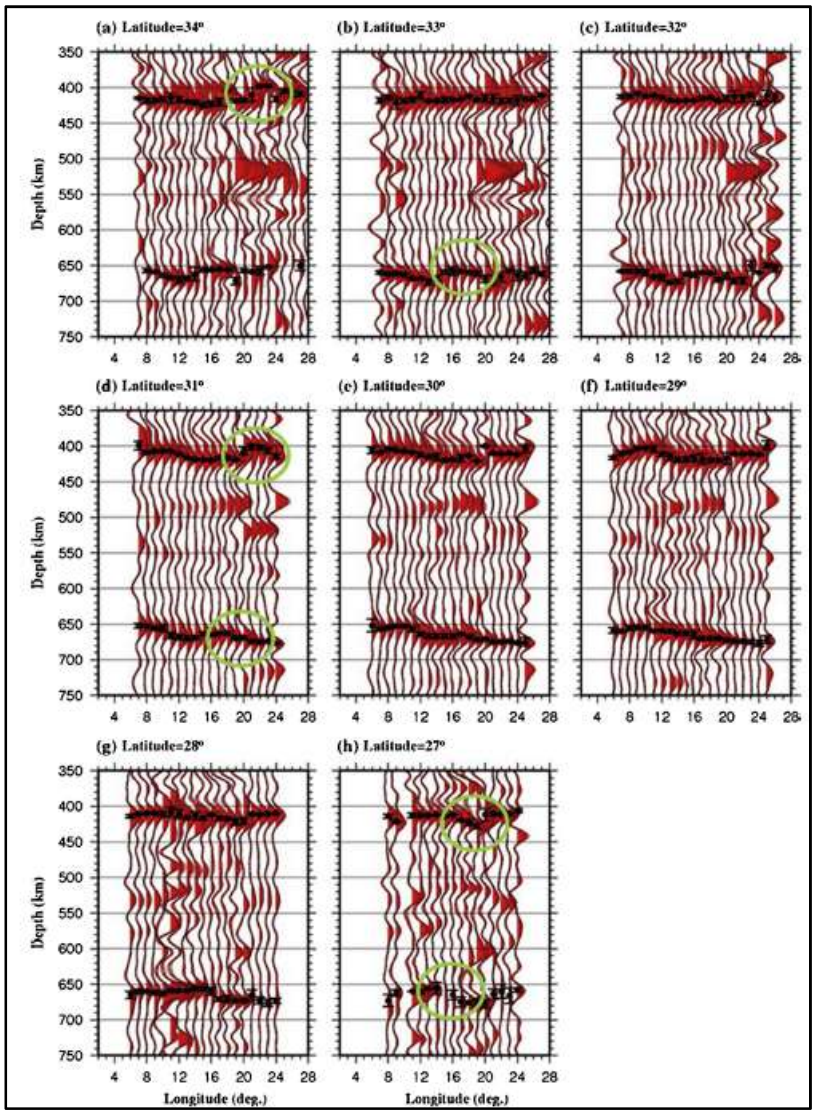

Figure 4.5. Profiles showing the RFs stacked in 2° radius bins at depths from 350 km and 750 km along eight latitudes. Thick gray lines of the stacked RFs show the depth series average; black lines around it represent the mean±2σ; black circles represent the average depths of the d410 and the d660, with error bars showing 2σ of the peak's depth.

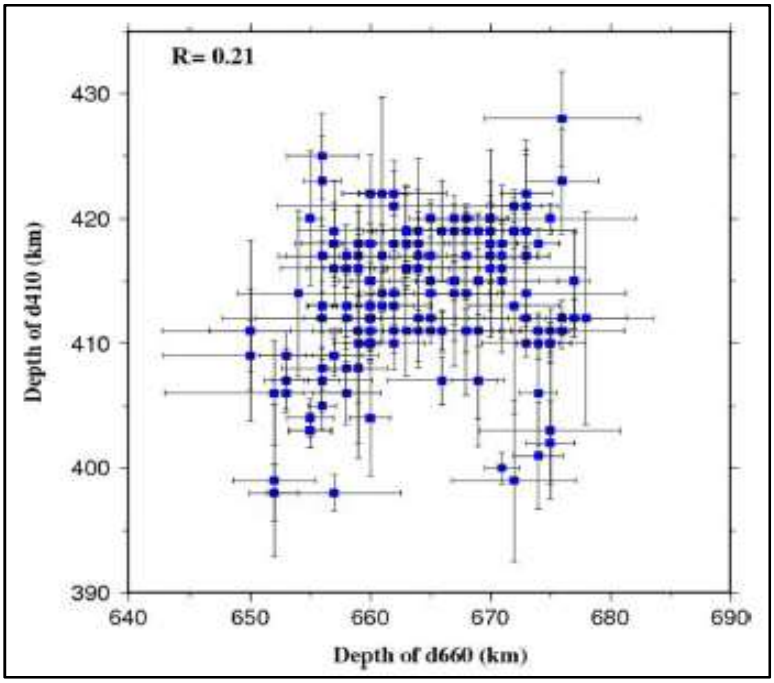

Figure 4.6. Cross correlation plot (R) of the d410 and d660 apparent depths. The error bars represent the (σ) standard deviation.

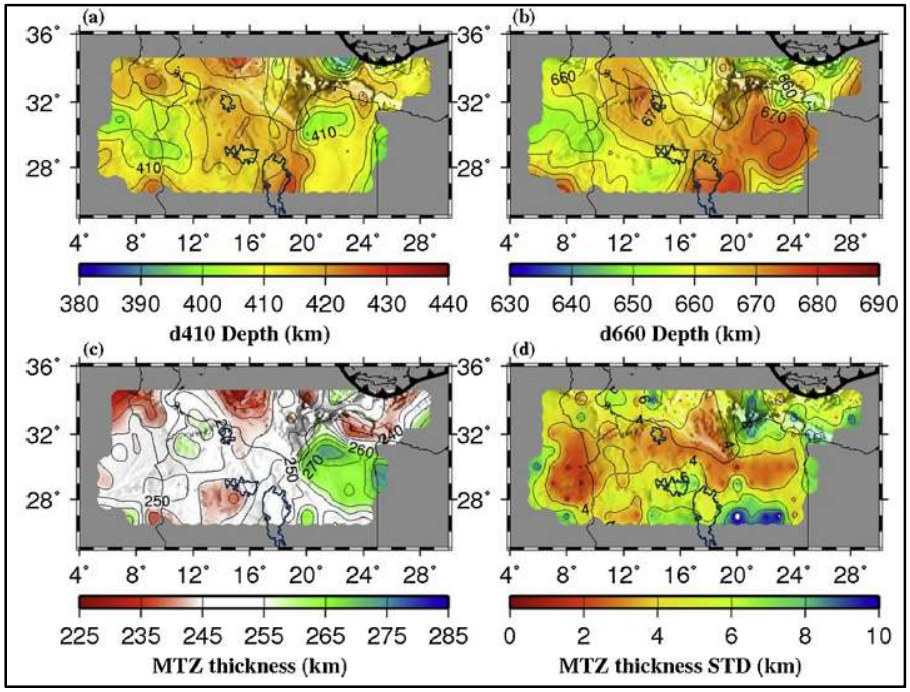

Figure 4.7. (a) Results showing the topography of the d410, (b) same as (a) but for the d660, (c) MTZ thickness, and (d) MTZ standard deviation (STD). Contour lines are spaced at 10 km intervals for in (a)-(c), but at 2 km (d).

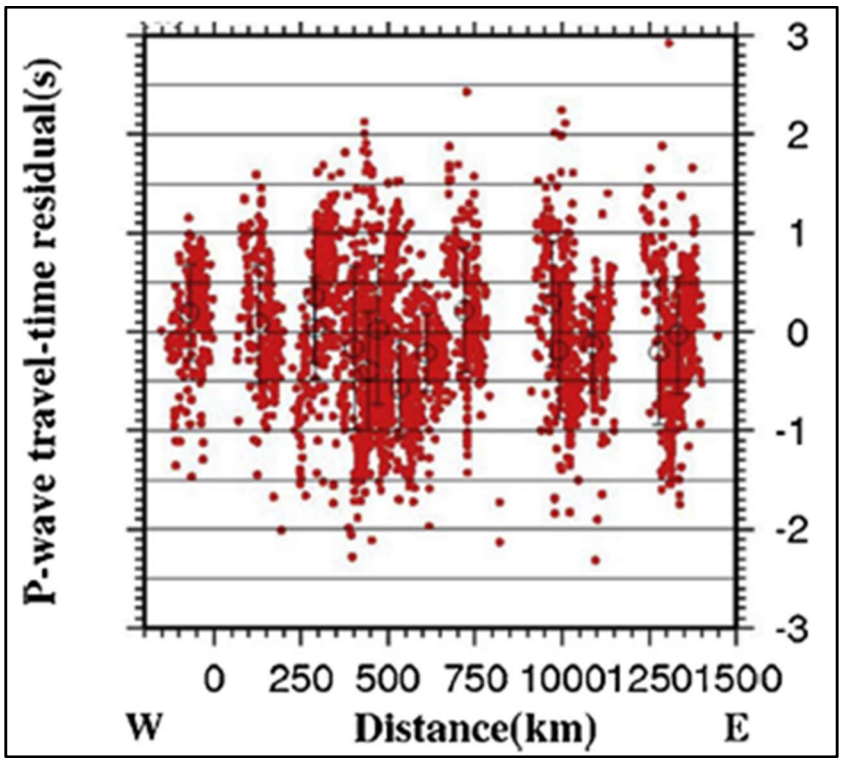

Figure 4.8. Teleseismic P-wave travel time residuals displayed above the ray-piercing points at 100 km depth and projected from west to east of the study area. The red points are individual event values, and circles with error bars are station-averaged values. (For interpretation of the references to color in this figure legend, the reader is referred to the web version of this article).

4.4. SUMMARY

This section covers the results from three methods that we used in this project. Furthermore, applying the sedimentary thickness technique of Yu et al. (2015), as mentioned before, provides the sediment thickness beneath the stations in the study area. The sedimentary thickness ranges from 0.40 km to 3.70 km with κ values ranging from 1.50 to 4.80 (Table 4.2). Results from all methods confirm each other. The results from p wave tomography support the results from receiver function that the surface volcanic materials are mainly coming from deep source. The discussion and interpretation of the results are captured in Section 5.

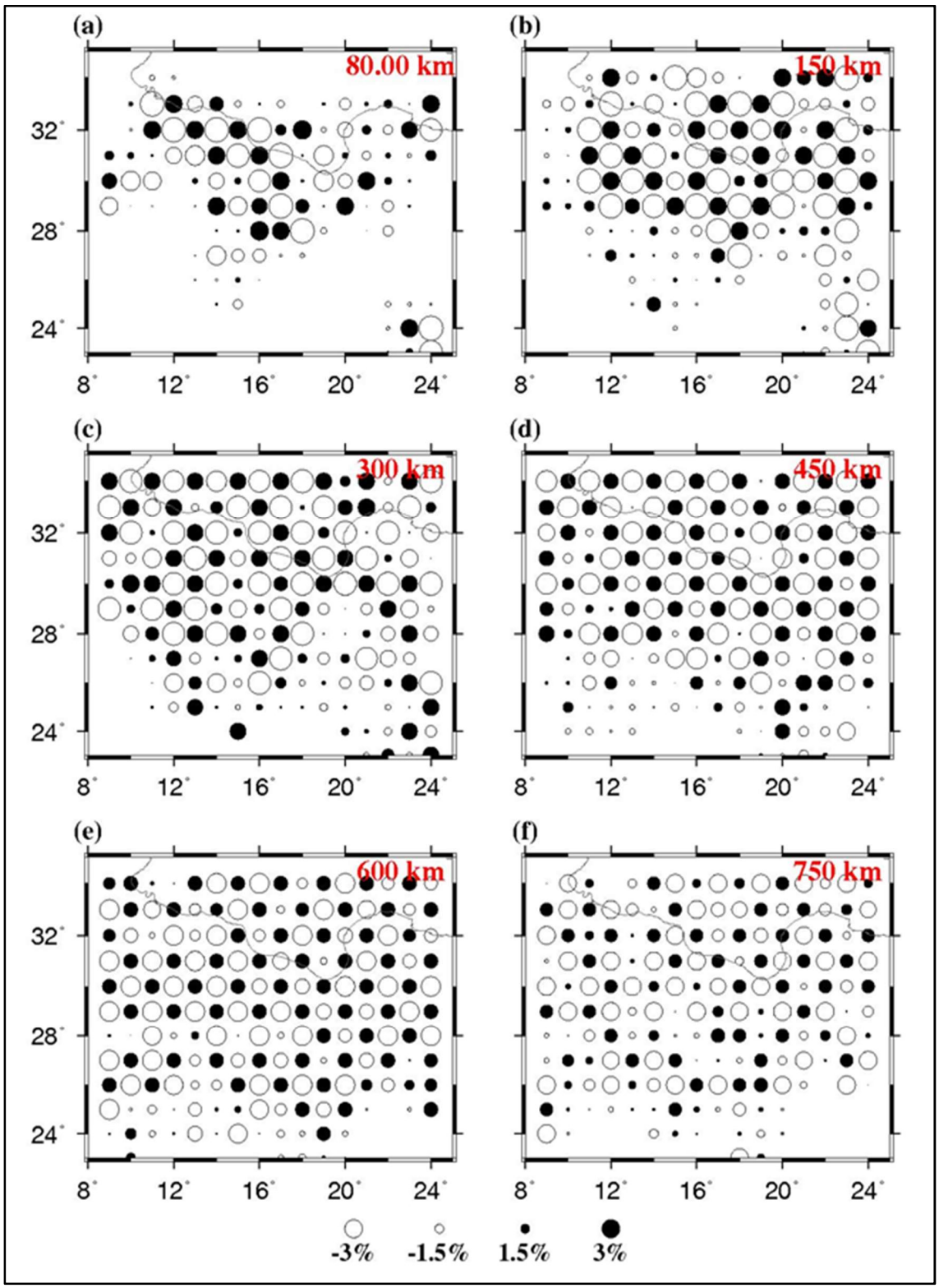

Figure 4.9. Maps view of different depth slices through a checkerboard resolution test beneath the region with a lateral grid interval of 1° and input velocity anomalies of ± 3%. The layer depth is shown in the upper right corner of each map.

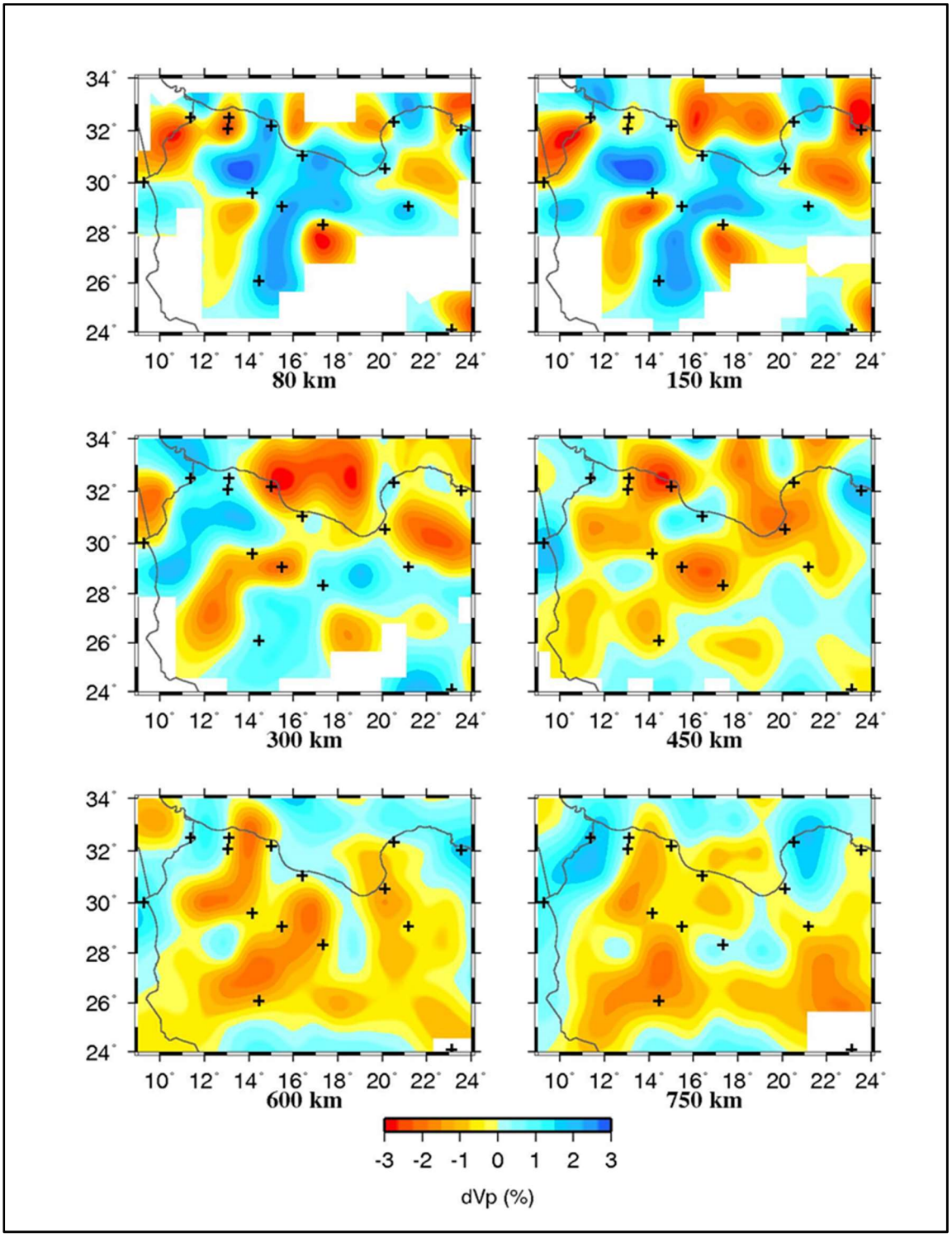

Figure 4.10. Map views of our obtained P-wave tomography results of the study area. The layer depth is shown below each map. Red colors represent low-velocity anomalies, and blues color represent high-velocity anomalies. The velocity perturbation scale (in %) is shown at the bottom. The black crosses show the seismic station locations.

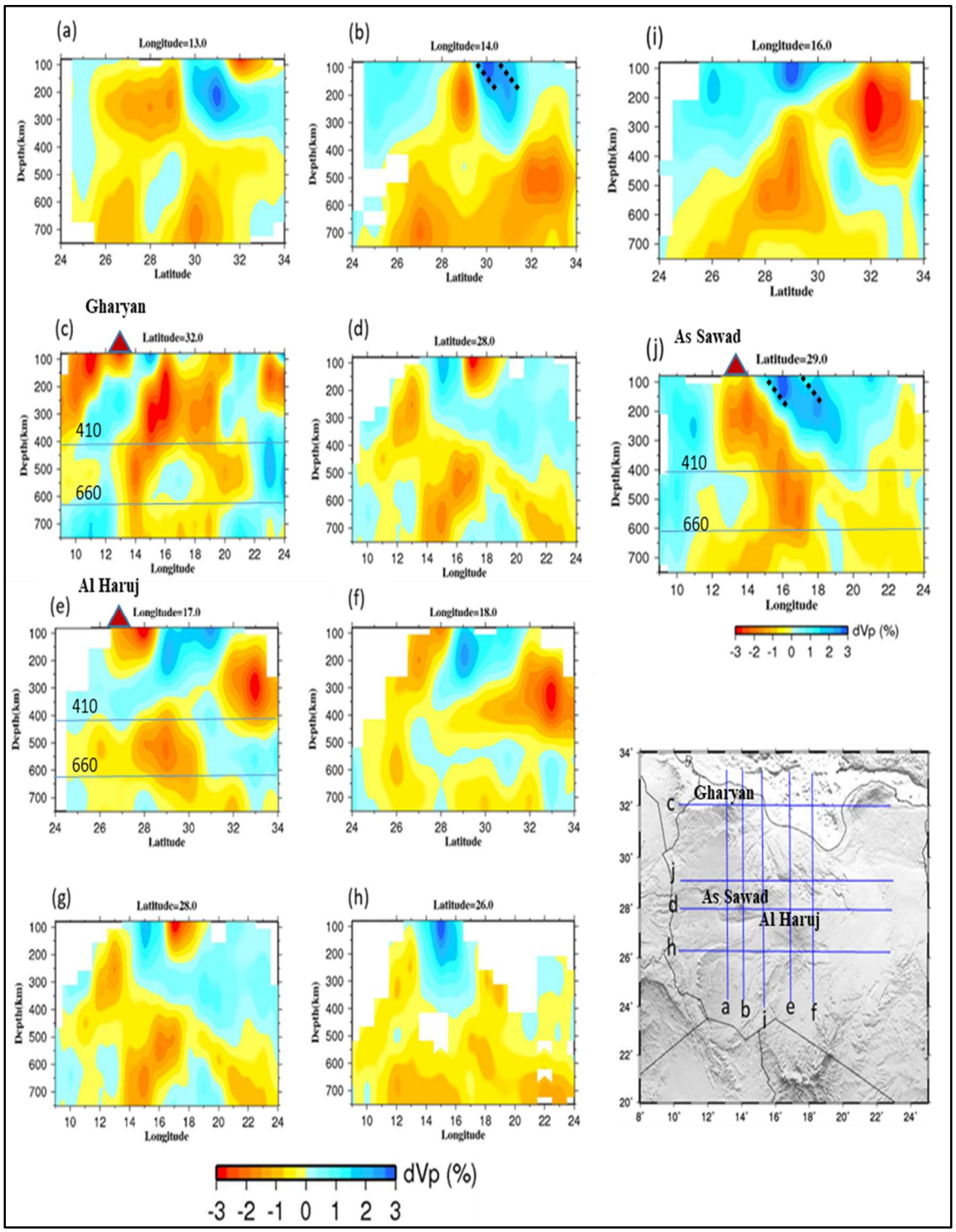

Figure 4.11. Cross-sections of the P-wave tomography results along longitude 13° (a), longitude 14° (b), latitude 32° (c), latitude 28° (d), longitude 17° (e), longitude 18° (f), latitude 28° (g), latitude 26° (h), longitude 16° (i) and latitude 29° (j). The black dashed lines represent the remaining microslab. The blue lines on the topographic map show the locations of the vertical cross-sections.

5. DISCUSSION

5.1. CONSTRAINTS ON THE SEDIMENT THICKNESS

One of the drawbacks of using the receiver function technique is the existence of interferences resulting from sedimentary layers (Ammon, 1991; Langston, 1979; Owens et al., 1984; Zandt & Ammon, 1995; Zhu & Kanamori, 2000). Previously, some geophysical studies were conducted in the study area, especially along the coast, to estimate the thickness of the sedimentary layers using global velocity models (Cowie & Kusznir, 2012; Pasyanos & Nyblade, 2007). According to these previous studies, the thickness of these layers' ranges from 1 to 7 km in the study area (e.g., Abadi et al., 2008). Hassan and Kendall (2014) summarized the geological and basin evolution in Libya, finding that the sediment thickness in the Sirt Basin varies from 1 km to 7 km; in the Murzuk Basin, it exceeds 4 km; in the Ghadamis Basin, it is about 7 km; in the Al Kufrah Basin, it is around 3 km; and in the northeast part of Libya, it varies from 3 km to 4 km.

This study finds that the unconsolidated sediment layers beneath the seismic stations range from 0.40 km to 3.70 km, with κ ranging from 2.20 to 4.80. Anomalously high measurements of κ at some seismic stations might result from the presence of loose sediments, such as at stations ASA, JDB, MSR, and UJL (Table 4.2). Some seismic stations, such as stations TRP and SHF, show low κ values ranging from 2.20 to 3.0, suggesting that the areas beneath these stations have less compact sediments.

Due to the availability of seismic data, and the importance of oil, within the Sirt Basin region, we focus the discussion on this sedimentary basin. The results show that there is a significant change in the unconsolidated sediment layer thickness, ranging from 1.50

km to 2.20 km, the lowest value beneath stations UJL and MSR, and highest value at eastern boundary of the basin. This change may be related to extension within the basin and typeset of rocks. Furthermore, most of the previous studies (Abadi et al., 2008; Hassan & Kendall, 2014) did not consider the κ value of the sedimentary layers of the region. We have shown, as did Yu et al. (2015), that this is an important variable. The κ value in the Sirt Basin ranges from 3.50 to 4.80, which indicates that the sediments differ in their compactness. The technique that we used here did not work in some seismic stations, probably due to strong interfaces inside the sedimentary layer in the basins.

5.2. CRUSTAL COMPOSITION PATTERN OF HEAT FLOW AND PARTIAL MELTING BENEATH CENTRAL LIBYA

The Cenozoic igneous rocks, which are exposed mainly in the central part of the region, comprise a low percentage of the region's surface geology (Suleiman, 1985). Geological studies (Al-Hafdh & El-Shaafi, 2015; Anketell, 1996; Cvetkovi´c et al., 2010; Klitzsch, 1971) suggest that the igneous rocks in these areas originated primarily from the partial melting of asthenospheric mantle materials.

Based on the classification of Holbrook et al. (1992), the crust composition in the study area is variable (Figure 4.1), with small κ values (1.72 to 1.77) occurring beneath stations SRT, UMB, and KFR, indicative of felsic rocks. For other stations, the values range from 1.80 to 1.86 and are indicative of intermediate rocks, except for station JFR, where a value above 1.86 suggests mafic rocks. In addition, Watanabe (1993) interpreted rapid reduction of Vs relative to Vp, the κ value, as being a function of melt percentage, the melt being primarily noticeable for values above 1.86. Reed et al. (2014) inferred that

the high κ (>1.86) beneath the Red Sea rift and adjacent regions indicates widespread partial melting. The observed low values of Vs are interpreted as reflecting present-day thermal effects within the central part of Libya (cf. Begg et al., 2009; Deen et al., 2006).

Overall, the crustal composition in the study area is intermediate to mafic. In the volcanic and coastal areas, κ values are high, especially at stations JFR, TATN, JDB, ASA, and TRP. This indicates that the crustal composition beneath these stations is predominantly mafic. Other κ values suggest that the crustal composition is mainly intermediate. Our observations of velocities obtained from seismic stations at the volcanic provinces (SHF, JFR, and GHR) broadly agree with other geochemical and petrological studies on the composition of crustal materials (e.g., Aboazomet al., 2006; Al-Hafdh & El-Shaafi, 2015; Al-Hafdh & Gafeer, 2015).

As discussed by Abdelsalam et al. (2002) and Lemnifi et al. (2015) a negative of shear wave velocity at depth of 100–175 km reflects the delamination of a cratonic root. This is in agreement with our results, especially from data obtained from stations KFR and UMB, which give values of κ ranging between 1.75 and 1.77, respectively. The κ values are not high enough to indicate partial melt beneath the lower crust or delamination process beneath the Al Kufra and Murzuk Basins. However, these values may indicate that heat flux beneath the base of the lower crust is not high or, alternatively, the values may be an effect of the thickness in this part of Libyan territory.

Heat flow across the Sirt Basin has been shown to be normal to slightly elevated (49–91mWm2) and generally higher in platforms (horsts) than grabens (Figure 4.2) (Nyblade et al., 1996). It has been suggested that the heat flow in the Sirt Basin is too low, particularly compared with that of the Sahara basins (northwestern Africa), to support the

idea of a lithospheric thermal anomaly (Nyblade et al., 1996). Heat flow measurements suggest that the elevated heat flow is primarily concentrated in the western part of the Sirt Basin (77–91 mW m2) in areas close to the Al Haruj and AS Sawda Volcanic Provinces (Nyblade et al., 1996) (Figure 4.2). In addition, maturation depth trends in the western Sirt Basin are higher than in the eastern and central parts, suggestive of elevated paleogeothermal gradients in the late Cenozoic (up to 30°C/km) (Abadi et al., 2008; Gumati & Schamel, 1988). It is thus likely that elevated heat flow in the western Sirt Basin is related to enhanced crustal heat production rather than to thermal alteration of the lithosphere related to rifting of the Sirt Basin (Nyblade et al., 1996). However, a lack of heat flow data prevents a precise evaluation of heat flow in the northwestern part of Africa between Algeria and the Sirt Basin (Figure 4.2). In these regions the heat flow in volcanic areas, such as the western part of the Sirt Basin, are indeed likely to be much higher than central and eastern parts of the Sirt Basin.

The high κ values show velocity ratios suggesting the presence of fluids and melts (Deen et al., 2006; Reed et al., 2014; Watanabe, 1993). The κ values in the volcanic regions throughout Libyan territory are significantly greater than those found in other areas, particularly at the JFR station (AS Sawda Volcanic Province) (1.91) (Figure 3.5). These values are significantly greater than those found in other areas. This suggests the existence of partial melt within the crust beneath the volcanic areas. The modern-age dating for the last volcanic phase at the Al Haruj Volcanic Province, central Libya, indicates ages as young as 2.3 ± 0.8 ka (Nixon et al., 2011), indicating that the magma reservoir beneath this volcanic field is still active (Elshaafi & Gudmundsson, 2017a). In addition, the Al Haruj

and Waw an Namous volcanic fields in central Libya (Figure 3.1) are considered as still potentially volcanically active (Bardintzeff et al., 2012; Siebert & Simkin, 2002).

Isotope data and geochemical signatures for basaltic rocks within the Al Haruj Volcanic Province indicate that fractional crystallization of primitive magma took place at depths of 25–39 km and temperatures of 1215–1360∘C (Nixon et al., 2011). The majority of earthquakes in Libya occur at depths around 30–35 km (Al-Heety, 2013) that suggests that the increased seismogenic thickness in Libya corresponds to a thick lithosphere underlying the region (cf. Craig et al., 2011; Priestley & McKenzie, 2006). The depths of the proposed magma reservoirs and the earthquakes coincide with the depths that our results give for the Moho. The results suggest that the proposed magma reservoirs at the Al Haruj and AS Sawda Volcanic Provinces could be located in the transition zone between the lowermost crust and the upper mantle. Results from other volcanic areas, such as Iceland, suggest that many partially molten magma reservoirs tend to be located at the boundary between the upper mantle and the lower crust (Elshaafi & Gudmundsson, 2017a; Gudmundsson, 1986, 2016; cf. Hermance, 1981; Schmeling, 1985).

Magma reservoirs at the contact between the upper mantle and the lower crust can remain active for millions of years or more and mantle plumes exist for tens of millions of years, particularly when located away from plate boundaries (Courtillot et al., 2003; Elshaafi & Gudmundsson, 2017b; Gudmundsson et al., 2009, 2016) as in the present case. Consequently, the magma reservoirs beneath parts of Libya, particularly the central part (at Al Haruj, Waw an Namous and AS Sawda volcanic fields), are likely to be still active. In which case, mechanical interaction is possible over the same time spans as the magma chamber/reservoir acts to concentrate stress (Andrew & Gudmundsson, 2008; Biggs et al.,

2016; Elshaafi and Gudmundsson, 2017b). The magma reservoirs beneath the Libyan territory would contribute to the generation of zones of tensile and shear stresses within and in-between these volcanic provinces. The concentration of elevated stresses poses a significant earthquakes and volcanic hazard (for more details see Elshaafi & Gudmundsson, 2017b).

5.3. LIBYAN CONTINENTAL INTERIOR AND COASTAL AREA CRUSTAL THICKNESS

The H varies spatially throughout Libya, with the northern central portion having the thinnest crust and the interior having the thickest crust. Most of the seismic stations located along the uplifted areas, such as stations JFR and GHAR (Figure 4.1), suggest H of >32 km. From these thicknesses we deduce that uplift occurred in this area and volcanic activity played a contributing role in the determining H and composition. Results for H and κ represent aspects of crustal formation and evolution as illustrated in Figures 4.1 and 4.2.

The crust beneath the central and northwestern parts of Libya is as much as 5 km thinner than in the southeast and southwest parts. It is widely agreed (e.g., Faccenna et al., 2001; Marone et al., 2003) that the H might relate to the opening of the Paleozoic ocean to the north (Granot, 2016) and the heterogeneity of tectonic processes in the area.

5.4. COMPARING CRUSTAL THICKNESS WITH ELEVATION AND BOUGUER GRAVITY ANOMALIES

The question then arises: is the crust in Libya compensated only by isostasy or instead by mantle dynamics? Numerous studies have discussed the relationship between gravity anomalies and H (e.g., Aiken, 1976; Assumpcáo et al., 2013; Bashir et al., 2011;

Hendricks & Plescia, 1991; Sumner, 1989). We tested correlations between H, elevation, and Bouguer gravity anomalies (Figure 4.1) and found that they are correlated.

The studies by Egorkin (1998) and Zandt and Ammon (1995) indicate that geological processes of different ages can be distinguished by their relation of H and κ values. But our results do not support these suggestions since we find a weak correlation between H and κ values with $r = -0.02$ in the region (Figure 4.3e).

A number of previous studies (e.g., Boschi et al., 2010; Flament, 2014; Forte et al., 1993, 2010; Gurnis, 1993; Husson et al., 2014; Lithgow-Bertelloni & Silver, 1998; Liu & Gurnis, 2010; Moucha & Forte, 2011; Moucha et al., 2009) propose that surface elevations of >1 km are mainly controlled by mantle convention. Long-wavelength dynamic topography can account for topography smaller than 500 m, which supports the idea that surface topography can be created by mantle convection, whereas short wavelengths can be related to local thermal settings (Hoggard et al., 2016).

In Libya, surface elevations are <500 m except in some volcanic provinces where the surface elevation reaches above 850 m. We suggest that these elevation differences at volcanic areas are supported by mantle convection, which supports the findings of several previous studies (e.g., Hoggard et al., 2016). According to the correlation between surface elevation and H, we propose that the crust is isostatically compensated. It has been suggested that the crust near/within adjacent areas to the Eurasia-Africa plate boundary region are in close-to-isostatic equilibrium (Marone et al., 2003).

The results show that the crust is 30–36 km thick throughout the high elevation parts of the interior of Libya but much thinner, 24–28 km, under the lower topography parts along the coastal area, except in the northwest at the Gharyan Volcanic Province.

The available seismic data are still limited for explore the detailed relationships between elevation, crustal thickness, and the Bouguer anomalies. However, data from this analysis indicate a crustal thickness variation that is in agreement with studies by Assumpcáo et al. (2013), Oliveira and Medeiros (2012), and Van Der Meijde et al. (2013), who estimated the H using modeling gravimetric anomalies. The results thus indicate that the Moho depth might constrain the topography of Libya, as suggested in Brazil region (e.g., Assumpcáo et al., 2013; Feng et al., 2007; Lloyd et al., 2010).

The correlations in Figure 4.3 suggest an isostatically compensated crust: higher elevations correspond to lower Bouguer anomalies and thicker crust. Using the Airy model to crudely calculate the density of the crust beneath the study area, we find it to be approximately 3,140 kg/m3, which is above the average found using typical values of crustal density (2,850 kg/m3 to 2,880 kg/m3) (e.g., Darbyshire et al., 2000; Woollard, 1959) and lower than densities derived from Makris and Vees (1977), Makris and Stobbe (1984), and Makris and Yegorova (2006), which are 3,300 kg/m3. Therefore, we propose that the crust beneath Libya is old and dense, possibly having been formed during the Precambrian to Early Paleozoic age, which agree with the finding by Granot (2016) and Speranza et al. (2012) beneath the eastern Mediterranean Sea. Meanwhile, results of surface wave modeling by Fishwick (2010), who observed the thinner lithosphere beneath central Libya and delamination of cratonic roots beneath Sahara metacraton (Abdelsalam et al., 2011), tend to support the idea that the area is under isostatic equilibrium.

As such, the thinner lithosphere can lead to the rise of the asthenosphere and promote isostatic equilibrium, which leads to local mountain building. This follows because although volcanic eruptions during the late Cenozoic period supplied mafic

magmas to the underlying crust in some areas, hence the idea of having a dense crust suggests a poor correlation between Bouguer gravity anomalies and κ ratios, with r of 0.03 (Figure 4.3d) and inverse correlation between topography and Bouguer gravity anomalies (Figure 4.3b). However, the crustal thickness shows a good reverse relation with Bouguer gravity anomalies, which supports the assumption of an older origin for the overall denser crust.

Crustal thickness has been shown to vary significantly in the East Saharan Shield area depending on the models used (e.g., Bassin et al., 2000; Pasyanos & Nyblade, 2007). The Pasyanos and Nyblade (2007) velocity model gives H ranging from 25 to 35 km, while CRUST2.0 (Bassin et al., 2000) indicates crustal ranging from 35 km to 45 km. Results from this study agree closely with the more recent of the two studies yielding an overall denser crust, since such a crust would also have higher velocities. Crustal uplifts are generally interpreted as hot spot swells because association with intraplate volcanism and large gravity anomalies (Pirajno, 2004). However, the spatial distributions of Libya's volcanism have also been related to a warm upwelling asthenospheric mantle associated with a thinner lithosphere that promotes magma migration through metasomatized lithospheric channels (Ball et al., 2016; Elshaafi & Gudmundsson, 2017a; Nixon et al., 2011). Furthermore, a low-density anomaly sits beneath the lithospheric plate and Libya's volcanic provinces are distinguished by a series of long-wavelength topographic swells (Ball et al., 2016).

The major volcanic fields in Libyan territory are greatly correlated to the current elevated basement areas. The basement highs seem to reflect some form of subcrustal arching rather than magmatic intraplate accumulation as inferred from isotope geochemical

data that indicate that the magmas lack signals of crustal contamination and, hence, most likely magma propagated directly from deep-seated magma reservoirs at the crust-mantle boundary (Elshaafi & Gudmundsson, 2017a; Stuart et al., 2014). There are no large igneous bodies such as extensive sills observed in seismic lines in the western part of the Sirt Basin (e.g., Abdunaser & McCaffrey, 2015). Hence, the lack of large plutonic bodies or extinct shallow magma chambers beneath the Earth's crust may be one reason for the low Bouguer anomaly in volcanic areas as observed in this study. It is generally accepted that a hot upwelling mantle induces dynamic uplift (Courtillot et al., 2003; Pirajno, 2004) where the impact of a mantle plume onto the base of the lithosphere results in doming of the crust.

The dynamic topography is quite difficult to determine in the continents, particularly in Africa, due to the density structure of the lithosphere, which is still unknown and poorly documented (cf. Ball et al., 2016). Further geophysical studies such as heat flowdata, denser broadband seismic coverage, and geothermal data should be addressed in the future in order to obtain better constraints on the deep structure and density of the lithosphere beneath this important region.

5.5. SPATIAL VARIATION OF ANOMALOUS MTZ THICKNESSES AND TEMPERATURES

Here, our discussion will mainly focus in the area where the number of the RFs per station is high (above 105, see Figure 3.6). In the following section we highlight several key features of the MTZ from the receiver function analysis. The MTZ is of constant thickness in the west of the studied region, thins by 10 km in the central part, and thickens by about 20 km beneath the northeastern part of Libya (Figure 4.7c). We infer that the location of the thinner MTZ (Figure 4.7c) is spatially related to the location of Quaternary

volcanism, suggesting that there is a deep source of upwelling materials. To infer temperature changes the d410 Clapeyron slope of 2.9 MPa/K (Bina and Helffrich, 1994), and the d660 Clapeyron slope of -2.1 MPa/K (Fei et al., 2004) are adopted. Therefore, considering that our results show a standard variation of the MTZ thickness of 14 km, this is equivalent to normal thermal variations of ± 76° K. The change in MTZ thickness to 20 km thinner-than-average as controlled by deepening d410 corresponds to an excess temperature of 242° K centered in the central and northwestern part of Libya, implying higher temperatures in the transition zone beneath central Libya.

Mohamed et al. (2014) adapted several different models that take account of velocity, thermal, and water content anomalies in order to explain the variations in thickness of the MTZ beneath the Afro-Arabian Dome. Those models relate the change in MTZ discontinuity depths to the effect of olivine- and garnet-dominated phase changes, and MTZ hydration. The variation in thickness of the MTZ in the area of investigation can be most appropriately fitted to two of the proposed models of Mohamed et al. (2014). The first model explains that the thinnest part of the MTZ occurs because Libya's Quaternary volcanism is underlain by low seismic velocities in the upper and lower mantle. In the first model, the main depression occurs in the d410, with uplift in the d660, which corresponds to the observed values between the longitudes from 14° to 20° in the central part of this region. This agrees with the findings of Fishwich (2010) who found that the lithosphere is about 90 km thinner beneath this area. Given the fact that the area with the thinned MTZ has a thinner lithosphere, this model indicates that the upwelling material probably originated from the lower mantle. This agrees with a proposed heat source originating in the lower mantle that drives Cenozoic volcanism in northwest Africa (e.g., Hoggar)

(Courtillot et al., 2003). Courtillot et al. (2003) suggest that hotspots may derive from distinct mantle boundary layers. Thus, our findings propose that the origin of Libya's volcanism may come from higher-than-normal temperatures in the mantle transition zone (MTZ).

Apparently depressed MTZ discontinuities can also be explained through hydration mechanisms (Reed et al., 2016). The presence of water assists both to thicken the MTZ through an immediate uplift and depression of the d410 and d660 (Figure 4.7), respectively, and to decrease the seismic velocities in the MTZ. The occurrence of a strong, continuous 520 km discontinuity and also a negative arrival immediately above the d410 beneath Afar is expressive of hydrous upwelling across the MTZ (Thompson, 1992; Thompson et al., 2015; Reed et al., 2016). In principle, the thickening of the MTZ observed in the eastern part of the region can also be caused by the presence of water. Though, some studies proposed that under normal pressure temperature conditions (Yu et al., 2017), water might promote a low-velocity anomaly of the phase transition associated with the d410. This process would cause anomalously low stacking amplitudes (Wood, 1995). The velocity anomalies of about 0.5 s observed from picking P-wave travel-time velocities, fit well with what we observe at the volcanic provinces in the study area, especially at the As Sawda volcanic province (Figure 4.8). The profile from east to west of the study area observed through P-wave travel-time velocities shows a low average velocity in the central part of Libya where most of the volcanic provinces occur.

5.6. SLAB SEGMENTS IN THE MTZ

Water has previously been used to explain low-velocity anomalies associated with phase transitions at the d410 (Tauzin et al., 2010). Thicker portions of the MTZ in the northeastern part of Libya are cause partly by hydrated minerals, resulting in a general increase in water content. This hydration could be associated with African-Eurasian closure and the subduction of the Tethys Ocean plate (Stern, 1994). The thickening of the MTZ observed in other areas can also be caused by the presence of water (e.g., Litasov et al., 2005; Yu et al., 2017).

A positive anomaly at the depths of 400–600 km beneath the northeastern part of Libya likely reflect part of the past subduction of the Thethys slab (Simmons et al., 2012) (Figure 4.7). Here, we suggest that the thicker MTZ is related to 170°K colder-than-normal temperatures, since cooler temperatures are related to positive velocity anomalies. Higher water contents also cause anomalously low stacking amplitudes or the presence of negative receiver function signals at the upper portion of the d410 discontinuity (Bercovici and Karato, 2003). The velocity anomalies found in this study match this observation.

Generally, tomographic studies using the global S-wave model by Grand (2002) and P-wave model by Piromallo and Morelli (2003) indicate the positive velocity anomaly observed in the eastern part of the study area. Also, our analysis of the P-wave travel-time residuals indicate a slightly higher average velocity (Figure 4.8). Given the fact that the northeastern part of Libya has a thickened MTZ, this is likely a reflection of past subduction and African-Eurasian collision since the late Mesozoic, and is also in agreement with the findings and interpretation of Van der Meijde et al. (2005) and Bonatto et al. (2015) in neighboring areas.

5.7. P-WAVE TOMOGRAPHY

Global seismic tomography has been used to image various cratons (the West African, Congo, and Kalahari Cratons), otherwise known as blocks, and the roots of the cratons, which extend down to a depth of 250 km (e.g., Deen et al., 2006; Begg et al., 2009; Abdelsalam et al., 2011). Most of the cratons are separated by sutures (e.g., Stern, 1994; Abdelsalam et al., 2011). Some of these suture lines are interpreted as the collision zone between the Saharan Metacraton and the Tuareg Shield to the west of the study area (Liégeois et al., 1994, 2003; Henry et al., 2009). Abdelsalam et al. (2011) used the Grand (2002) model to generate S-wave velocity anomaly images of the Saharan Metacraton lithospheric column at different depths of 0–100 km, 100–175 km, and 175–250 km and showed that the craton has a positive S-wave velocity anomaly extending down to a depth of 250 km, reflecting the presence of a well-developed cratonic root. When we compare our imaged low-velocity anomalies with the Cenozoic volcanic provinces, a relation is apparent down to great depth (~>500 km).

A previous work (e.g., King and Anderson, 1998) suggested that the upwelling volcanic materials beneath the study region may be due to an edge effect at an underlying lithospheric step. However, other studies such as Liégeois et al. (2003) suggested that these materials may result from the reactivation of preexisting shear zones and fractures during the late Neoproterozoic. Using a global tomography model, Liegeois et al. [2005] revealed that the shallow mantle is warmer with melt fractions at depths between 100 km and 150 km but did not show the existence of a mantle plume. A recent study by Lemnifi et al. (2019) that used teleseismic receiver functions found that the volcanism in Libya originates from higher temperatures in the mantle transition zone. Our present tomographic model

supports the study by Lemnifi et al. (2019) but shows more features in greater detail than previous models. There are obvious low- and high-velocity anomalies. For example, Figure 4.11 shows the results of tomography beneath the As Sawada volcanic province, suggesting that the low-velocity anomalies therein are attributable to microslabs representing a series of microcontinental collisions that possibly terminated with the collision of the Saldania microcontinent. The observed remaining slabs are as stiff as the lithosphere and extend to a depth of ~300 km with a dip of ~ 40° (Figure 4.11). However, the high-velocity anomalies are caused by hot materials extending down to ~ 400 km depth.

It is generally accepted that microcontinental collisions during the Neoproterozoic Pan-African orogeny (Stoeser and Camp, 1985; Stern, 1994; Lemnifi et al., 2015) in the study region played an important role in the formation and evolution of North Central Africa. Therefore, the region is characterized by lithosphere with variable thickness owing to the extensive Pan-African orogenic suturing of blocks (Stern, 1994; Lemnifi et al., 2017). The Pan-African orogeny, which involved various cratons, including the West African Craton and the Saharan Metacraton, represents the amalgamation of a series of orogenic events. We suggest that the microslab beneath the Saharan Metacraton subducted eastward during microcontinental accretion. The slab in this case did not subduct down into the deep mantle. This may explain why the volcanic provinces are limited in this region. In this case, we propose that the remaining microslabs reflect part of the collision of the Saharan Metacraton with the Tethys Ocean. This can be clearly seen from the elevation of the northwestern part of the study area, which encompasses the boundaries between the Sirt Basin, Ghadamis Basin, and Murzuk Basin (Figure 3.1). The mechanism of this collision may have been increased localized stretching in the Sirt Basin. This stretching

increased abruptly between ~50 and ~48 Ma (e.g., Capitanio et al., 2009). During this period, volcanism in Libya began and continued to develop into the late Pleistocene (e.g., Nixon et al., 2011). Consequently, we suggest that the local structure in the study region played a major role in forming the structure of the Sirt Basin and that small-scale convection and the upwelling of materials may have been responsible for the observed surface tectonic features, especially in the Sirt Basin (Figures 3.1 and 5.1).

Using the receiver function technique, Lemnifi et al. (2017) suggested that the magma reservoirs beneath the study region are still active and that these reservoirs generated the zones of tensile and shear stresses within and between these volcanic provinces. Consequently, our model supports the study by Lemnifi et al. (2017); however, more detailed features are observed in this study.

Moreover, the tomography results suggest that the lithosphere beneath the region may extend to an estimated maximum depth of 200 km with a more variable thickness than that obtained from surface wave tomography, which estimated a lithospheric thickness of approximately 90–100 km (Fishwick, 2010). It is likely that this thinner lithosphere was observed beneath the volcanic provinces due to thermal erosion and the presence of partially molten magma reservoirs. This hypothesis is supported by slow S-wave velocities in comparison to the P-wave velocities (Lemnifi et al., 2017; 2019).

Our results provide the most convincing evidence that the microslabs and relative movements of rigid cratonic blocks in the region are the most important sources of earthquakes that occurred during the past century (Al-Heety, 2013). The localized low-velocity anomaly observed in the upper asthenosphere (Figures 20 and 21) is most likely caused by a down going slab; however, we suggest that the speed of subduction of these

microslabs is almost zero, which may be due to their location far from the major plate boundaries to the north of the study area, such as the Hellenic and Calabrian subduction zones. The results from this teleseismic P-wave tomography study beneath the study region in combination with those from recent anisotropy investigations (Miller et al., 2013; Lemnifi et al., 2015) indicate that most of the regional geodynamic processes are associated with the varying lithospheric thickness due to microsubduction, partial melting, and local mantle flow deflection.

Using the first P-to-S receiver function investigation of the mantle transition zone in the study region, the previous study by Lemnifi et al. (2019) found that the thicker mantle transition zone to the east and southeast was related to ancient subducted slabs caused by the convergence between Africa and Europe. In the southeastern part of the study, the Al Awaynat volcanic province, which was initially created during the Precambrian, was mostly built during the Proterozoic (Abdelsalam et al., 2002). In this area, the geodynamic processes and source of volcanic materials are debated. Due to the limited number of seismic stations to the east of the study area and on the basis of the new findings from this study, we suggest that additional seismic stations are needed for further detailed geophysical studies to obtain better constraints on the deep Earth structure.

5.8. SUMMARY

The results of this study, when using three methods was successfully confirmed eacth other. The results from the RFs and p wave tomography suggested that the source of volcanic materials on the surface came from deep sources. The technique that we used to determine the sedimentary thickness did not work in some seismic stations, probably due

to strong interfaces inside the sedimentary layer in the basins. Further studies are certainly still needed in the future in order to obtain better constraints on the ore deposits in Libya, and we hope that these results encourage further research into the origin of Libya's volcanism.

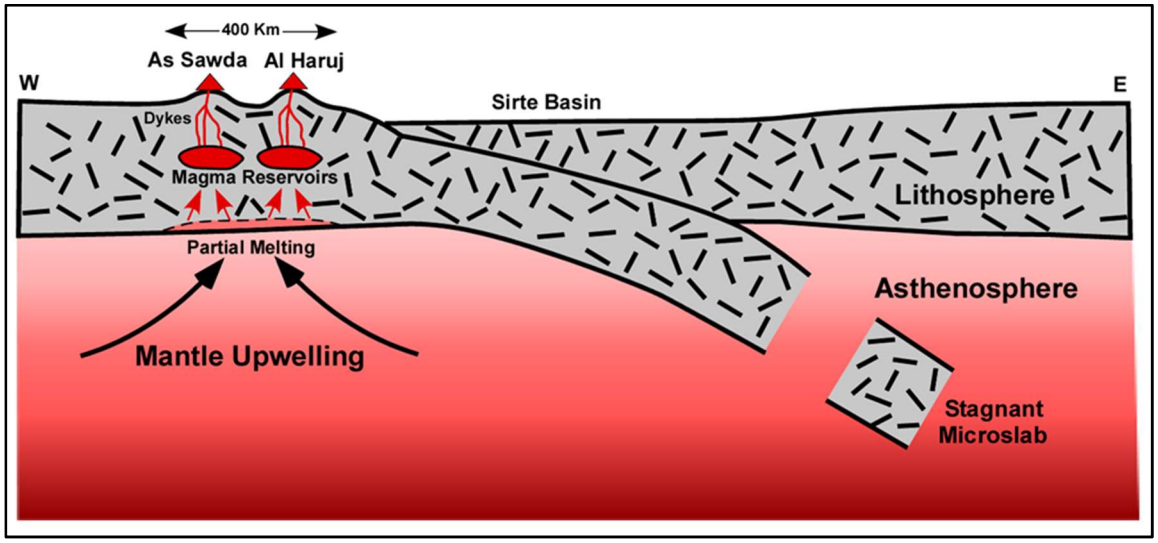

Figure 5.1. Schematic explanation of the proposed model for the study area from west to east.

6. CONCLUSIONS, PHD CONTRIBUTIONS AND RECOMMENDATIONS FOR FUTURE WORK

6.1. SUMMARY AND CONCLUSIONS

This is the first study to present crustal thickness measurements of Libya based on seismic data obtained from several seismic stations. The H ranges from 24 km to 36 km, specifically, the range in H is from a maximum of 30–36 km beneath the southern part of Libya to a minimum of 24–28 km along its coast. A significant correlation was observed between H, elevation, and Bouguer gravity, suggesting that the crust is isostatically compensated. However, there is a weak correlation between H and κ values. The main volcanic provinces in Libya mostly coincide with the current elevated areas and low Bouguer gravity anomalies, which indicates that the volcanic regions have been subject to subcrustal arching rather than magmatic under plating. This study showed that seismic stations close to the volcanic provinces detected more mafic crustal compositions because of basaltic magma underlying the crust, possibly forming partially molten magma reservoirs. The value at station JRF is 1.91, suggesting the existence of partial melt at the crust-mantle boundary beneath the associated volcanic field. Modern age dating by Nixon et al. (2011) at the Al Haruj Volcanic Province indicates that the volcanism in this region continued until recent times. If magma resides beneath central Libya in reservoirs, then the volcanic systems may pose significant earthquake and volcanic risks. Many previous earthquakes in Libya during the past century have depths between 30 km and 35 km (Al-Heety, 2013). Fractional crystallization of the primitive magmas at the Al Haruj Volcanic Province is also thought to have occurred at similar depths, namely, in reservoirs at depths of 25–39 km (Nixon et al., 2011). The inferred depths of the reservoirs match this study's

findings of the Moho depth variations. This study also finds that sediment thicknesses beneath the seismic stations range from 0.4 km to 3.7 km, with variable values of κ. Using an Airy isostasy model suggests that the density of the crust beneath the study area is 3,140 kg/m^3. This research study suggests that the crust in this region is denser than normal and therefore likely to be older than Phanerozoic time.

This is the first pioneering study to investigate the d410 and d660 depth variations, and mantle transition zone thicknesses beneath Libya using receiver functions. This study marks an important step in the quest to understand tectonic processes in the northern portion of the African continent. The results show that the d410 was depressed, while the d660 was uplifted within the Miocene – Quaternary volcanic areas and an anomalously thin MTZ in the central portion of Libya suggests that the Miocene – Holocene volcanoes heat source originated within the lower mantle. Hence, the study findings propose that the origin of Libya's volcanism may derive from higher temperatures in the mantle transition zone (MTZ), deeper than 410 km, beneath this region. This conclusion is in good agreement with the hypothesis of a mantle plume where Miocene-Holocene volcanic activity throughout Libya was/is directly related to an uprising mantle plume rather than related solely to extension of the lithosphere. Conversely, the MTZ is thickened in the north-east to approximately 270 km, indicating a colder-than-average MTZ. Thus, this study infers that this thicker and colder MTZ is most likely associated with slab stagnation.

In conclusion, this study provides new insights using P-wave velocity tomography to further enhance the details of the tomographic images in a local-scale model. This study provided a velocity model for the vertical structure that has a better resolution than that of

previous models. The tomography results in the region show different observables, which are governed by different temperatures in the crust, lithospheric mantle and asthenosphere.

The main finding of this study is that the low-velocity anomalies probably represent deep and hot materials that are visible under the volcanic provinces in North Central Africa and extend to depths between 350to 550 km. The observation of high-velocity anomalies, which indicate that microslabs still exist beneath the region, suggests that North Central Africa was mostly affected by microcontinental accretion during the Pan-African orogeny.

6.2. PHD RESEARCH CONTRIBUTIONS

Essentially the formation of ore and mineral deposits is governed by the flow of hot fluids through faults and fractures as known by permeability. It is well recognized that the geometrical arrangement of crustal structures influences the deposition of hydrothermal minerals [Hildenbrand et al., 2000]. Even as the relationship between ore formation and lithospheric thickness is still poorly constrained and unknown, therefore this study suggests signs of potential mineralization in the Libyan region.

The region is broadly categorized into an area hosting a thinner-than-normal mantle transition zone (and so thicker lithosphere) and an area hosting a thicker-than-normal mantle transition zone (and so a thinner lithosphere). The thinner MTZ is characterized by increased melt production which is associated with numerous shear and extensional fractures such as ring-faults and dykes and so also presumably significant hydrothermal circulation. The location of epithermal and porphyry precious and base metal deposits may

then form in such environments, whereas they are less likely to form in the colder stagnant slab region.

The results of this research study shed lights on the subsurface and surface economic minerals, sediment and crustal layering, deformation history of the lithosphere and the thermodynamic processing beneath Libya. In addition, it provides valuable information about the source of economic materials and future mine activities in the region.

The key contributions from this research are outlined below:

1. The value at some seismic stations show that the Vp/Vs ratio is high, suggesting the existence of partial melt beneath volcanic provinces.
2. This study also finds that sediment thicknesses beneath the seismic stations range from 0.4 km to 3.7 km, with variable values of Vp/Vs ratio.
3. The velocity anomaly shows a low average velocity in the central part of Libya where most of the volcanic provinces have formed.

6.3. RECOMMENDATIONS FOR FUTURE WORK

This research has made significant strides towards improving geophysical methods to discover ore deposits, further work is still necessary to achieve a complete certainty of ore deposits existence. There is a need for further study using different methods such as remote seining, because one of the drawbacks for example of using the receiver function technique is the low vertical resolution in shallow depth. Thus, this study concludes that to use the remote sensing is essential to complete the whole image.

APPENDIX A.

RECEIVER FUNCTION

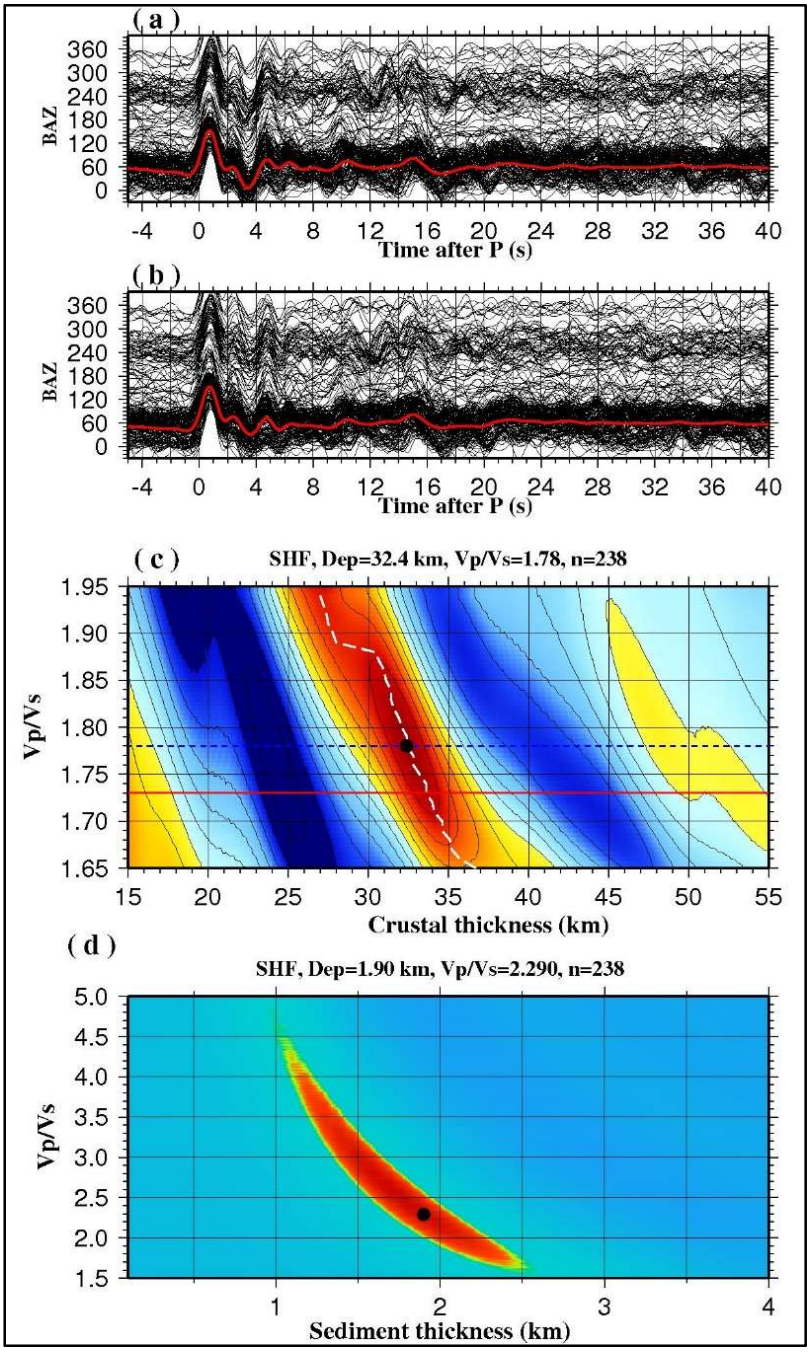

Figure A1. An H-κ plot for station SHF before and after the sediment correction. (a) Radial RFs plotted against the back-azimuth, with a simple time-series stack (red) before sediment move-out, (b) same as (a) but after resource-removal filtering, (c) H-κ grid plot for normalized stacking amplitude after the sediment move-out correction. The red line represents stacking amplitudes for κ = 1.73 (which is the mean κ for crustal rocks), the dash blue line represents stacking amplitudes for the optimal κ and stacking amplitude along the dashed white. The optimal H and κ pair is indicated by a black dot, (d) same as (c) but for the H-κ grid plot for the stacking amplitude to determine sediment thickness.

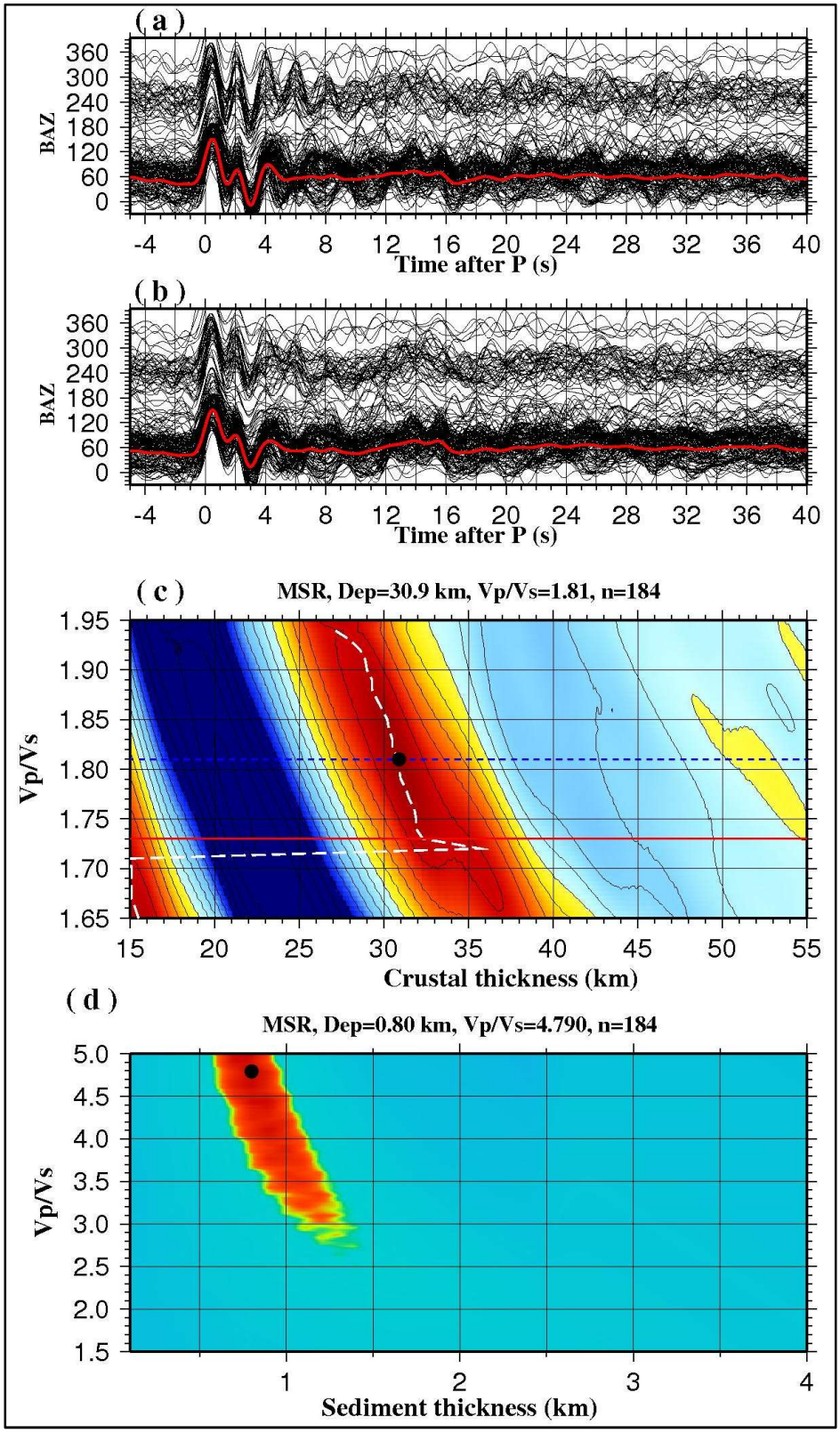

Figure A2. Same as Figure A1, but for station MSR.

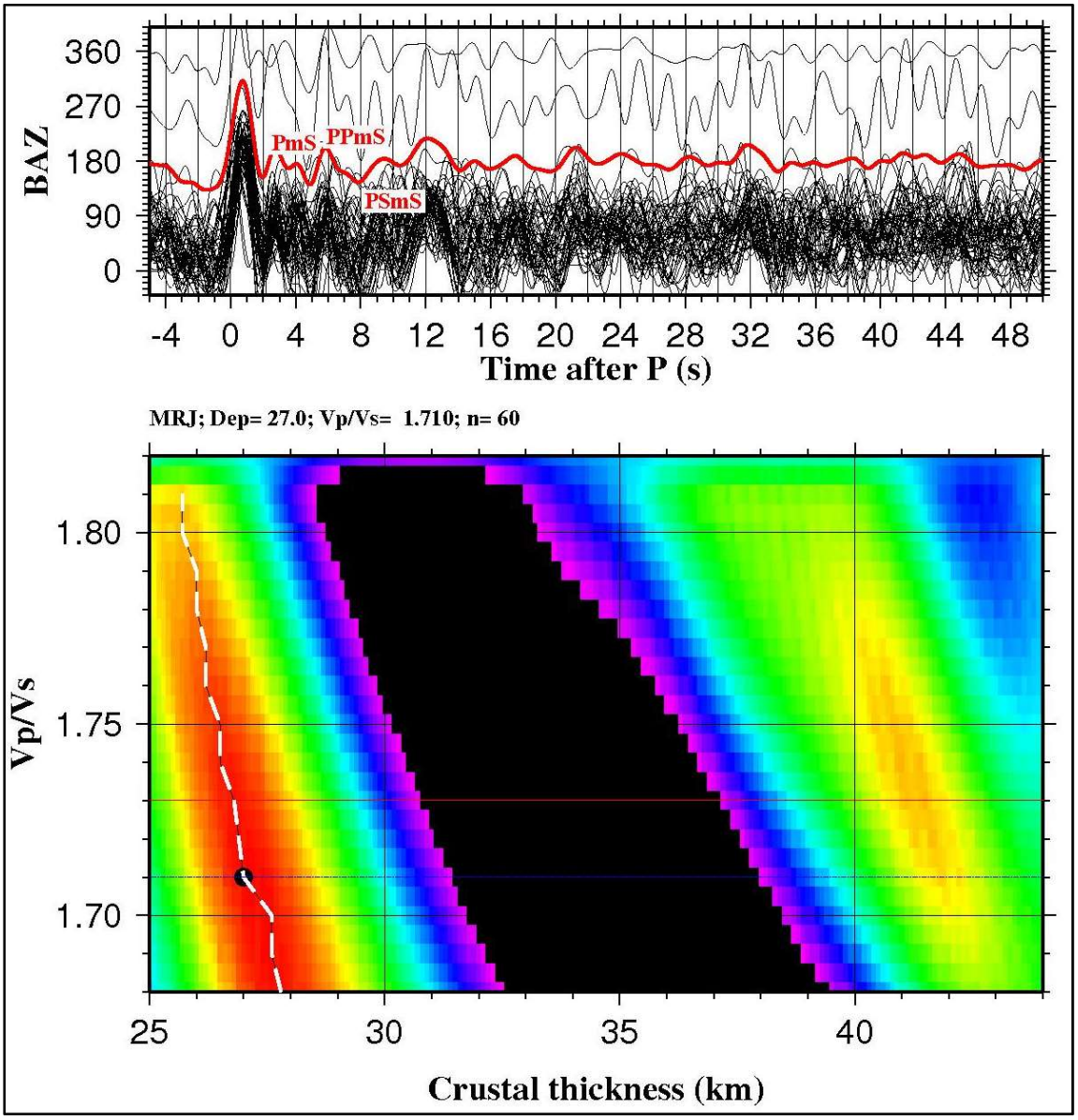

Figure A3. Application of H-κ stacking for MRJ station, located in the Northeastern part of the region. (Top) Radial RFs plotted against the back-azimuth. (Bottom) Normalized amplitude grid with optimal H and κ pair indicated by a black dot.

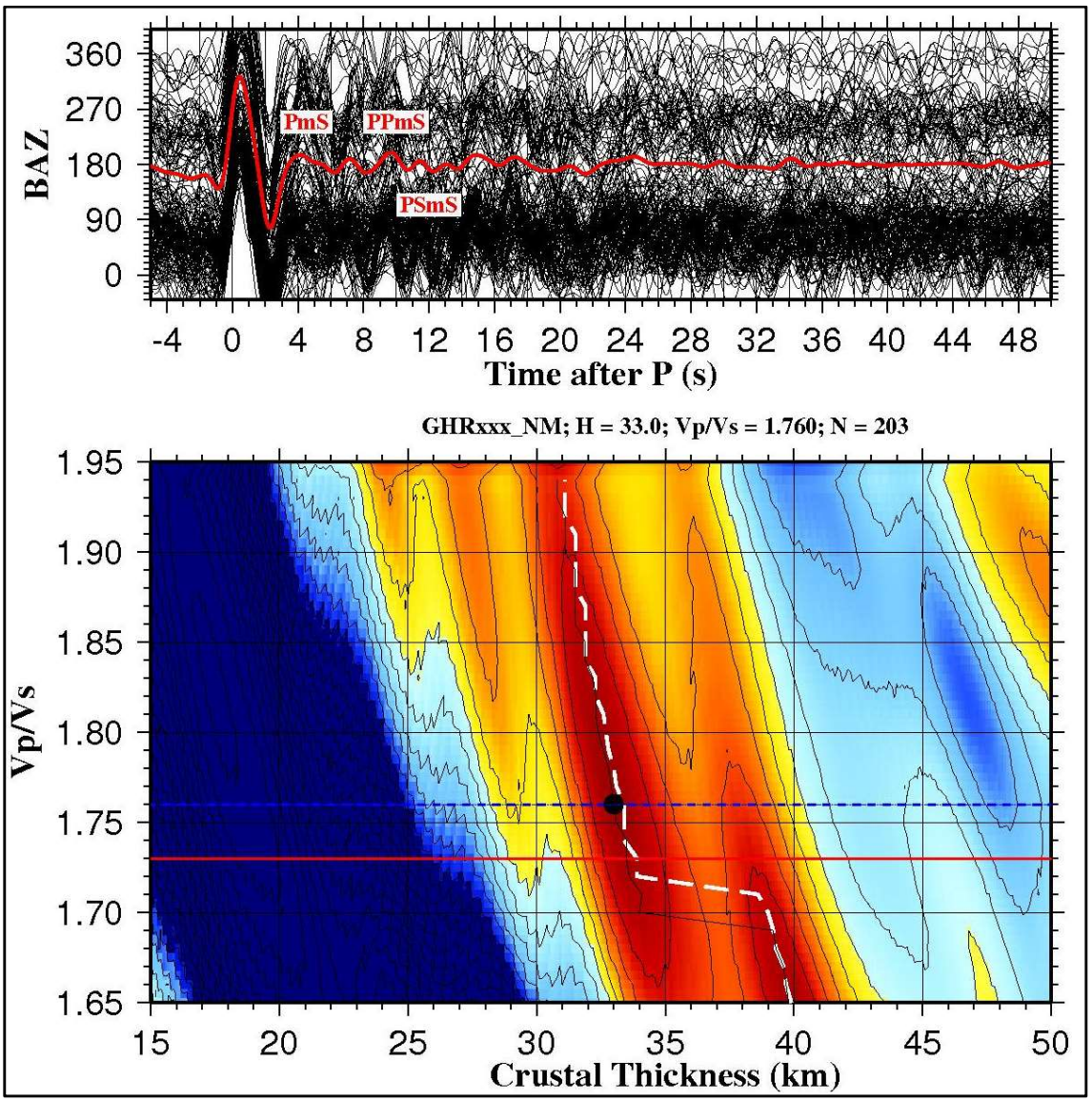

Figure A4. Same as Figure A3, but for station GHR and without sediment correction.

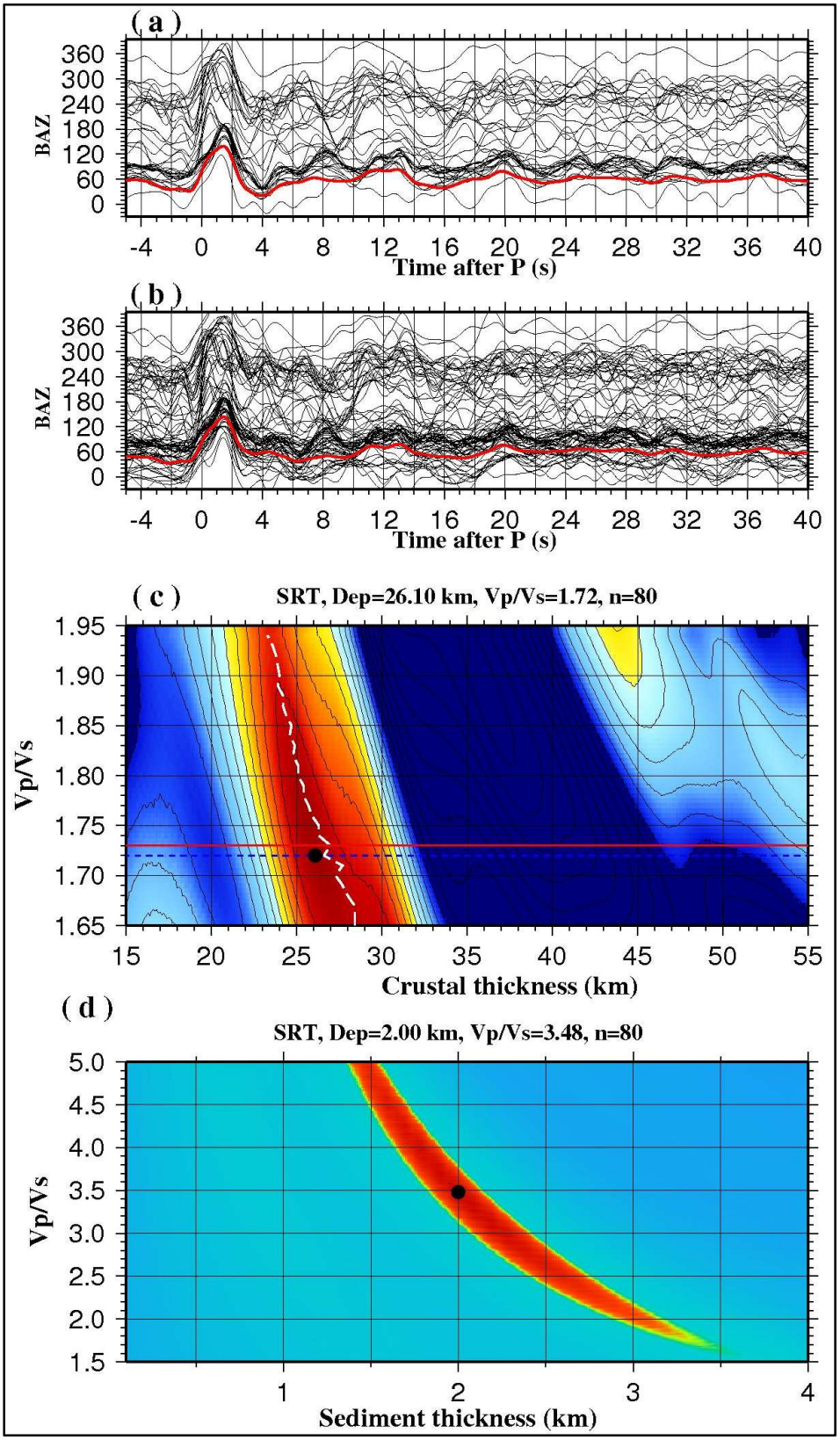

Figure A5. Same as Figure A1, but for station SRT.

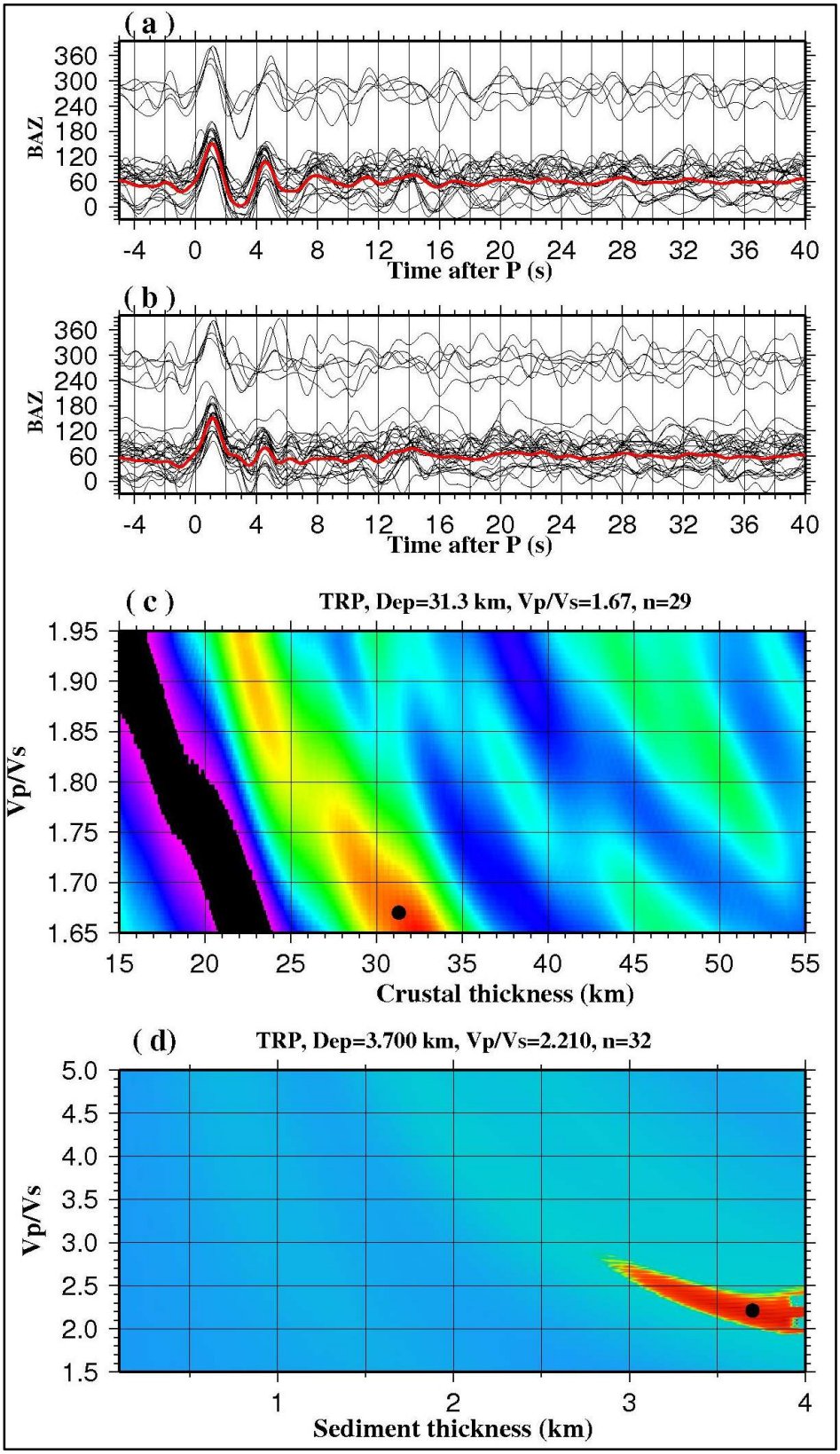

Figure A6. Same as Figure A1, but for station TRP.

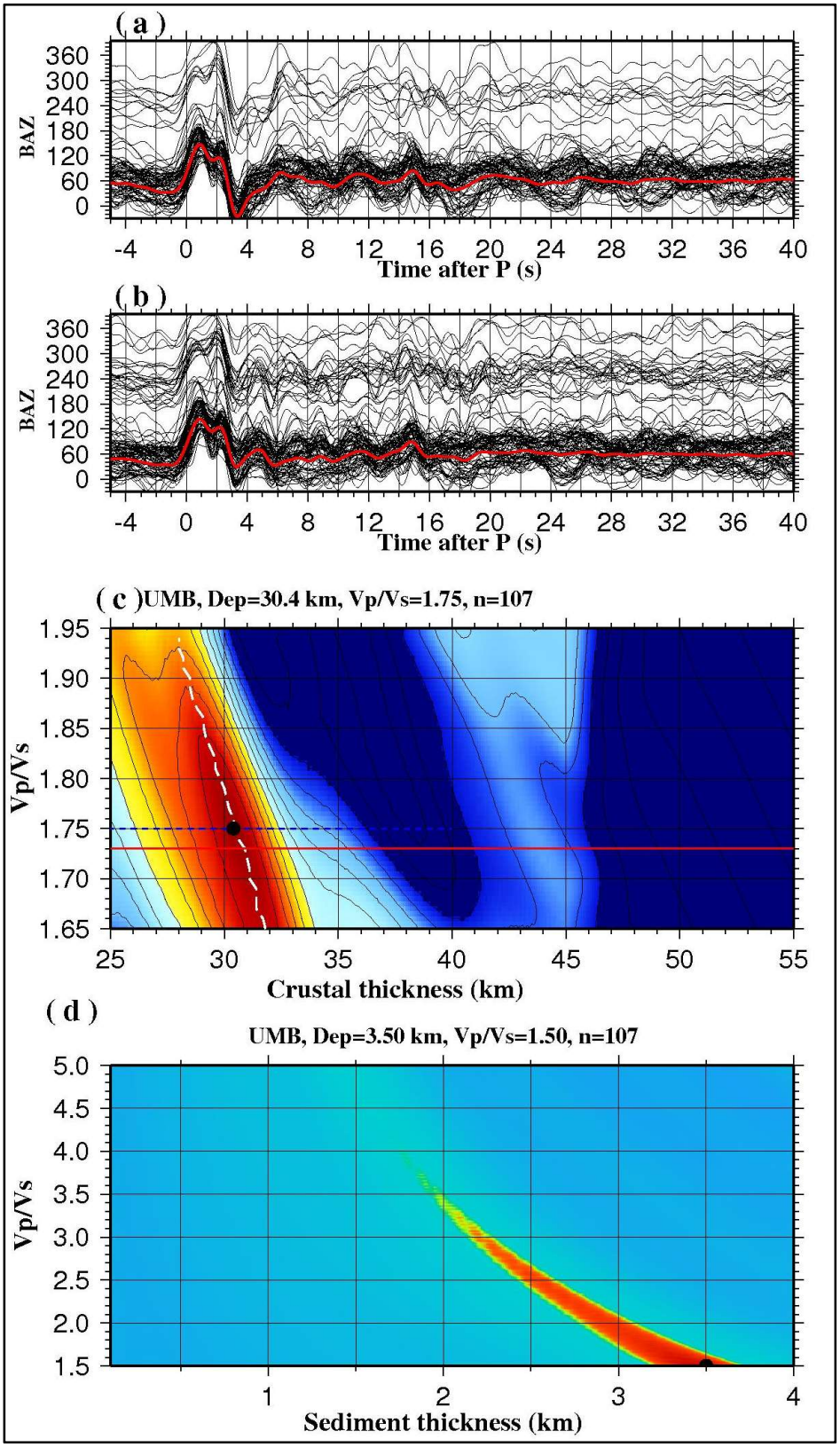

Figure A7. Same as Figure A1, but for station UMB.

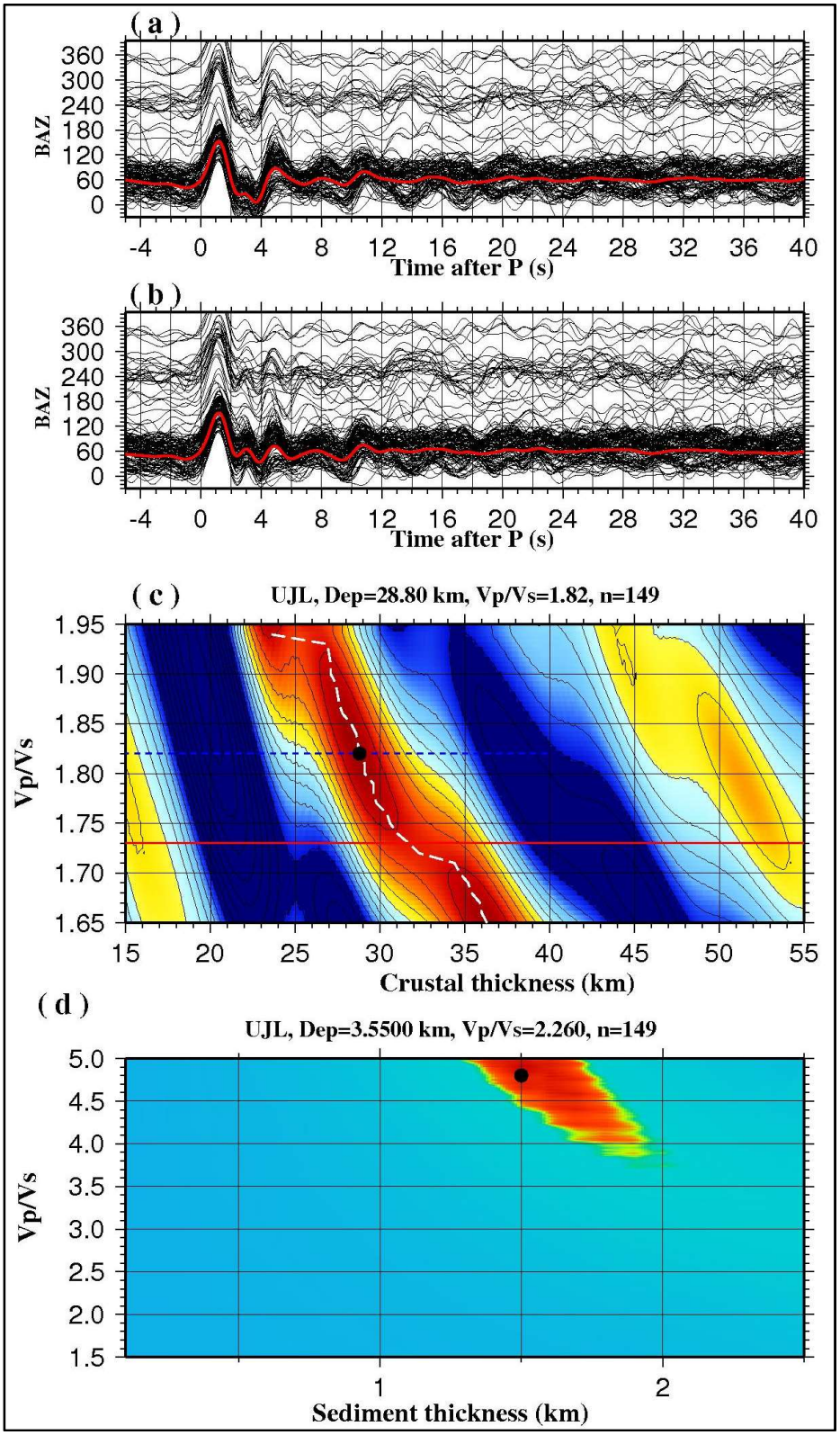

Figure A8. Same as Figure A1, but for station UJL.

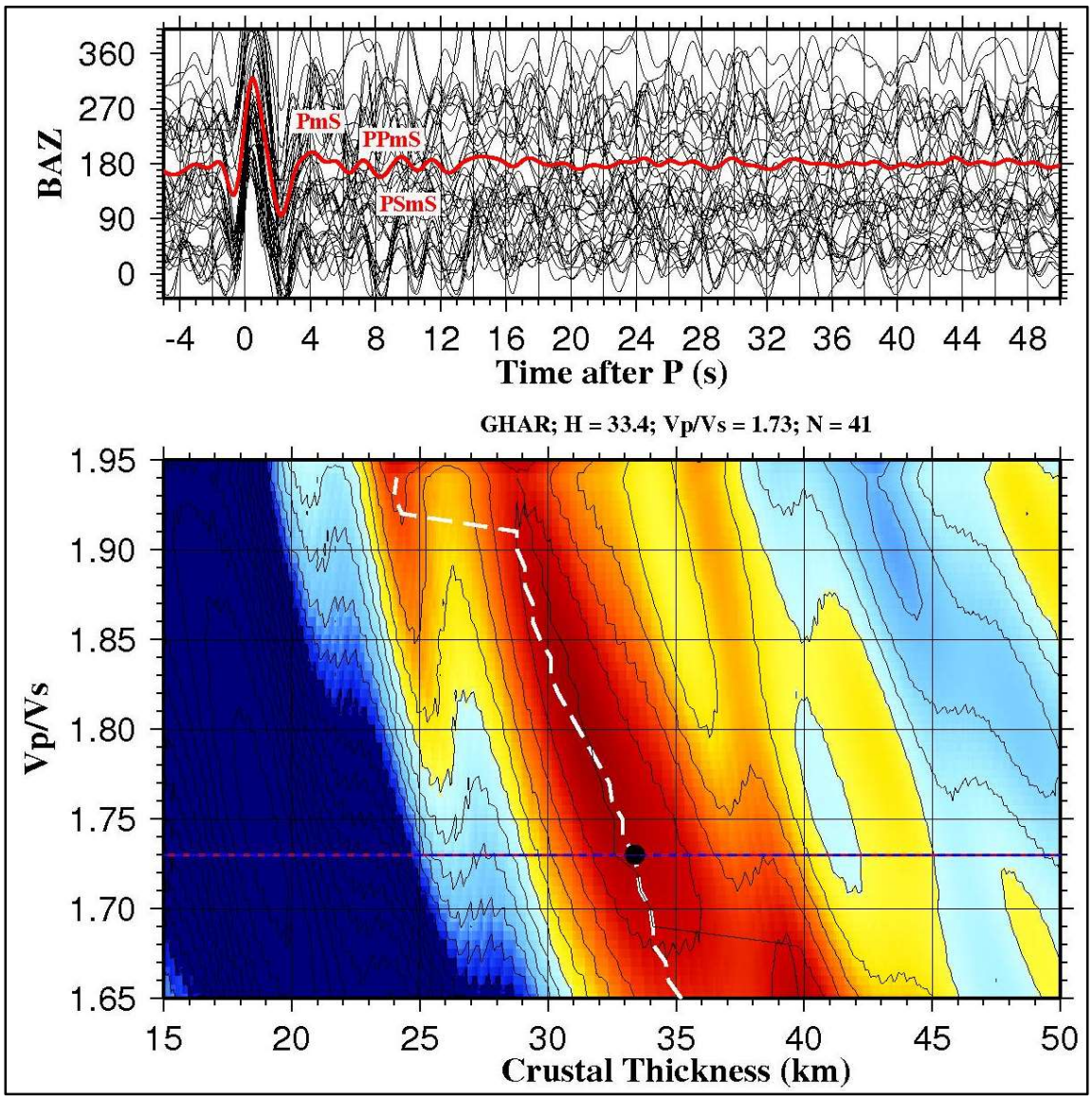

Figure A9. Same as Figure A3, but for station GHAR.

APPENDIX B.

MANTLE TRANSION ZONE (MTZ)

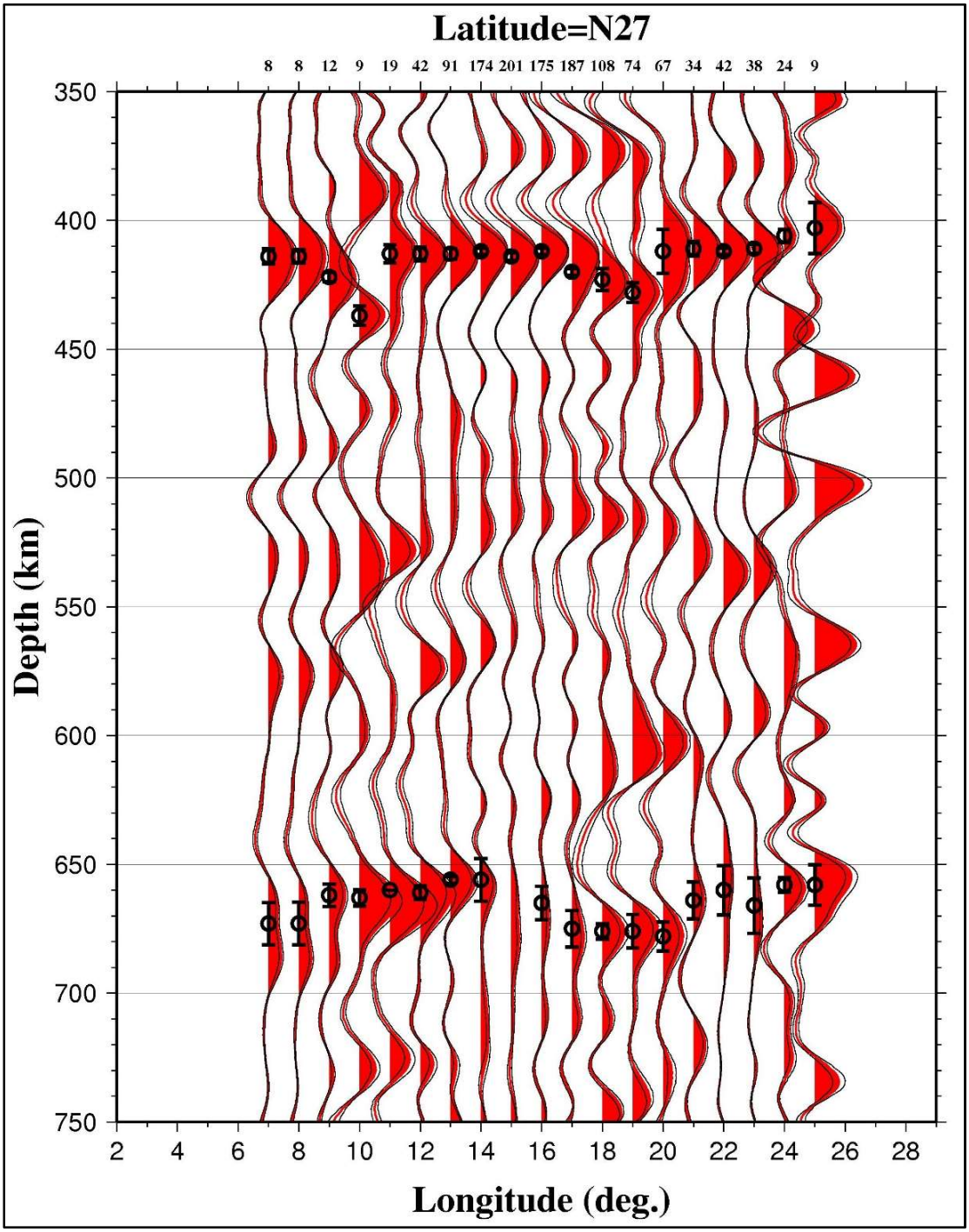

Figure B.1. Stacked latitudinal traces of time-series receiver functions (RFs) converted into depth-series RFs using the IASP91 Earth model velocities. Dashed lines represent the standard error of the binned trace amplitude from a bootstrap sample of 50 traces. Black dots with associated standard error mark the depth value obtained from bootstrap resampling of 50 resampled traces for each 2° radius bin.

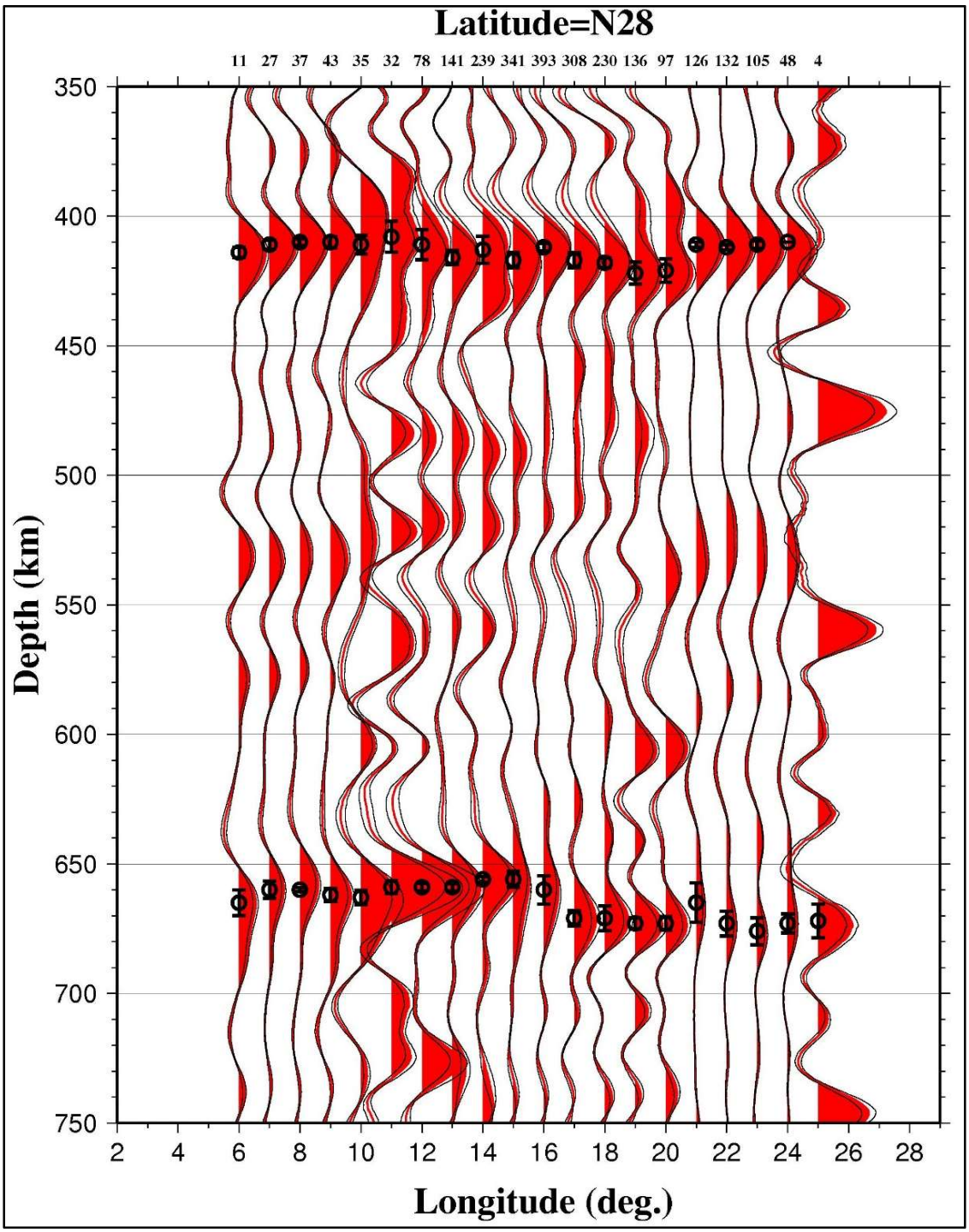

Figure B.2. Same as Figure B10.

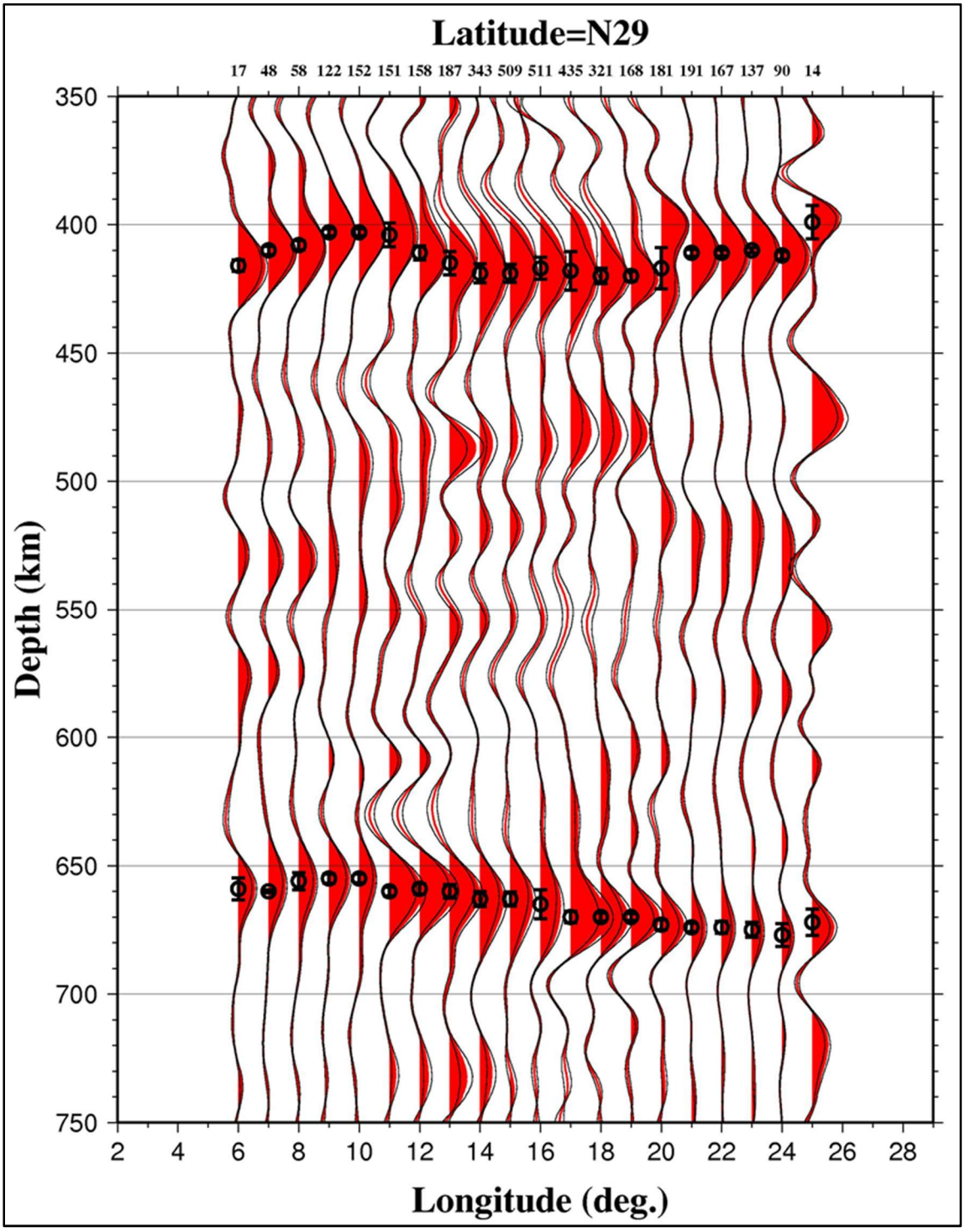

Figure B.3. Same as Figure B10.

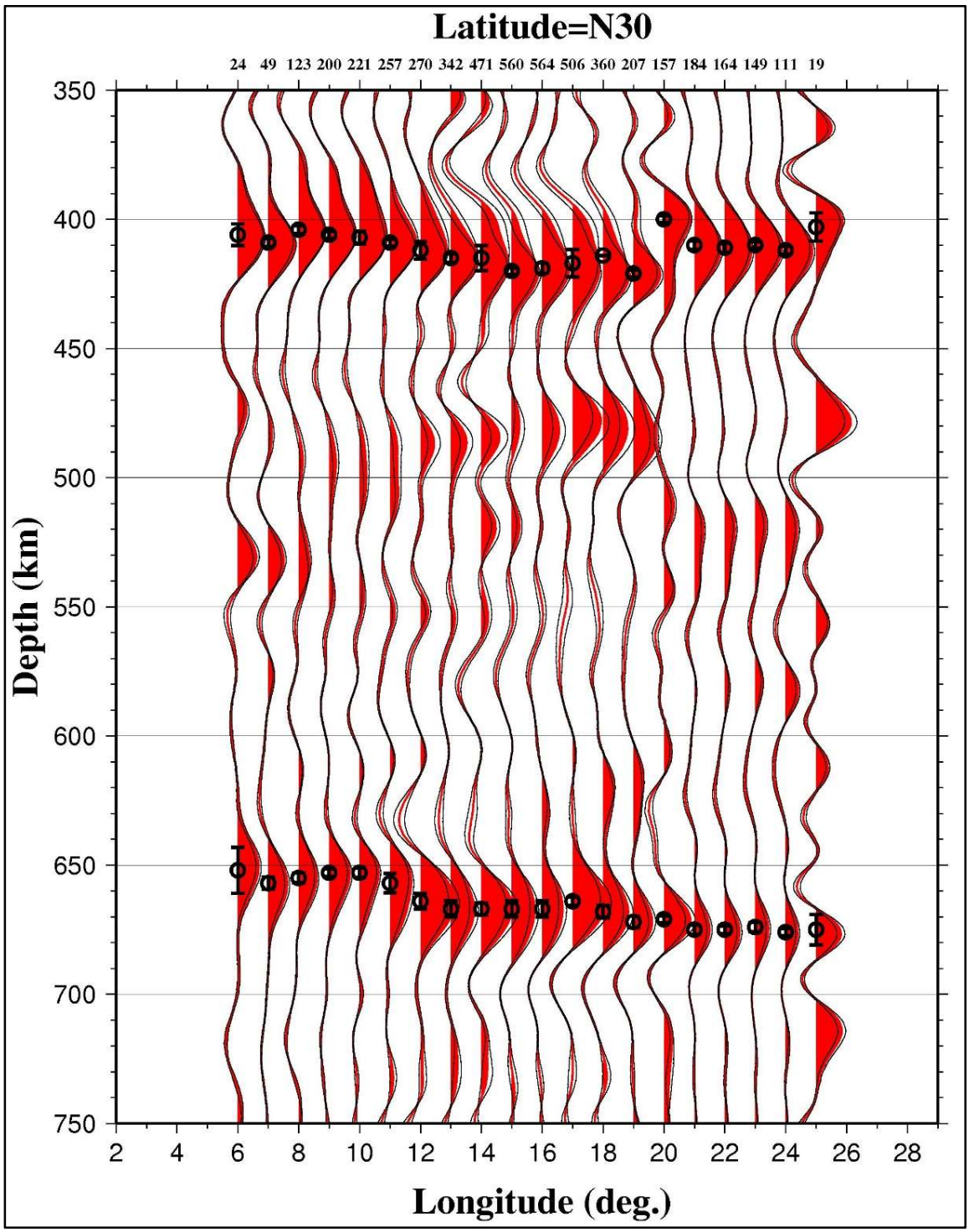

Figure B.4. Same as Figure B10.

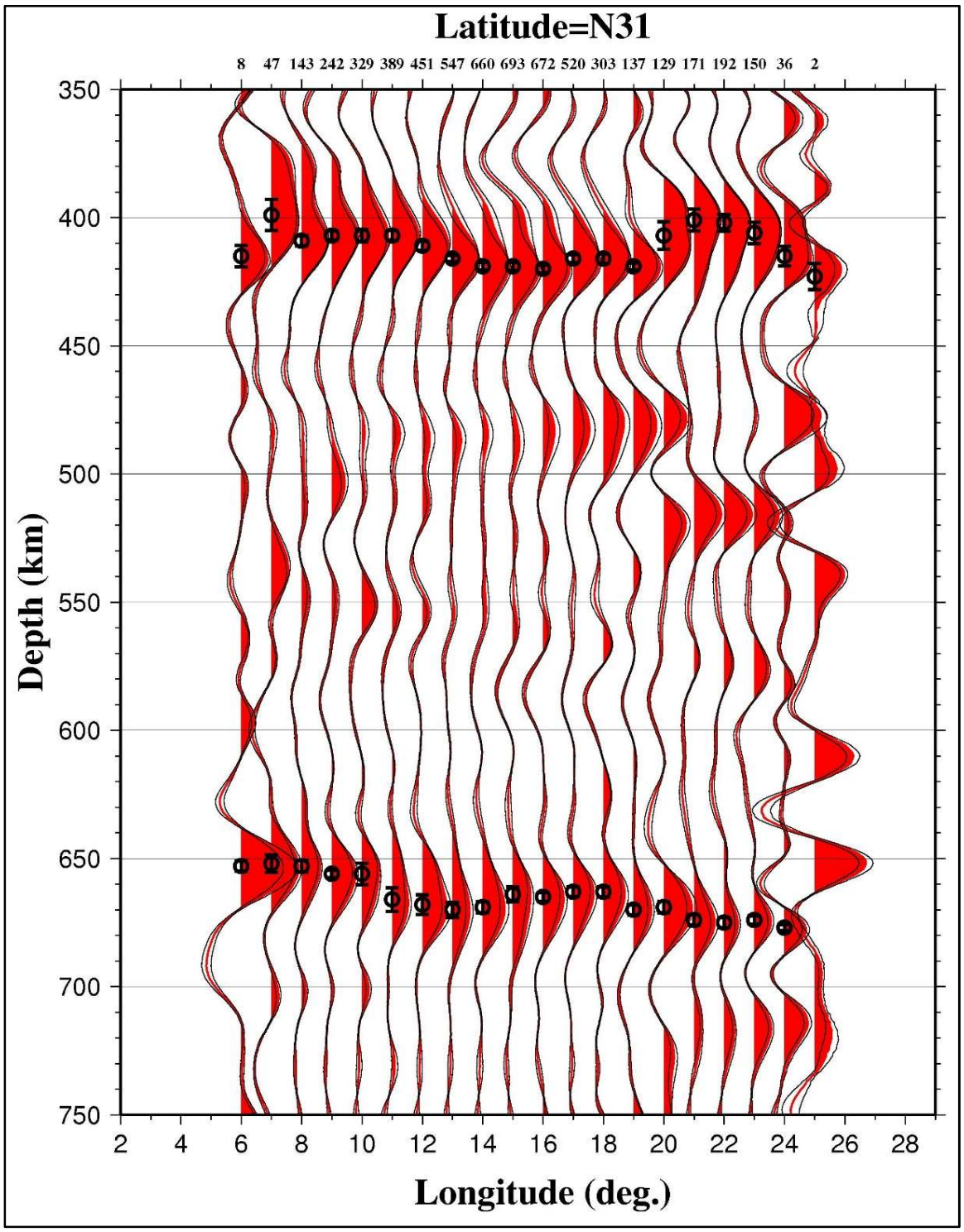

Figure B.5. Same as Figure B10.

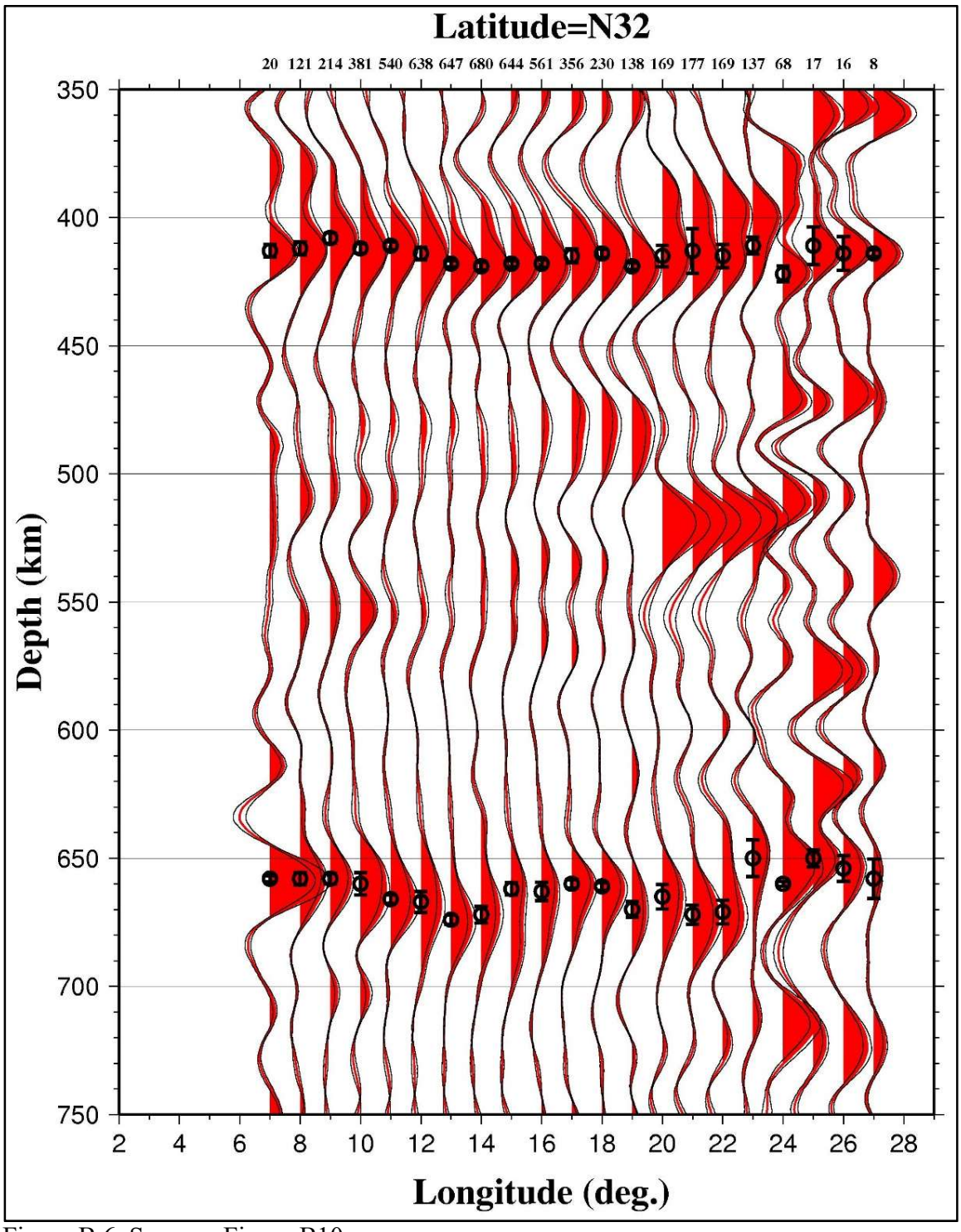

Figure B.6. Same as Figure B10.

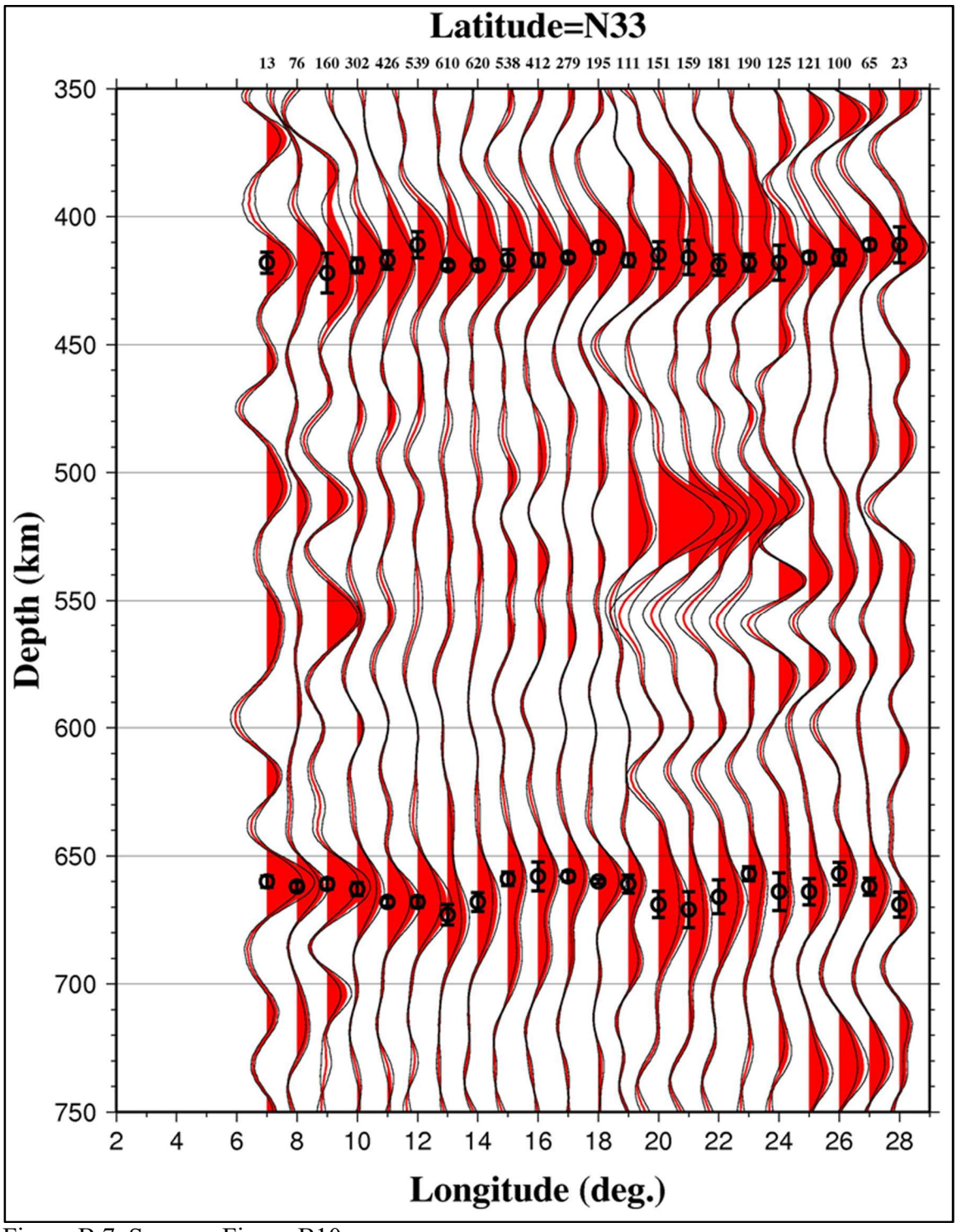

Figure B.7. Same as Figure B10.

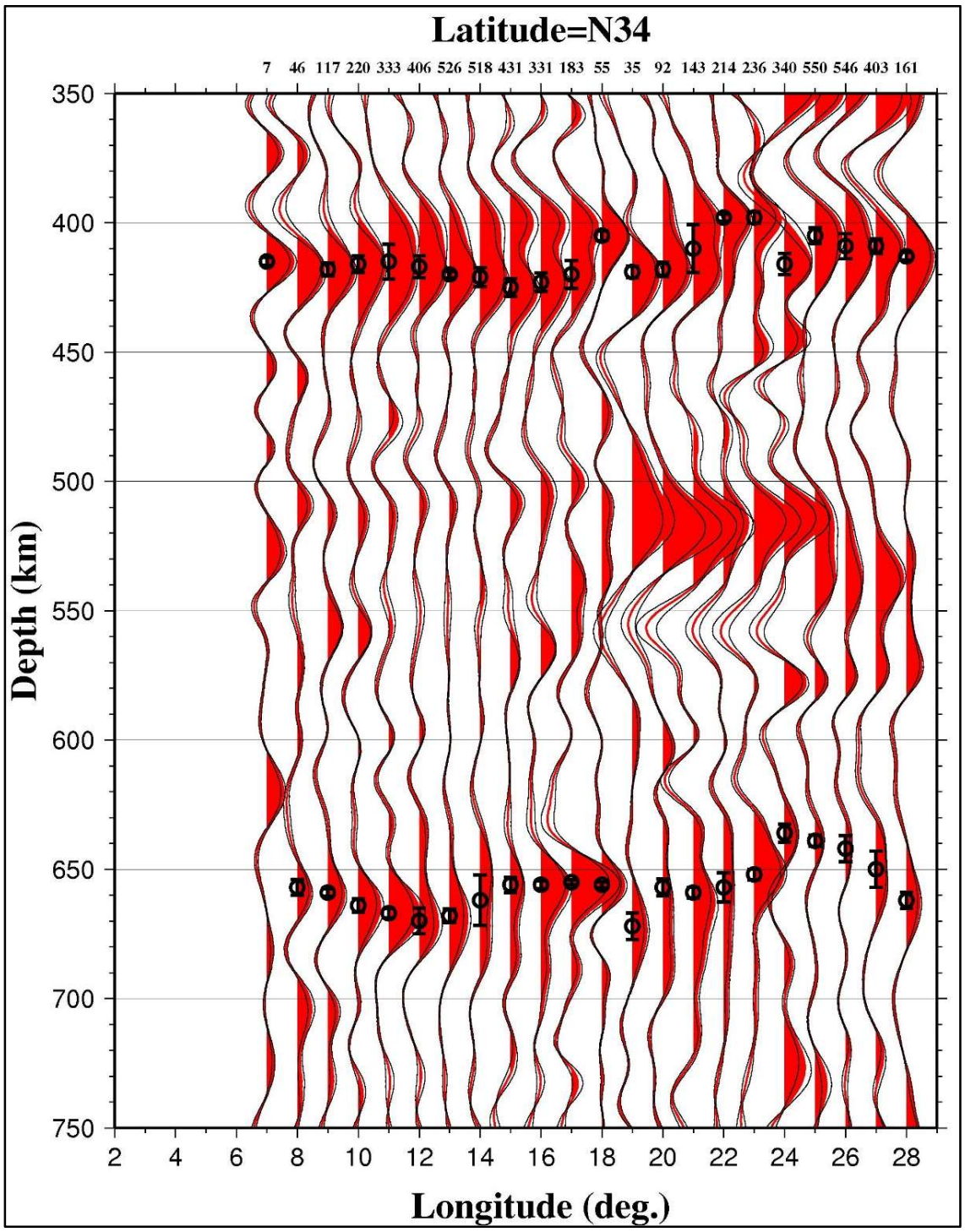

Figure B.8. Same as Figure B10.

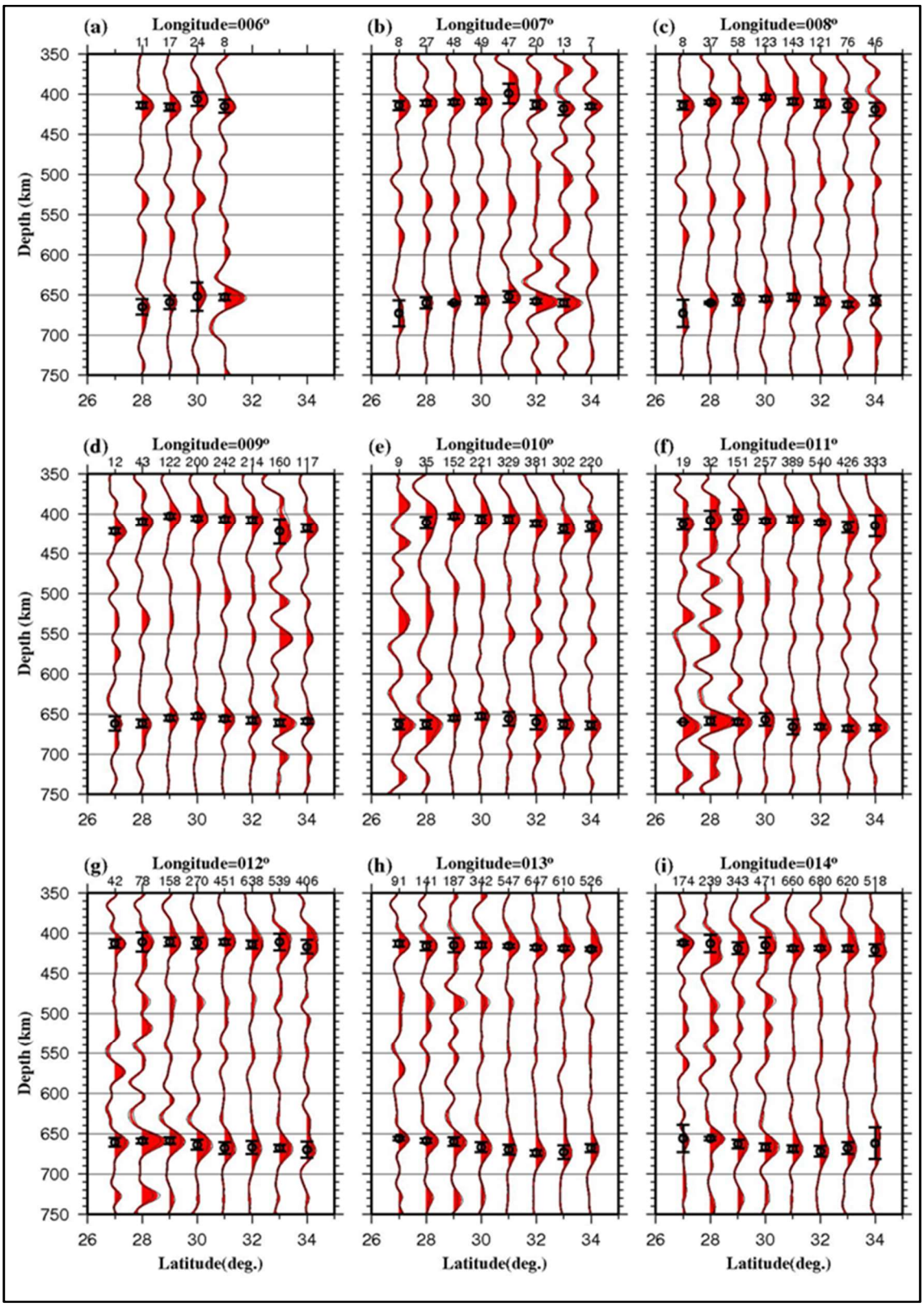

Figure B.9. Results of stacking moveout-corrected RFs within each bin plotted along 9 longitude profiles.

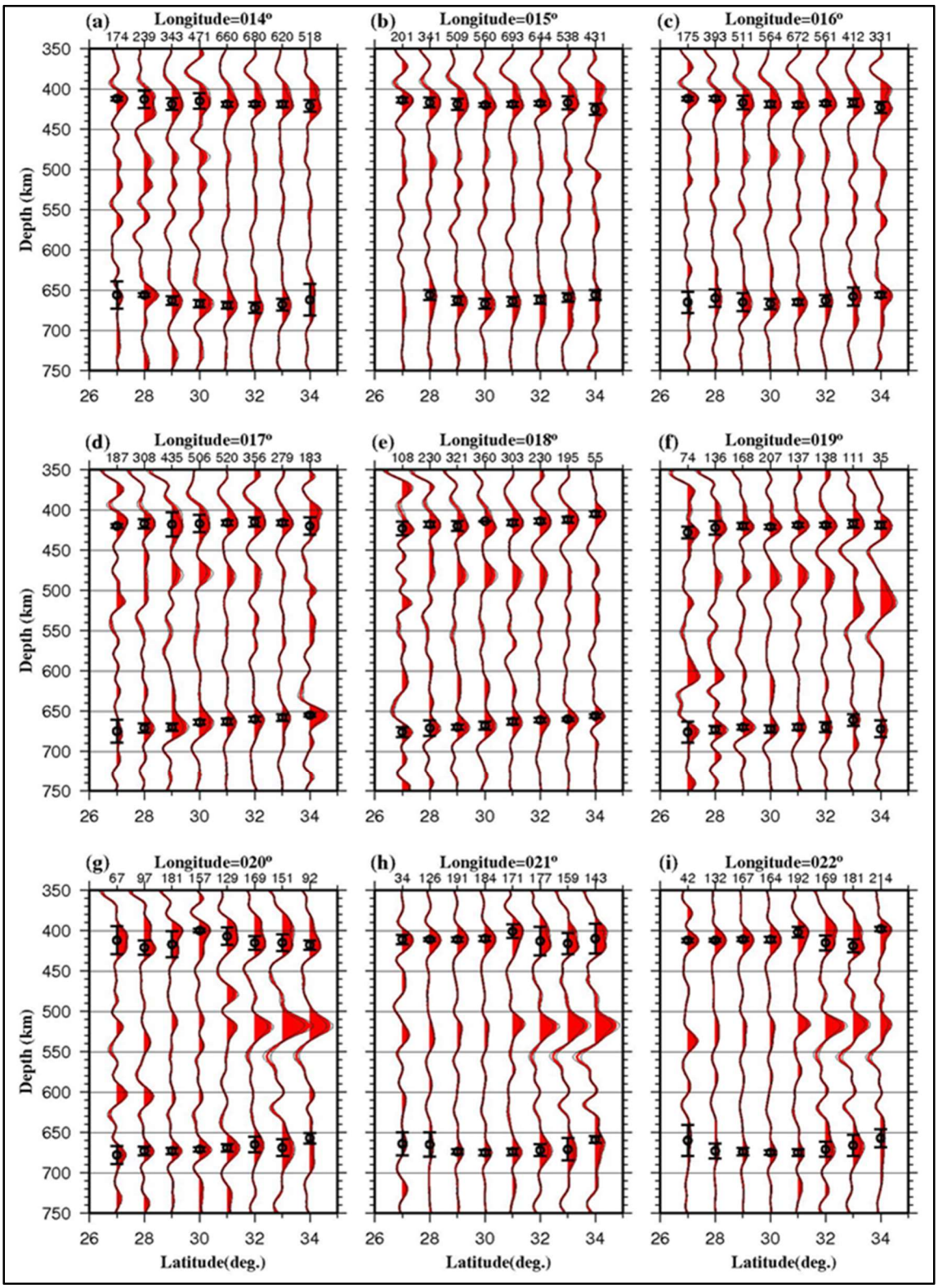

Figure B.10. With different 9 longitude profiles.

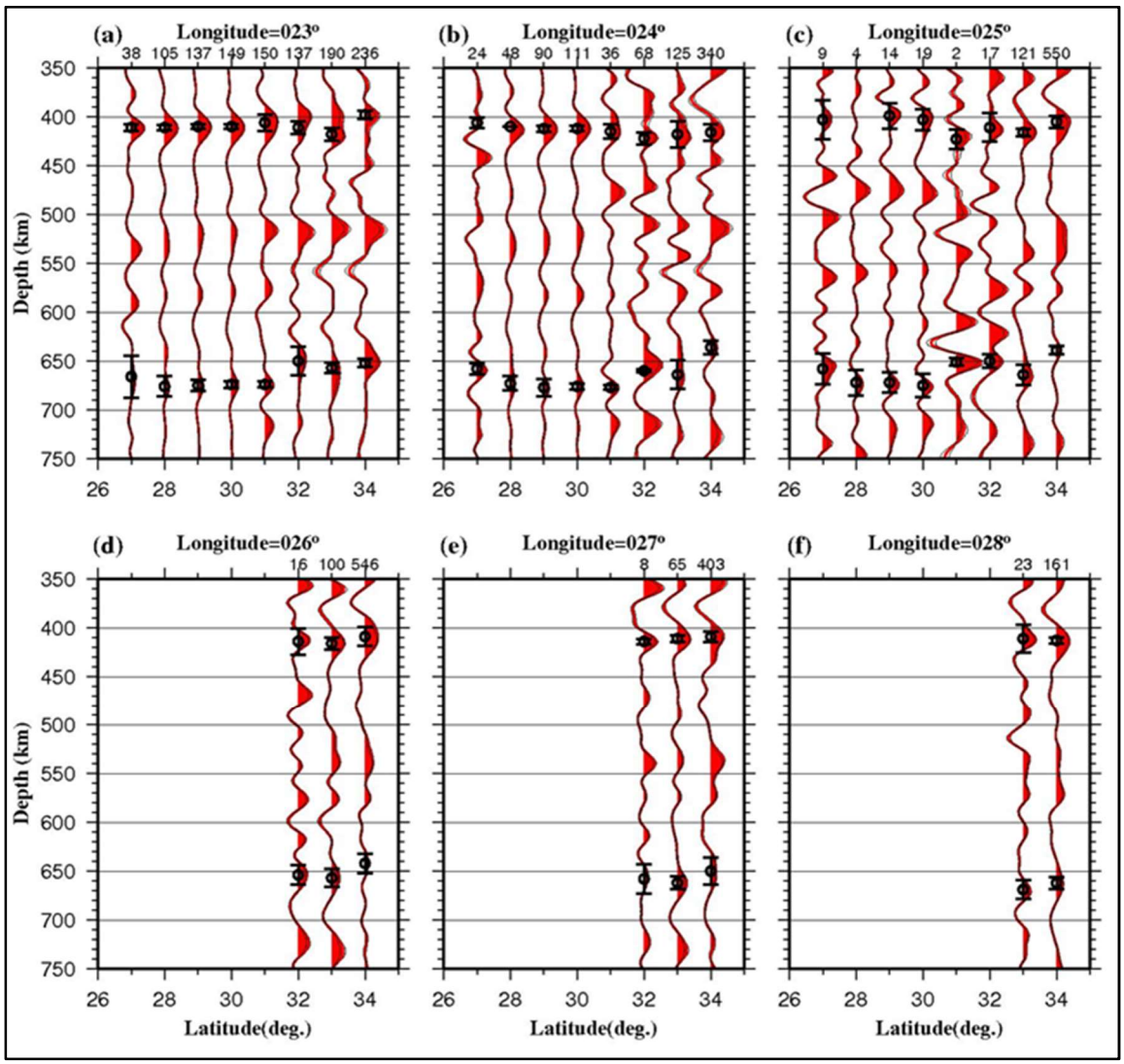

Figure B.11. With 6 longitude profiles.

BIBLIOGRAPHY

Abdelsalam, M. G., Gao, S. S., & Liegeois, J. P. (2011). Upper mantle structure of the Saharan Metacraton. Journal of African Earth Sciences, 60(5), 328–336. https://doi.org/10.1016/j.jafrearsci.2011.03.009.

Abdelsalam, M. G., Liegeois, J. P., & Stern, R. J. (2002). The Saharan Metacraton. Journal of African Earth Sciences, 34, 119–136. https://doi.org/10.1016/S0899-5362(02)00013-1

Abadi, A., van Wees, J., van Dijk, P., & Cloetingh, S. (2008). Tectonics and subsidence evolution of the Sirt Basin, Libya. Bulletin-American Association of Petroleum Geologists, 92, 993–1027. https://doi.org/10.1306/03310806070

Abdunaser, K, & McCaffrey, K. (2015). Tectonic history and structural development of the Zallah-Dur al Abd sub-basin, western Sirt Basin, Libya. Journal of Structural Geology, 73, 33–48. https://doi.org/10.1016/j.jsg.2015.02.006

Aboazom, A. S., Asran, A. S. H., Abdel Ghani, M. S., & Farhat, E. S. (2006). Geologic and geochemical constraints on the origin of some Tertiary alkaline rift volcanics, Gharyan area, northwestern Libya. Journal of Geology, 35, 25–47.

Aiken, C. (1976). The analysis of the gravity anomalies of Arizona (PhD dissertation), University of AZ, Tucson.

Al-Hafdh, N. M., & El-Shaafi, A. S. (2015). Geochemistry and petrology of basic volcanicrocks of Jabal Al Haruj Al-Aswad, Libya. International Journal of Geosciences, 6, 109–144. https://doi.org/10.4236/ijg.2015.61008

Al-Hafdh, N. M., & Gafeer, A. S. (2015). The petrology and geochemistry of Gharyan Volcanic Province of NW Libya. Journal of African Earth Sciences, 104, 71–102. https://doi.org/10.1016/j.jafrearsci.2014.11.006

Al-Heety, E. (2013). Seismicity and seismotectonics of Libya: As an example of intraplate environment. Arabian Journal of Geosciences, 6,193–204. https://doi.org/10.1007/s12517-011-0347-y

Ammon, C. J. (1991). The isolation of receiver effects from teleseismic P waveforms. Bulletin of the Seismological Society of America, 81, 2504–2510.

Anderson, D.L. (1967). Phase changes in the upper mantle. Science 157, 1165–1173.

Andrew, R., & Gudmundsson, A. (2008). Volcanoes as elastic inclusions: Their effects on the propagation of dykes, volcanic fissures, and volcanic zones in Iceland. Journal of Volcanology and Geothermal Research, 177, 1045–1054. https://doi.org/10.1016/j.jvolgeores.2008.07.025

Anketell, J. M. (1996). Structural history of Sirt Basin and its relationship to the Sabratah Basin and Cyrenaica platform, northern Libya. In M. J. Salem et al. (Eds.), The Geology of sirt basin (Vol. 3, pp. 57–89). Amsterdam: Elsevier.

Asran, A.M.H., & Aboazom, A.S. (2004). CRZ Al-haruj tertiary basalts, Libya: petrological and geochemical approach. Proceedings of the 6th International Conference on the Geology of the Arab World (GAW6).

Assumpcao, M., Bianchi, M., Julia, Dias, F. L., Frana, G. S., Nascimento, R., & Lopes, A. E. V. (2013). Crustal thickness map of Brazil: Data compilation and main features. Journal of South American Earth Sciences, 43, 74–85. https://doi.org/10.1016/j.jsames.2012.12.009

Azzouni-Sekkal, A., Bonin, B., Benhallou, A., Yahiaoui, R., & Liégeois, J. (2007). Cenozoic alkalinevolcanism of the atakor massif, hoggar, Algeria. J. Soc. Am. 418, 321–340. https://doi.org/10.1130/2007.2418(16).

Ball, P. N., White, N. J., Maclennan, J., & Stuart, F. (2016). Magmatism and Dynamic Topography of Libya and Tibesti, North Africa, American Geophysical Union, Fall General Assembly, Abstract DI51B-2667.

Bardintzeff, J. M., Deniel, C., Guillou, H., Platevoet, B., T´clouk, P., & Oun, K. H. (2012). Miocene to recent alkaline volcanism between Al Haruj and Waw an Namous (southern Libya). International Journal of Earth Sciences, 101, 1047–1063. https://doi.org/10.1007/s00531-011-0708-5

Bashir, L., Gao, S. S., Liu, K. H., & Mickus, K. (2011). Crustal structure and evolution beneath the Colorado Plateau and the southern Basin and Range Province: Results from receiver function and gravity studies. Geochemistry, Geophysics, Geosystems, 12, Q06008. https://doi.org/10.1029/2011GC003563

Bassin, C., Laske, G., & Masters, G. (2000). The current limits of resolution for surface wave tomography in North America. Eos Transactions American Geophysical Union, 81, F897.

Beccaluva, L., Azzouni-Sekkal, A., Benhallou, A., Bianchini, G., Ellam, R.M., Marzola, M., Siena, F., & Stuart, F.M. (2007). Intracratonic asthenosphere upwelling and lithosphere rejuvenation beneath the Hoggar swell (Algeria): evidence from HIMU metasomatized lherzolite mantle xenoliths. Earth Planet. Sci. Lett. 260 (3), 482–494. https:// doi.org/10.1016/j.epsl.2007.05.047.

Begg, G. C., Griffin, W. L., Natapov, L.M., O'Reilly, S. Y., Grand, S. P., & O'Neill, C. J. Bowden, P. (2009). The lithospheric architecture of Africa: Seismic tomography, mantle petrology, and tectonic evolution. Geosphere, 5, 23–50. https://doi.org/10.1130/GES00179.1

Ben, S. A. (2000). Hydrocarbon prospectivity to the north-west of the assumoodeld, Sirt Basin, Libya (Durham theses), (http://etheses.dur. ac.uk/4379/). Durham University.

Bercovici, D., & Karato, S. (2003). Whole mantle convection and transition-zone water filter.Nature 425, 39–44.

Biggs, J., Robertson, E., & Cashman, K. (2016). The lateral extent of volcanic interactions during unrest and eruption. Nature Geoscience, 9, 308–311. https://doi.org/10.1038/ngeo2658

Bina, C.R., & Helffrich, G. (1994). Phase-transition Clapeyron slopes and transition zone seismic discontinuity topography. J. Geophys. Res. 99 (B8), 15853–15860.

Bonatto, L., Schimmel, M., Gallart, J., & Morales, J. (2015). The upper-mantle transition zone beneath the Ibero-Maghrebian region as seen by teleseismic Pds phases. Tectonophysics 212–224. https://doi.org/10.1016/j.tecto.2015.02.002.

Boschi, L., Faccenna, C., & Becker, T. W. (2010). Mantle structure and dynamic topography in the Mediterranean Basin. Geophysical Research Letters, 37, L20303. https://doi.org/10.1029/2010GL045001

Burke, K. (1996). The African plate. South Afr. J. Geol. 99, 339–410.

Capitanio, F. A., Faccenna, C., & Funiciello, R. (2009). The opening of Sirte Basin: Result of slab avalanching? Earth and Planetary Science Letters, 285, 210–216. https://doi.org/10.1016/j.epsl.2009.06.019

Christensen, N. I. (1996). Poisson's ratio and crustal seismology. Journal of Geophysical Research, 101, 3139–3156. https://doi.org/10.1029/95JB03446

Christensen, N. I., & Mooney, W. D. (1995). Seismic velocity structure and composition of the continental crust: A global view. Journal of Geophysical Research, 100, 9761–9788. https://doi.org/10.1029/95JB00259

Clarke, T. J., & Silver, P. G. (1993). Estimation of crustal Poisson's ratio from broadband teleseismic data. Geophysical Research Letters, 20, 241–244. https://doi.org/10.1029/92GL02922

Cochran, J. R., & Karner, G. D. (2007). Constraints on the deformation and rupturing of continental lithosphere of the Red Sea: The transition from rifting to drifting, in The Origin and Evolution of the Caribbean Plate, edited by K. H. James, M. A. Lorente, and J. L. Pindell, Geol. Soc. Spec. Publ., 282, 265–289, doi:10.1144/SP282.13.

Collier, J.D., Helffrich, G.R., & Wood, B.J. (2001). Seismic discontinuities and subduction zones. Phys. Earth Planet. Inter. 127, 35–49.

Contenti, S., Gu, Y.J., Okeler, A., & Sacchi, M.D. (2012). Shear wave reflectivity imaging of the Nazca-South America subduction zone: Stagnant slab in the mantle transition zone? Geophys. Res. Lett. 39https://doi.org/10.1029/2011GL050064. L02310.

Courtillot, V., Davaille, A., Besse, J., & Stock, J. (2003). Three distinct types of hotspots in the Earth's mantle. Earth and Planetary Science Letters, 205, 295–308. https://doi.org/10.1016/S0012-821X(02)01048-8

Cowie, L., & Kusznir, N. (2012). Gravity inversion mapping of crustal thickness and lithosphere thinning for the Eastern Mediterranean. The Leading Edge, 31, 810–814. https://doi.org/10.1190/tle31070810.1

Craig, J., Jackson, J., Priestley, A., & McKenzie, D. (2011). Earthquake distribution patterns in Africa: Their relationship to variations in lithospheric and geological structure, and their heological implications. Geophysical Journal International, 185, 403–434. https://doi.org/10.1111/j.1365-246X.2011.04950.x

Craig, J., Rizzi, C., Said, F., Thusu, B., Luning, S., Asbali, A., Hamblett, C. (2008). Structural styles and prospectivity in the Precambrian and Palaeozoic hydrocarbon systems of North Africa. In M. J. Salem, K. M. Oun, & A. S. Essed (Eds.), The Geology of East Libya (Vol. 4, pp. 51–122). Earth Science Society of Libya.

Cvetkovi´c, V., Tolji´c, M., Ammar, N. A., Rundi´c, L., & Trish, K. B. (2010). Petrogenesis of the eastern part of the Al Haruj basalts (Libya). Journal of African Earth Sciences, 58, 37–50.

Dahm, H.H., Gao, S.S., Kong, F., Liu, & K.H. (2017). Topography of the mantle transition zone discontinuities beneath Alaska and its geodynamic implications: constraints from receiver function stacking. J. Geophys. Res. Solid Earth 122 (10). https://doi.org/10.1002/2017JB014604. 352–10,363.

Darbyshire, F. A., White, R. S., & Priestley, K. F. (2000). Structure of the crust and uppermost mantle of Iceland from a combined seismic and gravity study. Earth and Planetary Science Letters, 181, 409–428. https://doi.org/10.1016/S0012-821X(00)002065

Deen, T., Griffin, W. L., O'Reilly, G., Begg, S. Y., & Natapov, L. M. (2006). Thermal and compositional structure of the subcontinental lithospheric mantle: Derivation from shear-wave seismic tomography. Geochemistry, Geophysics, Geosystems, 7, Q07003. https://doi.org/10.1029/2005GC001164

Doucoure, C. M., & de Wit, M. J. (2003). Old inherited origin for the present near-bimodal topography of Africa. Journal of African Earth Sciences, 36, 371–388. https://doi.org/10.1016/S0899-5362(03)00019-8

Ebinger, C. J., & Sleep, N. H. (1998). Cenozoic magmatism throughout East Africa resulting from impact of a single plume. Nature, 395, 788–791. https://doi.org/10.1038/27417.

Ebinger, C.J., Deino, A.L., Drake, R.E., & Tesha, A.L. (1989). Chronology of volcanism and rift basin propagation: rungwe volcanic province, East Africa. J. Geophys. Res. 94 (15) 785–15.

Ebinger, C.J., & Sleep, N.H. (1998). Cenozoic magmatism throughout East Africa resulting
from impact of a single plume. Nature 395, 788–791. https://doi.org/10.1038/
27417.

Efron, B., & Tibshirani, R. (1986). Bootstrap methods for standard errors, confidence intervals, and other measures of statistical accuracy. Statistical Science, 1, 54–77.

Egorkin, A. V. (1998). Velocity structure, composition and discrimination of crustal provinces in the former Soviet Union. Tectonophysics, 298, 395–404. https://doi.org/10.1016/S0040-1951(98)00192-9

Elshaafi, A., & Gudmundsson, A. (2016). Volcano-tectonics of the Al Haruj Volcanic Province, central Libya. Journal of Volcanology and Geothermal Research, 325, 189–202. https://doi.org/10.1016/j.jvolgeores.2016.06.025

Elshaafi, A., & Gudmundsson, A. (2017a). Distribution and size of lava shields on the Al Haruj al Aswad and the Al Haruj al Abyad volcanic systems, central Libya. Journal of Volcanology and Geothermal Research, 338, 46–62. https://doi.org/10.1016/j.jvolgeores.2017.03.012

Elshaafi, A., & Gudmundsson, A. (2017b). Mechanical interaction between volcanic systems in Libya, Tectonophysics, https://doi.org/10.1016/j.tecto.2017.11.031

Elshaafi, A., & Gudmundsson, A. (2018). Mechanical interaction between volcanic systems in Libya. Tectonophysics 722, 549–565. https://doi.org/10.1016/j.tecto.2016.

Faccenna, C., & et al. (2014). Mantle dynamics in the Mediterranean. Rev. Geophys. 52, 283–332. https://doi.org/10.1002/2013RG000444.

Faccenna, C., Funiciello, F., Giardini, D., & Lucente, P. (2001). Episodic backarc extension during restricted mantle convection in the central Mediterranean. Earth and Planetary Science Letters, 187, 105–116. https://doi.org/10.1016/S0012-821X(01)002801

Feng, M., Van Der Lee, S., & Assumpca, M. (2007). Upper mantle structure of South America from joint inversion of waveforms and fundamental-mode group velocities of Rayleigh waves. Journal of Geophysical Research, 112, B04312. https://doi.org/10.1029/2006JB004449

Fei, Y., & et al. (2004). Experimentally determined postspinel transformation boundary in Mg2SiO4 using MgO as an internal pressure standard and its geophysical implications. J. Geophys. Res. Solid Earth 109 (B2), 1978–2012. https://doi.org/10.1029/ 2003JB002562.

Fishwick, S. (2010). Surface wave tomography: Imaging of the lithosphere-asthenosphere boundary beneath central and southern Africa? Lithos, 120(1), 63–73. https://doi.org/10.1016/j.lithos.2010.05.011

Flament, N. (2014). Linking plate tectonics and mantle flow to Earth's topography. Geology, 42, 927–928. https://doi.org/10.1130/focus102014.1

Flanagan, M.P., & Shearer, P.M. (1998). Global mapping of topography on transition zone velocity discontinuities by stacking SS precursors. J. Geophys. Res. 103 (B2), 2673–2692.

Forte, A. M., Peltier, W. R., Dziewonski, A. M., & Woodward, R. L. (1993). Dynamic surface topography: A new interpretation based upon mantle flow models derived from seismic tomography. Geophysical Research Letters, 20, 225–228. https://doi.org/10.1029/93GL00249.

Forte, A. M., Quere, S., Moucha, R., Simmons, N. A., Grand, S. P., Mitrovica, J. X., & Rowley, D. B. (2010). Joint seismic-geodynamic-mineral physical modeling of African geodynamics: A reconciliation of deep mantle convection with surface geophysical constraints. Earth and Planetary Science Letters, 295, 329–341. https://doi.org/10.1016/j.epsl.2010.03.017

Gao, S.S., & Liu, K.H. (2014a). Imaging mantle discontinuities using multiply reflected P-to-S conversions. Earth Planet. Sci. Lett. 402, 99–106. https://doi.org/10.1016/j.epsl. 2013.08.025. 294.

Gao, S.S., & Liu, K.H. (2014b). Mantle transition zone discontinuities beneath the contiguous United States. J. Geophys. Res. 119 (6), 452–456. https://doi.org/10.1002/ 2014JB011253. 468.

Gourgaud, A., & Vincent, P.M. (2004). Petrology of two continental alkaline intraplate series at Emi Koussi volcano, Tibesti, Chad. J. Volcanol. Geotherm. Res. 129, 261–290.

Grand, S.P. (2002). Mantle shear-wave tomography and thefate of subducted slabs. Philos. Trans. R. Soc. London A 360, 2475–2491. https://doi.org/10.1098/rsta.2002.1077.

Granot, R. (2016). Palaeozoic oceanic crust preserved beneath the Eastern Mediterranean. Nature Geoscience, 9, 701–705. https://doi.org/10.1038/ngeo2784

Griffin, W., & O'Reilly, S. (1987). Is the continental Moho the crust-mantle boundary? Geology,15,241–244.https://doi.org/10.1130/0091 7613(1987)15<241: ITCMTC>2.0.CO;2

Gu, Y., Dziewonski, A.M., & Agee, C.B. (1998). Global de-correlation of the topography of transition zone discontinuities. Earth Planet. Sci. Lett. 157, 57–67.

Gudmundsson, A. (1986). Mechanical aspects of postglacial volcanism and tectonics of the Reykjanes Peninsula, southwest Iceland. Journal of Geophysical Research, 91, 12711–12721.

Gudmundsson, A. (2016). The mechanics of large volcanic eruptions. Earth-Science Reviews, 163, 72–93. https://doi.org/10.1016/j.earscirev.2016.10.003.

Gudmundsson, A., Friese, N., Andrew, R., Phillpp, S. L., Ertl, G., & Letourneur, L. (2009). Effects of dyke emplacement and plate pull on mechanical interaction between volcanic systems and central volcanoes in Iceland. In T. Thordarson et al. (Eds.), Studies in volcanology: The legacy of George Walker, Special Publication of IAVCEI (Vol. 2, pp. 331–347). London, UK: Geological Society.

Guiraud, R., & Bosworth, W. (1997). Senonian basin inversion and rejuvenation of rifting in Africa and Arabia: Synthesis and implications to plate-scale tectonics. Tectonophysics, 282, 39–82. https://doi.org/10.1016/S0040-1951(97)00212-6

Gumati, Y., & Schamel, S. (1988). Thermal maturation history of the Sirte Basin, Libya. Journal of Petroleum Geology, 11, 205–218. https://doi.org/10.1111/j.1747-5457.1988.tb00814.X

Gurnis, M. (1993). Phanerozoic marine inundation of continents driven by dynamic topography above subducting slabs. Nature, 364, 589–593. https://doi.org/10.1038/364589a0

Hansen, P.C. (1992). Analysis of discrete ill-posed problems by means of the L-curve: SIAM (Society for Industrial and Applied Mathematics) Review, v. 34, p. 561–580, doi: 10 .1137 /1034115.

Hassan, H. S., & Kendall, C. G. (2014). Hydrocarbon provinces in Libya: A petroleum system study. In L. Marlow et al. (Eds.), Petroleum systems of the Tethyan region (Vol. 106, pp. 101–142). London: Geological Society Special Publication.

Hegazy, A. H. (1999). Tertiary volcanics in Libya: Evidence for the direction and rate of the African plate motion, paper presented at Proceeding of the 4th International Conference on Geochemistry, (pp. 401–419). Egypt: Alexandria University.

Helffrich, G. (2000). Topography of the transition zone seismic discontinuity. Rev. Geophys. 38, 141–158.

Hendricks, J. D., & Plescia, J. B. (1991). A review of the regional geophysics of the Arizona transition zone. Journal of Geophysical Research, 96, 12,351–12,373. https://doi.org/10.1029/90JB01781

Henry, B., Liégeois, J. P., Nouar, O., Derder, M. E. M., Bayou, B., Bruguier, O., Ouabadi, A.,Belhai, D., Amenna, M., Hemmi, A., Ayache, M. (2009). Repeated granitoid intrusionsduring the Neoproterozoic along the western boundary of the Saharan metacraton,Eastern Hoggar, Tuareg shield, Algeria: an AMS and U–Pb zircon age study. Tectonophysics 474 (3), 417–434.

Hermance, J. (1981). Crustal gensis in Iceland: Geophysical constraints on crustal thickening with age. Geophysical Research Letters, 8, 203–206. https://doi.org/10.1029/GL008i003p00203

Hildenbrand, T.G., Berger, B., Jachens, R.C., & Ludington, S. (2000). Regional crustal structures and their relationship to the distribution of ore deposits in the western United States based on magnetic and gravity data. Econ. Geol. 95 (8), 1583–1603.

Hoernle, K., Zhang, Y.S., & Graham, D. (1995). Seismic and geochemical evidence for largescale mantle upwelling beneath the eastern Atlantic and western and central Europe. Nature 374, 34–39. https://doi.org/10.1038/374034a0.

Hoggard, M. J., White, N. J., & Al-Attar, D. (2016). Global dynamic topography observations reveal limited influence of large-scale mantle flow. Nature Geoscience, 9, 456–463. https://doi.org/10.1038/ngeo2709

Holbrook, W. S., Mooney, W. D., & Christensen, N. I. (1992). The seismic velocity structure of the deep continental crust. In D. Fountain, R. Arculus, & R. Kay (Eds.), Continental lower crust (Vol. 23, pp. 1–43). New York: Elsevier.

Husson, L., Bernet, M., Guillot, S., Huyghe, P., Mugnier, J. L., Replumaz, A., & Van der Beek, P. (2014). Dynamic ups and downs of the Himalaya. Geology, 42, 839–842. https://doi.org/10.1130/G36049.1

Ito, E., & Takahashi, E. (1989). Postspinel transformations in the system Mg2SiO4-Fe2SiO4 and some geophysical implications. J. Geophys. Res. 316 94:10 637-10 646.

Kennett, B.L.N., & Engdahl, E.R. (1991). Traveltimes for global earthquake location and phase identification. J. Geophys. Intern. 105 (2), 429–465. https://doi.org/10.1111/ j.1365-246X.1991.tb06724. x.

Kennett, B.L.N., Engdahl, E.R., & Buland, R. (1995). Constraints on seismic velocities in the Earth from traveltimes. Geophys. J. Int. 122, 108–124.

Keppie, J., Dostal, J., & Murphy, J. (2011). Complex geometry of the Cenozoic magma plumbing system in the central Sahara. NW Africa, ISI.ISSN: 0020-6814 (Print) 1938-2839 (Online) J. homepage: http://www.tandfonline.com/loi/tigr20

King, S. D., & Anderson, D. L. (1998). Edge-driven convection. Earth Planet. Sci. Lett. 160, 289–296.

Klitzsch, E. (1971). The structural development of parts of North Africa since Cambrian time. In C. Gray (Ed.), Symp. on the geology of Libya: Tripoli (pp. 256–260). University of Libya: Faculty of Sciences.

Kröner, A., & Stern, R. J. (2005). Pan-African orogeny. Encyclopedia of Geology, 1. Elsevier, Oxford, 1–12.

Langston, C. A. (1979). Structure under Mount Rainier, Washington, inferred from teleseismic body waves. Journal of Geophysical Research, 84, 4749–4762. https://doi.org/10.1029/JB084iB09p04749

Lawrence, J.F., & Shearer, P.M. (2006). A global study of transition zone thickness using receiver functions. J. Geophys. Res. 111https://doi.org/10.1029/2005JB003973.B06307.

Lei, J., & Zhao, D. (2016). Teleseismic P-wave tomography and mantle dynamics beneatheastern Tibet. Geochem. Geophys. Geosyst. 17, 1861–1884.

Lemnifi, A.A., Liu, K.H., Gao, S.S., Elsheikh, A.A., Reed, C.A., Yu, Y., & Elmelade, A.A. (2014). Investigations of Libya Upper Mantle Anisotropy and Crustal Structure Using
Shear Wave Splitting and Receiver Function Analyses, Eos trans. AGU, Fall Meet.

Lemnifi, A. A., Liu, K. H., Gao, S. S., Reed, C. A., Elsheikh, A. A., Yu, Y., & Elmelade, A. A. (2015). Azimuthal anisotropy beneath north central Africa from shear wave splitting analyses. Geochemistry, Geophysics, Geosystems, 16, 1105–1114. https://doi.org/10.1002/2014GC005706

Lemnifi, A., Elshaafi, A., Browning, J., El Ebadi, S., & Gudmundsson, A. (2017a). Crustal thickness beneath Libya and the origin of partial melt beneath AS Sawda Volcanic Province from receiver-function constraints. J. Geophys. Res. Solid Earth. https://doi.org/10.1002/2017JB014291.

Lemnifi, A. A., Elshaafi, A., Karaoglu, O., Salah, M. K., Aouad, N., Reed, C. A., & Yu, Y. (2017b). Complex seismic anisotropy and mantle dynamic beneath Turkey. Journal of Geodynamics, 0264–3707. https://doi.org/10.1016/j.jog.2017.10.004

Lesquer, A., Takheris, D., Dautria, J., & Hadiouche, O. (1990). Geophysical and petrological evidence for the presence of anomalous upper mantle beneath Sahara basin (Algeria). Earth and Planetary Science Letters, 96, 407–418. https://doi.org/10.1016/0012-821X(90)90016-Q

Less, G., Turki, S., Suwesi, K., Peregi, L., Koloszar, L., Kalmar, J., Sherif, K., Csaszar, G., Gulasci, Z., Dalum, H., & Al Tajuri, A. (2006). Explanatory Booklet. Geological Map of Libya1: 250.000. Sheet: Waw Al Kabir NG 33-12. Industrial Research Centre, pp. 295.

Li, X., & Yuan, X. (2003). Receiver functions in northeast China—Implications for slab penetration into the lower mantle in northwest Pacific subduction zone. Earth Planet. Sci. Lett. 216, 679–691. https://doi.org/10.1016/S0012-821X(03)00555-7.

Liegeois, J. P., Abdelsalam, M. G., Ennih, N., & Ouabadi, A. (2013). Metacraton: Nature, genesis and behavior. Gondwana Research, 23, 220–237. https://doi.org/10.1016/j.gr.2012.02.016.

Liegeois, J. P., Benhallou, A., Azzouni-Sekkal, A., Yahiaoui, R., & Bonin, B. (2005). The Hoggar swell and volcanism: Reactivation of the Precambrian Tuareg shield during Alpine convergence and West African Cenozoic volcanism. Geological Society of America, Special Papers, 388, 379–400. https://doi.org/10.1130/0-8137-2388-4.379

Liegeois, J.P., Latouche, L., Boughrara, M., Navez, J., & Guiraud, M. (2003). The LATEA (Central Hoggar, Tuareg shield, Algeria): Behavior of an old passive margin during the Pan-African orogeny. J. Afr. Earth Sci. 37, 161–190. https://doi.org/10.1016/j.jafrearsci.2003.05.004.

Liégeois, J. P., Black, R., Navez, J., & Latouche, L. (1994). Early and late Pan-African orogeniesin the Aïr assembly of terranes (Tuareg shield, Niger). Precambrian Res. 67, 59–66.

Lithgow-Bertelloni, C., & Silver, P. G. (1998). Dynamic topography, plate driving forces and the African superswell. Nature, 395, 269–272. https://doi.org/10.1038/26212

Liu, K.H., Gao, S.S., Silver, P.G., & Zhang, Y.K. (2003). Mantle layering across central South America. J. Geophys. Res. 108 (B11), 2510. https://doi.org/10.1029/2002JB002208.

Liu, K. H., & Gao, S. S. (2010). Spatial variations of crustal characteristics beneath the Hoggar swell, Algeria, revealed by systematic analyses of receiver functions from a single seismic station. Geochemistry, Geophysics, Geosystems, 11, Q08011. https://doi.org/10.1029/2010GC003091

Liu, L., & Gurnis, M. (2010). Dynamic subsidence and uplift of the Colorado Plateau. Geology, 38, 663–666. https://doi.org/10.1130/G30624.1

Liu, L., Gao, S. S., Liu, K. H., & Mickus, K. (2017). Receiver function and gravity constraints on crustal structure and vertical movements of the Upper Mississippi Embayment and Ozark Uplift. Journal of Geophysical Research: Solid Earth, 122, 4572–4583. https://doi.org/10.1002/2017JB014201

Lloyd, S., Van Der Lee, S., Frana, G. S., Assumcao, M., & Feng, M. (2010). Moho map of South America from receiver functions and surface waves. Journal of Geophysical Research, 115, B11315. https://doi.org/10.1029/2009JB006829

Makris, J., & Stobbe, C. (1984). Physical properties and state of the crust and upper mantle of the Eastern Mediterranean Sea deduced from geophysical data. Marine Geology, 55, 347–363.

Makris, J., & Vees, R. (1977). Crustal structure of the Aegean Sea and the Islands Evia, Crete, Greece, obtained by refraction seismic experiments. Journal of Geophysical Research, 42, 329–341.

Makris, J., & Yegorova, T. (2006). A 3-D density-velocity model between the Cretan Sea and Libya. Tectonophysics, 417, 201–220. https://doi.org/10.1016/j.tecto.2005.11.003

Marone, F., Van Der Meijde, M., Van Der Lee, S., & Giardini, D. (2003). Joint inversion of local, regional and teleseismic data for crustal thickness in the Eurasia-Africa plate boundary region. Geophysical Journal International, 154, 499–514. https://doi.org/10.1046/j.1365-246X.2003.01973.x

Meert, J. G., & Lieberman, B.S. (2008). The Neoproterozoic assembly of Gondwana and its relationship to the Ediacaran-Cambrian radiation. Gondwana Res. 14, 5–21. https://doi.org/10.1016/j.gr.2007.06.007.

Meier, U., Trampert, J., & Curtis, A. (2009). Global variations of temperature and water content in the mantle transition zone from higher mode surface waves. Earth Planet. Sci. Lett. 282, 91–101. https://doi.org/10.1016/j.epsl.2009.03.004.

Miller, M.S., Allam, A.A., Becker, T.W., Di Leo, J.F., & Wookey, J. (2013). Constraints on the tectonic evolution of the westernmost Mediterranean and northwestern Africa from shear wave splitting analysis. Earth Planet. Sci. Lett. 375, 234–243. https://doi.org/10.1016/j.epsl.2013.05.036.

Mohamed, A.A., Gao, S.S., Elsheikh, A.A., Liu, K.H., Yu, Y., & Fat-Helbary, R.E. (2014). Seismic imaging of mantle transition zone dis-continuities beneath the northern Red Sea and adjacent areas. 361. J. Geophys. Int. 199, 648–657. https://doi.org/10.1093/gji/ggu284.

Montagner, J.-P., & et al. (2007). Mantle upwellings and convective instabilities revealed by seismic tomography and helium isotope geochemistry beneath eastern Africa. Geophys. Res. Lett. 34https://doi.org/10.10129/2007GL031098. L21303.

Moucha, R., & Forte, A. M. (2011). Changes in African topography driven by mantle convection. Nature Geoscience, 4, 660–661. https://doi.org/10.1038/ngeo1235

Moucha, R., Forte, A. M., Rowley, D. B., Mitrovica, J. X., Simmons, N. A., & Grand, S. P. (2009). Deep mantle forces and the uplift of the Colorado Plateau. Geophysical Research Letters, 36, L19310. https://doi.org/10.1029/2009GL039778

Nair, S. K., Gao, S. S., Liu, K. H., & Silver, P. G. (2006). Southern African crustal evolution and composition: Constraints from receiver function studies. Journal of Geophysical Research, 111, B02304. https://doi.org/10.1029/2005JB003802

Nixon, S., Maclennan, J., & White, N. (2011). Generation of alkali and tholeiitic basalts: The Al Haruj volcanic field, Paper presented at Volcanic and Magmatic Studies Group Annual Meeting, Queen's College Cambridge.

Nolet, G. (2008). A Breviary of Seismic Tomography. Cambridge Univ. Press.

Nyblade, A., Suleiman, I., Roy, R., Pusell, B. A., Suleiman, A., Doser, D., & Keller, R. (1996). Terrestrial heat flow in the Sirt Basin, Libya, and the pattern of heat flow across northern Africa. Journal of Geophysical Research, 101, 17,737–17,746.

Oliveira, R. G., & Medeiros, W. E. (2012). Evidences of buried loads in the base of the crust of the Borborema Province (NE Brazil) from Bouguer admittance estimates. Journal of South American Earth Sciences, 37, 60–76. https://doi.org/10.1016/j.jsames.2012.02.004

Owens, T. J., Zandt, G., & Taylor, S. R. (1984). Seismic evidence for an ancient rift beneath the Cumberland Plateau, Tennessee: A detailed analysis of broadband teleseismic P waveforms. Journal of Geophysical Research, 89, 7783–7795. https://doi.org/10.1029/JB089iB09p07783

Paige, C. C., & Saunders, M. A. (1982). LSQR: An algorithm for sparse linear equations and sparse least squares: ACM (Association for Computing Machinery) Transactions on Mathematical Software, 8, 43–71, doi: 10 .1145 /355984 .355989.

Pasyanos, M. E., & Nyblade, A. A. (2007). A top to bottom lithospheric study of Africa and Arabia. Tectonophysics, 444, 27–44. https://doi.org/10.1016/j.tecto.2007.07.008.

Pasyanos, M. E., & Walter, W. R. (2002). Crust and upper-mantle structure of North Africa, Europe and the Middle East from inversion of surface waves. Geophysical Journal International, 149, 463–481. https://doi.org/10.1046/j.1365-246X.2002.01663.x

Peregi, Z., Less, G., Konrad, G., Fodor, L., Gulacsi, Z., Gyalog, L., Turki, S., Suwesi, S., Sherif, Kh., & Dalub, H. (2003). Explanatory Booklet. Geological Map of Libya 1: 250.000. Sheet: Al Haruj Al Abyad NG 33-8. Industrial Research Centre, Tripoli, pp. 248

Pirajno, F. (2004). Hotspots and mantle plumes: Global intraplate tectonics, magmatism and ore deposits. Journal of Petroleum Science and Engineering, 82, 183–216. https://doi.org/10.1007/s00710-004-0046-4

Piromallo, C., & Morelli, A. (2003). P wave tomography of the mantle under the Alpine-Mediterranean area. J. Geophys. Res. Solid Earth 108 (B2). https://doi.org/10.1029/ 2002JB001757. (1978-2012).

Priestley, K., & McKenzie, D. (2006). The thermal structure of the lithosphere from shear wave velocities. Earth and Planetary Science Letters, 244, 285–301. https://doi.org/10.1016/j.epsl.2006.01.008

Reed, C. A., Almadani, S., Gao, S. S., Elsheikh, A. A., Cherie, S., Abdelsalam, M. G., & Liu, K. H. (2014). Receiver function constraints on crustal seismic velocities and partial melting beneath the Red Sea rift and adjacent regions, Afar Depression. Journal of Geophysical Research: Solid Earth, 119, 2138–2152. https://doi.org/10.1002/2013JB010719.

Reed, C.A., Liu, K.H., Chindandali, P.R.N., Massingue, B., Mdala, Mutamina, H.D., Yu, Y., & Gao, S.S. (2016). Passive rifting of thick lithosphere in the southern East African Rift: evidence from mantle transition zone discontinuity topography. J. Geophys. Res. 121, 8068–8079. https://doi.org/10.1002/2016JB013131.

Ringwood, A.E., 1975. Composition and Petrology of the Earth's Mantle, 1st edn. pp. 672.

Rudnick, R. L., & Fountain, D. M. (1995). Nature and composition of the continental crust: A lower crustal perspective. Reviews of Geophysics, 33, 267–309. https://doi.org/10.1029/95RG01302

Rudnick, R. L., & Gao, S. (2003). Composition of the continental crust. The Crust, 3, 1–64. https://doi.org/10.1016/B0-08-043751-6/03016-4

Sandvol, E., Seber, D., Calvert, A., & Barazangi, M. (1998). Grid search modeling of receiver functions: Implications for crustal structure in the Middle East and North Africa. Journal of Geophysical Research, 103, 26,899–26,917. https://doi.org/10.1029/98JB02238

Schmeling, H. (1985). Partial melt below Iceland: A combined interpretation of seismic and conductivity data. Journal of Geophysical Research, 90, 10,105–10,116.

Shearer, P.M., & Masters, T.G. (1992). Global mapping of topography on the 660-km discontinuity. Nature 355, 791–796 McGraw-Hill, New York.

Siebert, L., & Simkin, T. (2002). Volcanoes of the world: An illustrated catalog of Holocene volcanoes and their eruptions, Global Volcanism Program Digital Inf. Ser., GVP-3, Washington, DC. http://www.volcano.si.edu/world/

Simmons, N.A., Myers, S.C., Johannesson, G., & Matzel, E. (2012). LLNLG3Dv3: global P-wave tomography model for improved regional and teleseismic travel time prediction. J. Geophys. Res. Solid Earth 117 (B10). https://doi.org/10.1029/ 2012JB009525. 1978-2012.

Smith, W.H.F., & Wessel, P. (1990). Gridding with continuous curvature splines in tension. Geophysics 55, 293–305.

Speranza, F., Minelli, L., Pignatelli, A., & Chiappini, M. (2012). The Ionian Sea: The oldest in situ ocean fragment of the world? Journal of Geophysical Research, 117, B12101. https://doi.org/10.1029/2012JB009475

Stern, R.J. (1994). Arc-assembly and continental collision in the Neoproterozoic African orogen:Iimplications for the consolidation of Gondwanaland. Annu. Rev. Earth Planet Sci. 22, 319–351. https://doi.org/10.1146/annurev.ea.22.050194.001535.

Stoeser, D. B., & Van Camp, V. E. (1985). Pan-African miscroplate accretion of the Arabian–Nubian shield. Bull. Geol. Soc. Am. 96,817–826.

Stuart, F., Masoud, A., & Mark, D. (2014). The origin of Cenozoic magmatism of Libya. Geophysical Research Abstracts (Vol. 16, EGU2014-15877).

Suleiman, I. S. (1985). Gravity and heat flow studies in the Sirte Basin, Libya (PhD dissetation), University of Texas, El Paso.

Sumner, J. (1989). Regional geophysics of Arizona. In J. Jenny, & S. Reynolds (Eds.), Geological evolution of Arizona (Vol. 17, pp. 717–739). Tucson, AZ: Geological Society Digest.

Tauzin, B., & Ricard, Y. (2014). Seismically deduced thermodynamics phase diagrams for the mantle transition zone. Earth Planet Sci. Lett. 401, 337–346. https://doi.org/10. 1016/j.epsl.2014.05.039.

Tauzin, B., Debayle, E., & Wittlinger, G. (2010). Seismic evidence for a global low velocity layer in the Earth's upper mantle. Nat. Geosci. 3, 718. https://doi.org/10.1038/NGEO969.

Thompson, A.B. (1992). Water in the Earth's upper 383 mantle. Nature 358, 295–302. https://doi.org/10.1038/358295a0.

Thompson, D.A., Hammond, J.O.S., Kendall, J.-M., Stuart, G.W., Helffric, G.R.h., Keir, D., Ayele, A., & Goitom, B. (2015). Hydrous upwelling across the mantle transition zone beneath the Afar Triple Junction. Geochem. Geophys. Geosyst. 16, 834–846. https:// doi.org/10.1002/2014GC005648.

Tontini, F. C., Graziano, F. L., Cocchi, C., Carmisciano, L., & Stefanelli, P. (2006). Determining the optimal Bouguer density for a gravity data set: Implications for the isostatic setting of the Mediterranean Sea. Geophysical Journal International, 169, 380–388.https://doi.org/10.1111/j.1365-246X.2007.03340.x

Van Der Meijde, M., Julia, J., & Assumpcao, M. (2013). Gravity derived Moho for South America. Tectonophysics, 609, 456–467.https://doi.org/10.1016/j.tecto.2013.03.023

Van der Meijde, M., Van der Lee, S., & Giardini, D. (2005). Seismic discontinuities in the Mediterranean mantle. Phys. Earth Planet. Inter. 148 (2), 233–250. https://doi.org/ 10.1016/j.pepi.2004.09.008.

Van Der Meijde, M., Van Der Lee, S., & Giardini, D. (2003). Crustal structure beneath broad-band seismic stations in the Mediterranean region. Geophysical Journal International, 152, 729–739. https://doi.org/10.1046/j.1365-246X. 2003.01871.x

Vail, J. R. (1971). Dikes swarms and volcanic activity in northeastern Africa, Symposium Geology of Libya (pp. 341–347). University of Libya.

Watanabe, T. (1993). Effects of water and melt on seismic velocities and their application to characterization of seismic reflectors. Geophysical Research Letters, 20, 2933–2936. https://doi.org/10.1029/93GL03170

Wood, B.J. (1995). The effect of H2O on the 410-kilometer seismic discontinuity. Science 268–276.

Woollard, G. P. (1959). Crustal structure from gravity and seismic measurements. Journal of Geophysical Research, 64, 1521–1544. https://doi.org/10.1029/JZ064i010p01521

Yamazaki, D., & Karato, S. (2001). Some mineral physics constraints on the rheology and geothermal structure of Earth's lower mantle. Am. Mineral. 86, 385–391. https://doi. org/10.2138/am-2001-0401.

Yu, Y., Song, J., Liu, K. H., & Gao, S. S. (2015). Determining crustal structure beneath seismic stations overlying a low-velocity sedimentary layer using receiver functions. Journal of Geophysical Research: Solid Earth, 120, 3208–3218. https://doi.org/10.1002/2014JB011610

Yu, Y., Gao, S.S., Liu, K.H., Yang, T., Xue, M., & Phon Le, K. (2017). Mantle transition zone discontinuities beneath the Indochina Peninsula: Implications for slab subduction and mantle upwelling. Geophys. Res. Lett. 44, 7159–7167. https://doi.org/10.1002/2017GL073528.

Zandt, G., & Ammon, C. J. (1995). Continental crust composition constrained by measurements of crustal Poisson's ratio. Nature, 374, 152–154. https://doi.org/10.1038/374152a0

Zhao, D. (2015). Multiscale Seismic Tomography: Tokyo, Springer Japan, 304 p.

Zhao, D., Hasegawa, A., & Horiuchi, S. (1992). Tomographic imaging of P and S wave velocity structure beneath northeastern Japan. J. Geophys. Res., 97, 19,909–19,928, doi: 10 .1029 /92JB00603.

Zhao, D., Hasegawa, A., & Kanamori, H. (1994). Deep structure of Japan subduction zone as derived from local, regional, and teleseismic events. J. Geophys. Res., 99, 22,313–22,329, doi: 10 .1029 /94JB01149 .

Zhu, L. P., & Kanamori, H. (2000). Moho depth variation in Southern California from teleseismic receiver functions. Journal of Geophysical Research, 105, 2969–2980. https://doi.org/10.1029/1999JB900322

VITA

Awad Abdussalam Henish Lemnifi was born in Benghazi, Libya. He received his bachelor's degree in Geology from Benghazi University in 1997. In 2007, he earned a master's degree in Marine Geoscience from Bremen University, Bremen, Germany. In 2011, he received his PhD degree in Geology and Geophysics at Missouri University of Science and Technology, Rolla, Missouri. Lemnifi joined the PhD program in Mining Engineering at Missouri University of Science and Technology, Rolla, Missouri. His research interest included mining exploration, receiver function, petroleum exploration, and seismic data interpretation. In May 2020 he received his PhD degree in Mining Engineering from Missouri University of Science and Technology.

Awad was a member of the Society of Exploration Geophysics (SEG), American Geophysical Union (AGU), American Association of Petroleum Geologist (AAPG), Society of Petroleum Engineering (SPE), and Geologic Society of America (GSA). He has also been involved in many academic activities on campus.